Universidade de Aveiro
Departamento de
Electrónica, Telecomunicações e Informática,
2020

Somayeh Ziaie

Tecnologias Coerentes para Redes Óticas Flexíveis

Coherent Technologies for Flexible Optical Networks

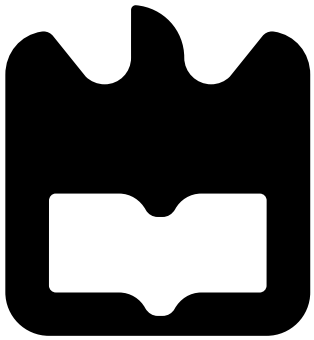

Somayeh Ziaie

Tecnologias Coerentes para Redes Ópticas Flexíveis

Coherent Technologies for Flexible Optical Networks

Tese apresentada à Universidade de Aveiro para cumprimento dos requisitos necessários à obtenção do grau de Doutor em Engenharia Eletrotécnica, realizada sob a orientação científica do Doutor Armando Humberto Moreira Nolasco Pinto, Professor Associado com Agregação do Departamento de Eletrónica, Telecomunicações e Informática da Universidade de Aveiro, e coorientação do Doutor Nelson de Jesus Cordeiro Muga, Investigador Auxiliar do Instituto de Telecomunicações.

This work was supported in part by Fundação para a Ciência e a Tecnologia (FCT) through national funds and when applicable co-funded by FEDER-PT2020 partnership agreement under the projects UID/EEA/50008/2013 (action SoftTransceiver and Optical-5G), UIDB/50008/2020-UIDP/50008/2020 (action DigCORE), and DSPMetroNet (POCI-01-0145-FEDER-029405) and PhD grant SFRH/BD/120665/2016. The Instituto de Telecomunicações was the host institution of this research work.

Dedicated to

My mother, Masoumeh and my father, Mohammadtaghi

My husband, Ali and my son, Arman

o júri / the jury

presidente / president

Doutor Victor Miguel Carneiro de Sousa Ferreira
Professor Catedrático da Universidade de Aveiro

vogais / examiners committee

Doutor Paulo Sérgio de Brito André
Professor Catedrático da Instituto Superior Técnico

Doutor Henrique Manuel de Castro Faria Salgado
Professor Associado da Universidade do Porto

Doutor Paulo Miguel Nepomuceno Pereiro Monteiro
Professor Associado da Universidade de Aveiro

Doutor Tiago Manuel Alves
Professor Auxiliar Convidado do Instituto Universitário de Lisboa

Doutor Armando Humberto Nolasco Pinto
Professor Associado com Agregação da Universidade de Aveiro (Orientador/Supervisor)

Agradecimentos / Acknowledgements

First and foremost, I would like to express my deepest gratitude to my research advisor and supervisor, Prof. Dr. Armando Nolasco Pinto for his constant encouragement, guidance and assistance throughout my graduate studies. During my Ph.D. he never stopped to support me and provide me the resources that I needed, he was always accessible and willing to help his students with their research.

I would like to express my appreciation to my co-supervisor, Dr. Nelson Muga, for his attention, motivation and constructive comments throughout my research work.

Moreover, I would like to appreciate Dr. Fernando Guiomar, for his motivating role and inspiring for my doctorate, he kept offering endless support throughout my Ph.D. studies.

I am very appreciated of Prof. José Rodrigues Ferreira da Rocha, Prof. António Luís Jesus Teixeira and Prof. Mário José Neves de Lima for their friendship and help. I also extend my sincere thanks to my colleges and friends from the optical communication group for sharing their time and experience with me and for many fruitful discussions. I would also like to thanks Gil Fernandes, Álvaro Almeida, Vitor Ribeiro, Artur Sousa, Vanessa Duarte, Cátia Pinho and Zeinab Rahmani. Special thanks to Ricardo Ferreira, who kindly helped me in clarifying many ideas during my Ph.D. work and sharing his experience.

With great pride for all the life experience that was given to me, my special thanks to the University of Aveiro, in particular to the Department of Electronics, Telecommunications and Informatics (DETI) and Instituto de Telecomunicações, and its director Prof. José Neves for his important supports. I also acknowledge Fundação para a Ciência e a Tecnologia for invaluable support in funding in order to complete this thesis. I would also like to acknowledge DiNEq, PANAROMA2, SoftTransceiver and Optical-5G projects for providing some of the equipment used in this work.

Furthermore, a special debt of gratitude is own to my husband Dr. Ali Shahpari, first as a college at the Instituto de Telecomunicações and then as a trainee advisor. I take this opportunity to thank for his endless love, unconditional support, guidance and exchange of knowledge throughout this work. I appreciate my lovely son Arman. You are indeed the greatest thing ever happened in my life. I couldn't have come this far without patience that you have shown during my studies and without seeing your smile and your cute eyes every morning.

At last, but not at least, I would like to pay my humble respects to my mother, my father, my uncle, and my brothers. I am extremely grateful to them to have sacrificed themselves to give me the finest education and the best in everything. And special thanks for their permanent encouragement from thousands of kilometers away.

Palavras-chave

Redes Óticas Flexiveis, Redes Óticas Passivas, Deteção Coerente, Processamento Digital de Sinal, Multiplexação e Desmultiplexação na Polarização, Multiplexagem em Subportadoras.

Resumo

As redes de telecomunicações futuras permitirão uma ampla gama de serviços inovadores e com melhor desempenho. No entanto, o desenvolvimento das futuras redes implicará vários avanços nas redes de fibra ótica, como transcetores óticos de alto desempenho capazes de suportar ligações de muito elevada capacidade, e a otimização da estrutura da rede, permitindo uma redução drástica do custo por bit transportado.

Simultaneamente, todos os segmentos de rede ótica (metropolitanas, acesso e longo alcance) necessitam de novas opções tecnológicas para suportar uma maior capacidade, maior eficiência espetral e flexibilidade. Neste contexto, a deteção coerente surge como uma oportunidade, fornecendo alta sensibilidade e elevada eficiência espetral. A tecnologia de deteção coerente pode ainda ser associada à multiplexação na polarização. Apesar de um potencial aumento ao nível do custo e da complexidade, a migração para transcetores coerentes de dupla polarização deve ser ponderada, pois permite duplicar a eficiência espetral. Esses sistemas de dupla polarização requerem um subsistema de processamento digital de sinal (DSP) adicional para desmultiplexagem da polarização. Este trabalho procura fornecer e caracterizar novos transcetores coerentes de baixo custo para o desenvolvimento de uma nova geração de transcetores mais práticos, flexíveis e de elevada capacidade, para interconexões óticas ao nível das futuras redes de acesso e metro. Assim, serão analisados diferentes algoritmos para a desmultiplexagem da polarização, incluindo uma abordagem adaptativa baseada no espaço de Stokes.

Além disso, são propostas técnicas de DSP independentes do formato de modulação e de baixa complexidade baseadas na desmultiplexagem de Stokes adaptativa para sistemas óticos coerentes flexíveis. Neste contexto, o desempenho do algoritmo adaptativo de desmultiplexagem na polarização baseado no espaço de Stokes é avaliado experimentalmente num sistema U-DWDM, tanto em análises off-line como em tempo real, considerando um percurso ótico hibrido que combina um sistema de transmissão suportado por fibra e outro em espaço livre. Foi ainda analisada a eficiência do algoritmo de desmultiplexagem na polarização numa rede ótica de acesso flexível U-DWDM com formatação de pulso do tipo Nyquist. Neste trabalho foi ainda analisada a aplicação da técnica de desmultiplexagem na polarização baseada no espaço de Stokes para sistemas de longo alcance. Assim, foi proposta uma solução de aplicação baseada no uso da multiplexagem digital de múltiplas sub-portadoras, tendo-se demonstrado uma melhoria na eficiência do desempenho dos sistemas óticos de longo alcance, sem aumentar significativamente a respetiva complexidade e custo.

keywords Flexible Networks, Passive Optical Networks, Coherent detection, Digital Signal Processing, Polarization Multiplexing and demultiplexing, Subcarrier multiplexing.

Abstract Next-generation networks enable a broad range of innovative services with the best delivery by utilizing very dense wired/wireless networks. However, the development of future networks will require several breakthroughs in optical networks such as high-performance optical transceivers to support a very-high capacity optical network as well as optimization of the network concept, ensuring a dramatic reduction of the cost per bit.
At the same time, all of the optical network segments (metro, access, long-haul) need new technology options to support high capacity, spectral efficiency and data-rate flexibility. Coherent detection offers an opportunity by providing very high sensitivity and supporting high spectral efficiency. Coherent technology can still be combined with polarization multiplexing. Despite the increased cost and complexity, the migration to dual-polarization coherent transceivers must be considered, as it enables to double the spectral efficiency. These dual-polarization systems require an additional digital signal processing (DSP) subsystem for polarization demultiplexing. This work seeks to provide and characterize cost-effective novel coherent transceivers for the development of new generation practical, flexible and high capacity transceivers for optical metro-access and data center interconnects. In this regard, different polarization demultiplexing (PolDemux) algorithms, as well as adaptive Stokes will be considered.
Furthermore, low complexity and modulation format-agnostic DSP techniques based on adaptive Stokes PolDemux for flexible and customizable optical coherent systems will be proposed. On this subject, the performance of the adaptive Stokes algorithm in an ultra-dense wavelength division multiplexing (U-DWDM) system will be experimentally evaluated, in offline and real-time operations over a hybrid optical-wireless link. In addition, the efficiency of this PolDemux algorithm in a flexible optical metro link based on Nyquist pulse shaping U-DWDM system and hybrid optical signals will be assessed. Moreover, it is of great importance to find a transmission technology that enables to apply the Stokes PolDemux for long-haul transmission systems and data center interconnects. In this work, it is also proposed a solution based on the use of digital multi-subcarrier multiplexing, which improve the performance of long-haul optical systems, without increasing substantially, their complexity and cost.

Contents

List of Figures

List of Tables

List of Acronyms

3-D three-dimensional

5G fifth generation

5GPPP 5G Public-Private Partnership

10GE-PON 10Gbps ethernet passive optical network

16QAM 16-ary quadrature amplitude modulation

ADC analog to digital converter

AFC automatic frequency control

AOM acousto-optical modulators

APC angled physical contact

APD avalanche photodiode

AON active optical network

ASE amplified spontaneous emission

AWG arbitrary waveform generator

BER bit error rate

BPF band pass filter

BP-SSF back propagation split step Fourier

BPSK Binary phase shift keying

BTB back-to-back

CD chromatic dispersion

CDE chromatic dispersion equalizer

CMA constant-modulus algorithm

CoRx coherent receiver

CPE carrier phase estimation

CUT channel under test

DBP digital backward propagation

DD-LMS decision directed least mean square

DFB distributed feedback

DM discrete mode

DOCP degree of circular polarization

DOF degree of freedom

DOLP degree of linear polarization

DOP degree of polarization

DP dual polarization

DP-16QAM dual polarization 16-ary quadrature amplitude modulation

DP-QPSK dual polarization quadrature shift keying

DPSK differential phase-shift keying

DPR dynamic power range

DSP digital signal processing

DQPSK differential quadrature shift keying

ECL external cavity laser

EDFA erbium-doped fiber amplifier

EPC electrical polarization controller

EPON Ethernet passive optical network

FEC forward error correction

FIR finite impulse response

FSAN full services access network

FSK frequency shift keying

FSO free space optics

FTTH fiber-to-the-home

FWM four-wave mixing

GEQ gain equalizer

GPON Gigabit passive optical network

IEEE institute of electrical and electronics engineers

IIR infinite impulse response

IM/DD intensity modulation/direct detection

IOT Internet of Things

IQM IQ modulator

LCP left circular polarization

LHP linear horizontal polarization

LMS least mean square

LO local oscillator

LVP linear vertical polarization

MSC multi-subcarrier

NG-PON2 next generation passive optical networks

NI nonlinear impairments

NLE nonlinearity equalization

NLPN nonlinear phase noise

NLSE nonlinear Schrodinger equation

NRZ non-return-to-zero

NLI nonlinear interference

ODL optical delay line

OFDM orthogonal frequency-division multiplexing

OLT optical line terminal

ONU optical networks unit

OOK on-off-keying

OPLL optical phase-locked loop

OSNR optical signal to noise ratio

PAM-4 4-ary pulse-amplitude modulation

PBC polarization beam combiner

PBS polarization beam splitter

PC polarization controller

PD polarization diversity

PDE partial differential equation

PDL polarization dependent losses

PDM polarization division multiplexing

PI polarization insensitive

PLL phase-locked loop

PMD polarization mode dispersion

PME polarization multiplexing emulation

PolDemux polarization demultiplexing

PolRot polarization rotation

PolTrack polarization tracking

PON passive optical network

PRBS pseudo random binary sequence

PS polarization scramble

PSCF pure silica core fiber

PSK phase shift keying

QAM quadrature amplitude modulation

QPSK quadrature phase shift keying

RCP right circular polarization

RDE radius directed equalizer

RF radio frequency

Rx receiver

RZ return to zero

SC single-carrier

SDN software defined networking

SE spectral efficiency

SNR signal to noise ratio

SOP state of polarization

SP single-polarization

SPM self-phase modulation

SRO symbol rate optimization

SSF split-step Fourier

SSM standard single-mode

TDHMF time-domain hybrid modulation format

TDM time division multiplexing

TDMA time division multiplexing access

TWDM-PON time and wavelength division multiplexing PON

TIA transimpedance amplifier

TOF tunable optical filter

Tx transmitter

U-DWDM ultra-dense wavelength division multiplexing

VOA variable optical attenuator

VSTF Volterra series transfer function

WDM wavelength division multiplexing

WS wavelength selective switch

XG-PON 10-Gigabit-capable passive optical network

XPM cross-phase modulation

Chapter 1

Introduction

Next-generation high-speed optical transmission systems expected to allow high capacity and low complexity networks with dynamic bandwidth assignment, in order to address the multiplicity of services and the plurality of end-users.

The organization of this chapter is as follows. Section 1.1 provides a comprehensive overview of the motivation for this Ph.D. thesis, which addresses the problem of improving optical networks to satisfy the technical requirements of future telecommunication services at a price affordable to end-users. The main goals of this thesis are identified in section 1.2. Also, the most important results reported in this thesis and a list of publications are presented in sections 1.3 and 1.4.

1.1 Introduction and Motivation

Bandwidth demand continues to rise exponentially in all optical networking sectors (metro, access, long-haul) and massive continuous growth is forecasted for the next decade. This is due to the subscriber's interest in the latest high bandwidth-demanding Internet applications and services [1], [2]. Such growth pushes the optical networking industry to update and develop next-generation transmission systems of 400-Gbps to 1-Tbps and even beyond [3]. The latest global Internet Protocol (IP) data traffic forecast, reported by Cisco Visual Networking Index, predicts a stable increase of about 26% per year, from 2017 to 2022, as presented in Fig.1.1 [4]. Due to the very heterogeneous nature of services, applications and end-user types, future optical networks need to include flexible equipment [5]. In order to support tomorrow's demands, fundamental changes from traditional static architectures in the optical communication networks to flexible, adaptive and energy-efficient networks are required [6].

Considering the actual growth of the data traffic, technologies are needed in optical communication systems, which efficiently using the fiber capacity. Optical transmission systems apply coherent detection technology to enhance receiver sensitivity and spectral efficiency (SE) as well as efficient usage of the fiber capacity [7]. Besides the higher receiver sensitivity of a coherent system, it can tremendously extend the reach and number of users per optical link. In addition, it can be used to exploit the spectral selectivity that may provide the required flexibility to optical networks [6]. It is a reality that coherent brings higher cost and complexity in optical transceiver modules. Although, with today's development of coherent transceivers in the long-haul transmission systems and recent advances in photonic integrated circuits, this cost can be reduced in the near future [6], [5]. Anyway, this transition

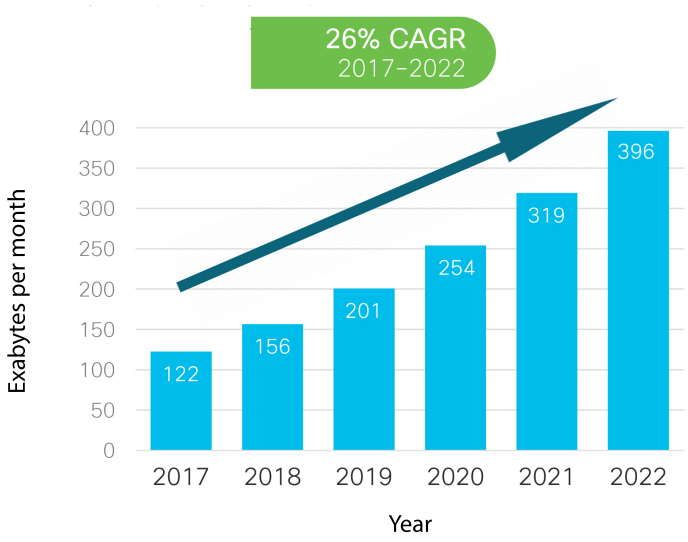

Figure 1.1: Global IP data traffic forecast, in exabytes per month, for the period of 2017 to 2022, reported in the Cisco Visual Networking Index [4].

period creates an opportunity for researchers to study new architectures and digital signal processing (DSP) to improve the performance and complexity of coherent transceivers, helping the standardization and industrial players to select the most efficient solutions in proper time.

The capacity of the coherent transmission systems can significantly increase with employing a powerful DSP, in order to compensate for the transmission impairments in the digital domain. A coherent receiver will benefit from DSP in main subsystems such as digital carrier recovery and frequency or phase compensation [8]. Furthermore, nonlinear impairments, can limit the SE and reach in the optical transmission systems. However, nonlinearities can also be compensated in the DSP subsystems [9]. In addition, wavelength-division multiplexing (WDM) technology has been successfully applied to improve capacity in the optical systems [10]. The association of ultra-dense wavelength division multiplexing (U-DWDM) and coherent transmission, allows SE of the fiber doubled by employing polarization division multiplexing (PDM) techniques [11], [12]. Besides coherent WDM, with applying a pure digital multi-subcarrier (MSC) multiplexing, instead of widely deployed single-carrier, bandwidth efficiency, power consumption and tolerance to dispersion of the optical system, can be significantly improved. [13], [14], [15], [16]. Moreover, remarkable improvements in the SE can be also achieved by using Nyquist pulse shaping. Although Nyquist pulse shaping creates an extra complexity for coherent transceivers due to the implementation of filter taps for the shaped signal [11].

These kinds of systems should be designed in a future-proof way to enable smoother transitions in future generations. The 5th generation of mobile broadband wireless networks is the proposed next major telecommunications standards, which are expected to provide the demands and service requirements of the application in 2020 and beyond [17]. The next-generation systems should be more effective comparing to previous generation in terms of energy consumption and hardware complexity and flexibility, and also they expected to support data rates exceeding 10 Gbps per end user [18]. On the other hand, due to the facilities provided by the optical metro-access networks, they can provide a high-capacity and

future-proof backhaul for 5G wireless networks and beyond [17], [19], [20]. Besides growing bandwidth requirements for future optical networks, increasing the capacity of backhaul and front-haul network links are inevitable. Such higher capacity inter-data centre connections are required to keep pace with the massive traffic growth in data centre networks.

In future optical metro networks, resiliency and granular control gain more and more attention in order to support and protect business and mobile users. Therefore, this kind of network should have backup links. For a special condition such as natural disaster or civil conflicts, optical wireless links using the RF system is helping to restore networks for lower data rate and unidirectional links [21, 22]. Recently, great attention has been given to free space optics links (FSO) in optical networks in the research community as well as industry. FSO is cost-efficient and a fast setup solution that could offer large bandwidths [23].

It has been shown that using dual-polarization (DP) and advanced modulation formats, the capacity of the optical-wireless link can be increased significantly [23, 24]. Although, with applying advanced modulation formats, higher-speed analog-to-digital converters (ADCs) and digital-to-analog converters (DACs) are needed, since advanced modulation formats will need converters with a higher effective number of bits. However, DP approaches improve the reliability of the FSO link with decreasing baud rate and consequently increasing sensitivity. Therefore, coherent U-DWDM using dual-polarization modulation formats and FSO can fully utilize the bandwidth and increase the transmission capacity, besides also extending the coverage area. In addition, implementing a flexible method for generating and detecting arbitrary complex-modulated signals in the access and metro networks can be an enabling technology for software-defined networking (SDN) architectures [25]. These flexible systems offer different degrees of freedom such as providing different modulation formats, offering various symbol rates, possibility to change the number and the spacing between the subcarriers.

An important milestone towards future optical networks is a proper design of optical transmitters-links-receivers, by changing architectures from traditional static to flexible, low complexity and energy-efficient structures in order to decrease the cost per bit and improve the performance of the system [17]. For instant, in flexible metro-access networks, different types of end-users with heterogeneous massive traffic and adaptive distance, with different optical powers and modulation formats can be joined to the system corresponding to the load of the network [26]. Therefore, besides flexible grids, SE and data rate, resiliency, optimization of the network regarding reach and capacity for this kind of multi-modulation formats systems are important factors [6]. However, sophisticated and high-performance transceivers in the optical networks are required to support very high capacity, while still guaranteeing other key features of optical networks, such as load balancing and resiliency. Nevertheless, in order to meet commercially viability, the quest for flexible and spectrally efficient optical networks must follow the path of simple and moderate-cost solutions by optimization on both network and system levels.

1.2 Thesis Main Goals

Given the above overview, we have identified the main objectives of this Ph.D. thesis. In this sense, this Ph.D. thesis focuses on research and development of numerical tools, DSP subsystems, and novel architecture designs that realize low complexity, moderate cost, energy-efficient and flexible coherent transceivers based on an enhanced optimization technique. The following goals were defined initially:

- Implement and integrate fiber and free space optics links to support metro and access networks based on high-performance transceivers.
- Develop a low-complexity polarization demultiplexing technique transparent to modulation formats for flexible and customizable optical coherent transceivers.
- Extend the developed polarization demultiplexing techniques for long-haul transmission systems.

1.3 Main Contributions

The author considers that the main contributions and most important results reported in this thesis can be summarized as follow:

- The adaptive Stokes polarization demultiplexing technique was experimentally validated for optical metro and access networks, based on dual-polarization quadrature shift keying (DP-QPSK) and dual-polarization 16-ary quadrature amplitude modulation (DP-16QAM) modulation formats. The performance and convergence speed of it were compared with the conventional constant-modulus algorithm (CMA) for 1-channel DP-QPSK and DP-16QAM Nyquist signals, with constant frequency state of polarization (SOP) rotation. The convergence of the adaptive Stokes algorithm has been found to be approximately three times quicker than that of CMA. This work was published in [27].
- Design a flexible optical system based on Nyquist pulse shaping coherent U-DWDM, supported by adaptive Stokes technique in bidirectional flexible optical metro networks. The optical fiber and FSO link support DP-QPSK and DP-16QAM modulation formats. A dynamic bandwidth and power range optical metro-access network were also demonstrated. These works were published in [28], [29].
- A real-time U-DWDM DP-QPSK system supported by the adaptive Stokes algorithm was implemented in real-time considering transmission over 100 km fiber. The resiliency of the adaptive Stokes PolDemux technique was evaluated in terms of nonlinearity and optical power budgets. This work was published in [30]
- Application of the adaptive Stokes PolDemux approach for long-haul transmission systems was experimentally tested. The enabling factor was the use of MSC modulation, which has been demonstrated to significantly enhance the PolDemux tolerance against residual accumulated CD. This work was published in [31].

1.4 List of Publications

The results obtained in the framework of this Ph.D. program were published in the following journals and conferences:

1.4.1 Journal Articles

5 S. Ziaie, F. P. Guiomar, N. J. Muga, A. Nespola, G. Bosco, A. Carena, A. N. Pinto, "Adaptive Stokes-based polarization demultiplexing for long-haul multi-subcarrier sys-

tems", IEEE Photonics Technology Letters, vol. 31, no. 10, pp. 759 - 762, March 2019.

4 C. S. Martins, F. P. Guiomar, S. B. Amado, R. M. Ferreira, S. Ziaie, A. Shahpari, A. L. Teixeira, A. N. Pinto, "Distributive FIR-Based Chromatic Dispersion Equalization for Coherent Receivers", IEEE/OSA Journal of Lightwave Technology, vol. 34, no. 21, pp. 5023 - 5032, November 2016.

3 A. Shahpari, R. M. Ferreira, F. P. Guiomar, S. B. Amado, S. Ziaie, C. Rodrigues, J. D. Reis, A. N. Pinto and A. L. Teixeira "Real-time bidirectional coherent Nyquist UDWDM-PON coexisting with multiple deployed systems in field-trial (Invited)", IEEE/OSA Journal of Lightwave Technology, vol. 34, no. 7, pp. 1643 - 1650, April 2016.

2 S. Ziaie, N. J. Muga, F. P. Guiomar, G. M. Fernandes, R. M. Ferreira, A. Shahpari, A. L. Teixeira, A. N. Pinto, "Experimental assessment of the adaptive Stokes Space-Based polarization demultiplexing for optical metro and access networks", IEEE/OSA Journal of Lightwave Technology, vol. 33, no. 23, pp. 4968 - 4974, December 2015.

1 A. Shahpari, R. M. Ferreira, V. M. Ribeiro, A. Sousa, S. Ziaie, A. Tavares, Z. Vujicic, F. P. Guiomar, J. D. Reis, A. N. Pinto and A. L. Teixeira, "Coherent ultra-dense wavelength division multiplexing passive optical networks [Invited paper]", Optical Fiber Technology -Elsevier, vol. 26, pp. 100- 107, December 2015.

1.4.2 International Conferences

11 S. Ziaie, R. M. Fereira, N. J. Muga, F. P. Guiomar, A. Shahpari, A. L. Teixeira and A. N. Pinto, "Coherent UDWDM transceivers based on adaptive Stokes space polarization demultiplexing in real-time", in Proc. European Conf. on Optical Communications (ECOC), Gothenburg, Sweden, paper Th.1.B, September 2017.

10 N. J. Muga, G. M. Fernandes, S. Ziaie, R. M. Fereira, A. Shahpari, A. L. Teixeira and A. N. Pin-to, "Advanced digital signal processing techniques based on Stokes space analysis for high-capacity coherent optical systems", in Proc. International Conf. on Transparent Networks (ICTON), Girona, Catalonia, Spain, paper We.A1.4, July 2017.

9 S. Ziaie, N. J. Muga, F. P. Guiomar, R. M. Fereira, A. Shahpari, A. L. Teixeira and A. N. Pinto, "Adaptive Stokes space based polarization demultiplexing for flexible UDWDM metro-access networks", in Proc. Optical Fiber Communication Conf. and Exposition (OFC), Los Angeles, CA, paper Th1K.6, March 2017.

8 S. Ziaie, N. J. Muga, F. P. Guiomar, R. M. Fereira, A. Shahpari, A. L. Teixeira and A. N. Pinto, "Flexible and hybrid bidirectional optical metro networking using adaptive Stokes space polarization demulti-plexing", in Proc. 21th Conf. on Network and Optical Communications (NOC), paper S9.5, pp 212-216, June 2016.

7 A. N. Pinto, S. B. Amado, C. S. Martins, S. Ziaie, N. J. Muga, and F. P. Guiomar, "Multi-carrier high-speed optical communication systems supported by digital signal processing (Invited Paper)", in Proc. International Conf. on Transparent Networks (ICTON), Trento, Italy, paper Mo. B1.2, July 2016.

6 N. J. Muga, S. Ziaie, A. Shahpari, and A. N. Pinto, "Using the Stokes space for equalization of polariza-tion impairments in digital coherent optical receivers (Invited Paper)", in Proc. International Conf. on Transparent Networks (ICTON), Trento, Italy, paper Mo. B2.3, July 2016.

5 Z. Vujicic, A. Shahpari, B. M. Neto, N. B. Pavlovic, A. J. Almeida, A. Tavares, M. Ribeiro, S. Ziaie, R. M. Ferreira, R. Bastos, and A. L. Teixeira, "Considerations on performance, cost and power consumption of candidate 100G EPON architectures", in Proc. International Conf. on Transparent Networks (ICTON), Trento, Italy, paper We. D1.1, July 2016.

4 S. Ziaie, F. P. Guiomar, R. M. Fereira, S. Amado, A. Shahpari, A. L. Teixeira and A. N. Pinto, "100 Gbps DP-QPSK transmission over 8000 km of standard single mode fiber using recirculating loop technique", in Proc. 10th Conf. on Telecommunications (Conftele), Aveiro, Portugal, paper CD, pp. 28 - 31, September 2015.

3 A. Shahpari, R. M. Ferreira, S. Ziaie, J. D. Reis, J. R. F. Oliveira, António L. Teixeira, "Multiple system configura-tion for next generation optical access networks with real-time Nyquist UDWDM-PON", in Proc. European Conf. on Optical Communications (ECOC), Valencia, Spain, paper P.7.18, September 2015.

2 A. N. Pinto, S. B. Amado, C. S. Martins, S. Ziaie, N. J. Muga, R. M. Ferreira, A. L. Teixeira and F. P. Guiomar, "Real-Time digital signal processing for coherent optical systems (Invited Paper)", in Proc. Inter-national Conf. on Transparent Networks (ICTON), Budapest, Hungary, paper Mo.C1.2, July 2015.

1 N. J. Muga, S. Ziaie, A. Shahpari, F. P. Guiomar, A. N. Pinto, "Optimizing polarization related dynamic equalization in coherent optical communications", in Proc. International Conf. on Transparent Optical Networks (ICTON), Budapest, Hungary, paper Mo.C1.6, July 2015.

1.5 Final Remarks

This chapter presented an overall view of the Ph.D. thesis. The motivation, objectives and main achievements were discussed, and a list of publications was presented.

Bibliography

[1] J. Kani, M. Yoshino, K. Asaka, H. Ujikawa, T. Yamada, K. Nishimoto, K. Suzuki, and A. Otaka, "Flexible access system architecture (FASA) to support diverse requirements and agile service creation," *Journal of Lightwave Technology*, vol. 36, no. 8, pp. 1510–1515, Apr 2018.

[2] N. Suzuki, H. Miura, K. Matsuda, R. Matsumoto, and K. Motoshima, "100 Gbps to 1 Tbps based coherent passive optical network technology," *Journal of Lightwave Technology*, vol. 36, no. 8, pp. 1485–1491, Apr 2018.

[3] R. Müller, J. Renaudier, P. Brindel, H. Mardoyan, P. Jennevé, L. Schmalen, and G. Charlet, "1-Terabit/s net data-rate transceiver based on single-carrier Nyquist-shaped 124 GBaud PDM-32QAM," in *Proc. Optical Fiber Communication Conf. and Exposition (OFC)*. IEEE, 2015, paper Th5B.1.

[4] Cisco, "Cisco visual networking index: Forecast and methodology 2017-2022," Tech. Rep., 2017.

[5] D. Hillerkuss and J. Leuthold, "Software-defined transceivers in dynamic access networks," *Journal of Lightwave Technology*, vol. 34, no. 2, pp. 792–797, Aug 2015.

[6] K. Roberts and C. Laperle, "Flexible transceivers," in *Proc. Optical Fiber Communication Conf. and Exposition (OFC)*, 2012, paper We.3.A.3.

[7] X. Liu, S. Chandrasekhar, X. Chen, P. Winzer, Y. Pan, T. Taunay, B. Zhu, M. Fishteyn, M. Yan, J. Fini, E. Monberg, and F. Dimarcello, "1.12-Tb/s 32-QAM-OFDM superchannel with 8.6-b/s/Hz intrachannel spectral efficiency and space-division multiplexed transmission with 60-b/s/Hz aggregate spectral efficiency," *Optics Express*, vol. 19, no. 26, pp. B958–B964, Dec 2011.

[8] R. M. Ferreira, A. Shahpari, F. P. Guiomar, S. Amado, M. Drummond, J. D. Reis, A. N. Pinto, and A. L. Teixeira, "Hardware optimization for carrier recovery based on mth power schemes," in *Proc. Optical Fiber Communication Conf. and Exposition (OFC)*, 2016, paper Th2A.43.

[9] R. J. Essiambre, G. Kramer, P. J. Winzer, G. J. Foschini, and B. Goebel, "Capacity limits of optical fiber networks," *Journal of Lightwave Technology*, vol. 28, no. 4, pp. 662–701, 2010.

[10] H. Rohde, E. Gottwald, A. Teixeira, J. D. Reis, A. Shahpari, K. Pulverer, and J. S. Wey, "Coherent ultra dense WDM technology for next generation optical metro and access networks," *Journal of Lightwave Technology*, vol. 32, no. 10, pp. 2041–2052, May 2014.

[11] J. D. Reis, A. Shahpari, R. M. Ferreira, S. Ziaie, D. M. Neves, M. Lima, and A. L. Teixeira, "Terabit+ (192x10 Gb/s) nyquist shaped UDWDM coherent PON with upstream and downstream over a 12.8 nm band," *Journal of Lightwave Technology*, vol. 32, no. 4, pp. 729–735, Feb. 2014.

[12] A. Shahpari, R. M. Ferreira, F. P. Guiomar, S. B. Amado, S. Ziaie, C. Rodrigues, J. D. Reis, A. N. Pinto, and A. L. Teixeira, "Real-time bidirectional coherent nyquist

UDWDM-PON coexisting with multiple deployed systems in field-trial," *Journal of Lightwave Technology*, vol. 34, no. 7, pp. 1643–1650, Apr 2016.

[13] M. Qiu, Q. Zhuge, M. Chagnon, Y. Gao, X. Xu, M. M. Osman, and D. V. Plant, "Digital subcarrier multiplexing for fiber nonlinearity mitigation in coherent optical communication systems," *Optics Express*, vol. 22, no. 15, pp. 18 770–18 777, Jul 2014.

[14] F. P. Guiomar, A. Carena, G. Bosco, L. Bertignono, A. Nespola, and P. Poggiolini, "Nonlinear mitigation on subcarrier-multiplexed PM-16QAM optical systems," *Optics Express*, vol. 25, no. 4, pp. 4298–4311, Feb 2017.

[15] T. Rahman, D. Rafique, B. Spinnler, A. Napoli, M. Bohn, A. Koonen, C. Okonkwo, and H. De Waardt, "Digital subcarrier multiplexed hybrid QAM for data-rate flexibility and ROADM filtering tolerance," in *Proc. Optical Fiber Communications Conf. and Exhibition (OFC)*. Optical Society of America, 2016, paper Tu3K–5.

[16] A. Nespola, L. Bertignono, G. Bosco, A. Carena, Y. Jiang, S. Bilal, P. Poggiolini, S. Abrate, and F. Forghieri, "Experimental demonstration of fiber nonlinearity mitigation in a WDM multi-subcarrier coherent optical system," in *European Conf. on Optical Communication (ECOC)*. IEEE, 2015, pp. 1–3.

[17] S. Aleksic, "Towards fifth-generation (5G) optical transport networks," pp. 1–4, 2015.

[18] M. Ruffini, "Multi-Dimensional convergence in future 5G networks," *Journal of Lightwave Technology*, vol. 35, no. 3, pp. 535–549, Feb 2017.

[19] M. Fiorani, B. Skubic, J. Martensson, L. Valcarenghi, P. Castoldi, L. Wosinska, and P. Monti, "On the design of 5G transport networks," *Photonic network communications*, vol. 30, no. 3, pp. 403–415, 2015.

[20] P. Vetter, "Next generation optical access technologies," in *Proc. European Conf. and Exhibition on Optical Communication (ECOC)*. Optical Society of America, 2012, paper Tu.3.G.1.

[21] I. Sugino, "Disaster recovery and the R&D policy in Japan's telecommunication," *Proc. Optical Fiber Communication Conf. and Exposition (OFC)*, March 2012.

[22] A. Shahpari, R. Ferreira, V. Ribeiro, A. Sousa, S. Ziaie, A. Tavares, Z. Vujicic, F. P. Guiomar, J. D. Reis, A. N. Pinto, and A. Teixeira, "Coherent ultra-dense wavelength division multiplexing passive optical networks," *Optical Fiber Technology, Elsevier*, vol. 26, pp. 100–107, December 2015.

[23] M. A. Khalighi and M. Uysal, "Survey on free space optical communication: A communication theory perspective," *IEEE Communications Surveys Tutorials*, vol. 16, no. 4, pp. 2231–2258, Fourthquarter 2014.

[24] G. Parca, A. Shahpari, G. M. T. B. V. Carrozzo and, and A. Teixeira, "Optical wireless transmission at 1.6-Tbitps (16 x 100 Gbitps) for next-generation convergent urban infrastructures," *Optical Engineering*, vol. 52, no. 11, pp. 1 161 021–5, November 2013.

[25] D. Hillerkuss and J. Leuthold, "Software-defined transceivers for dynamic access networks," in *Proc. Optical Fiber Communication Conf. and Exposition (OFC)*, 2015, paper Tu2E.4.

[26] M. Ruffini, "Metro-Access network convergence," in *Proc. Optical Fiber Communication Conf. and Exposition (OFC)*, 2016, paper Th4B–1.

[27] S. Ziaie, N. J. Muga, F. P. Guiomar, G. M. Fernandes, R. M. Ferreira, A. Shahpari, A. L. Teixeira, and A. N. Pinto, "Experimental assessment of the adaptive Stokes space-based polarization demultiplexing for optical metro and access networks," *Journal of Lightwave Technology*, vol. 33, no. 23, pp. 4968–4974, December 2015.

[28] S. Ziaie, N. J. Muga, R. Ferreira, F. Guiomar, A. Shahpari, A. L. Teixeira, and A. N. Pinto, "Adaptive Stokes space based polarization demultiplexing for flexible UDWDM metro-access networks," in *Proc. Optical Fiber Communication Conf. and Exposition (OFC)*, 2017, paper Th1K–6.

[29] S. Ziaie, N. J. Muga, R. Ferreira, A. Shahpari, F. Guiomar, A. L. Teixeira, and A. N. Pinto, "Flexible and hybrid bidirectional optical metro networking using adaptive stokes space polarization demultiplexing," in *21th European Conference on Networks and Optical Communications (NOC)*, 2016, paper S9.5, pp. 212–216.

[30] S. Ziaie, R. M. Ferreira, N. J. Muga, F. P. Guiomar, A. Shahpari, A. L. Teixeira, and A. N. Pinto, "Coherent UDWDM transceivers based on adaptive stokes space polarization demultiplexing in real-time," in *European Conf. on Optical Communication (ECOC)*. IEEE, 2017, p. Th1B4.

[31] S. Ziaie, F. P. Guiomar, N. J. Muga, A. Nespola, G. Bosco, A. Carena, and A. N. Pinto, "Adaptive Stokes-based polarization demultiplexing for long-haul multi-subcarrier systems," *IEEE Photonics Technology Letters*, vol. 31, no. 10, pp. 759–762, 2019.

Chapter 2

Coherent Optical Technology

A high capacity optical coherent communication system is a key technology for the next-generation networks. Recently, coherent detection technology has been applied to the optical transmission links to improve receiver sensitivity as well as efficient usage of spectrum. Coherent technologies have also been applied in passive optical networks. Therefore, the identification of different optical coherent technologies and understanding how these technologies can be combined to support the future high-speed networks are mandatory.

This chapter is organized as follows: in section 2.1, we start by discussing the demands and requirements for developing next-generation optical networks. In section 2.2, coherent optical communication systems will be reviewed. Especially, different anatomies of coherent systems consist of polarization and phase diverse coherent detection are analyzed. Furthermore, advanced optical modulation formats in the coherent system are discussed in this section. In section 2.3, an overview of digital post-processing algorithms for the coherent system is provided. Laboratory facilities developed at IT Aveiro, to implement long-haul optical and free-space optical links are presented in section 2.4. And finally, the main conclusions of this chapter are presented in section 2.5.

2.1 Future Optical Networks

Driven by the proliferation of heterogeneous bandwidth-consuming Internet services, the traffic demand has been growing exponentially year after year [1]. Fig. 2.1 shows the number of residential and business subscribers, the number of connected devices per subscriber and most important, bandwidth demands per device, which have been growing continuously. Therefore, an exponential increase in both peak and sustained data rate is needed which results in operator requests for optical transceivers with speeds of 25, 50, 100, and even 400 Gbps [2], [3].

Front-haul requirements target peak bandwidth of 10 Gbps will be required with the advent of the next-generation access networks [4]. Besides growing bandwidth requirements for future optical access networks, increasing the capacity of back-haul network links are inevitable [5], [6]. Such higher capacity inter-data center connections are required to keep pace with the massive traffic growth in data center networks [1], [7]. Moreover, back-haul also needs optical transceivers beyond 400 Gbps to carry traffic towards/from the core network or data-centers [8]. Therefore, future networks should be significantly different from today's networks. They should provide more energy efficiency and hardware flexibility, higher performance and capacity of the

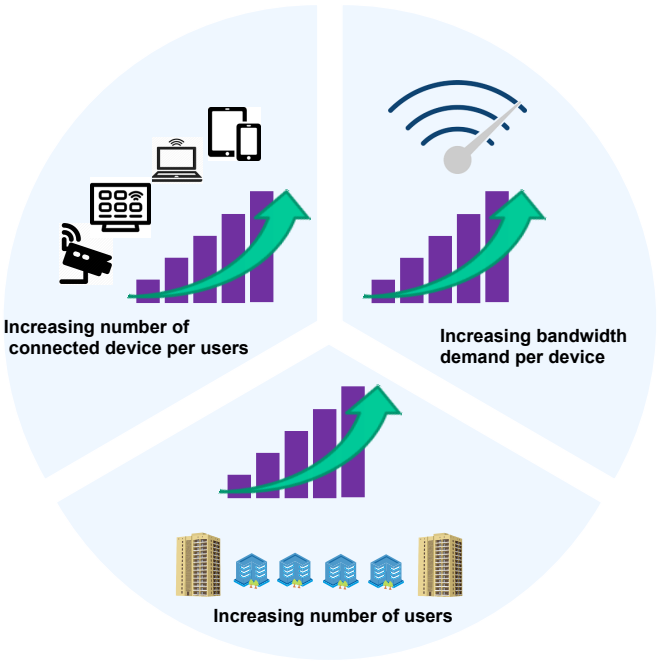

Figure 2.1: Bandwidth demand trends and broadband high-speed data services.

system, lower latency and power consumption, and beside them improve mobility, reliability and availability [9], [10]. In order to develop next-generation networks, which can support a very wide range of applications some requirements and facilities are needed, which can be listed in the following points [9], [11]:

- Flexibility

  The oncoming networks should be flexible to provide all the user demands without increasing the complexity of the system. The concept of the flexibility in the optical networks can be included the following points:

  - Possibility to support different technologies;
  - Capability to employ different modulation formats;
  - Cover different users with different distance from the central office;
  - Ability to manage load balancing at a different time of the day;
  - Possibility to extend network components in order to accommodate future unknowable scenarios;

- Reliability

  A reliable network is one of the critical objectives for network operators in order to deploy secure high-capacity fiber networks. Upcoming optical networks should prepare a reliable connection with very high availability namely:

  - Provide the most reliable link based on the user's application needs, location, and mobility;

- Being able to make secure connections in the network;
- Ability to recover itself when any natural disaster happens;
- Being able to solve any failure in the system very fast;
- Ability to adapt and switch to another technology when any problem occurs;
- Possibility to prepare a system with very low latency;

- Massive Network Capacity

  Using the maximum capacity of the fiber with enormous connectivity and providing ultra-high capacity density, is expected from the future optical infrastructure. By applying new techniques, the upcoming networks can present massive improvements in the capacity of the system.

- Higher Data Rate

  One of the most expectations of the networks is achieving higher data rates than the previous generation. The main idea is that while keeping the cost of the device down, providing maximum data rate up to 10 Gbps for each user. In this regard, upcoming networks should apply dense wavelength division multiplexing (DWDM) technology in order to further increase data rates.

- Low latency

  In order to develop the ultra-high-performance network and support communication applications, reducing latency for the link within the system is one of the most critical points [11]. Reducing end-to-end latencies is the key to provide applications that require real-time interactivity and data transmission with almost zero latency.

- Cost efficient devices

  Although, great speed comes with cost, but increasing the performance of a system should lead to a decrease in the total cost per bits of the devices in a network. Therefore, it is necessary that future devices be available at a very low cost.

Due to the highly heterogeneous environments in years ahead, optical metro and access networks need to be scalable to support multiple types of services and applications simultaneously to different types of end-users [5], [12]. Furthermore, oncoming optical networks should provide new services, such as virtual reality, cloud computing, smart homes and connected cars [6], [13].

In addition, mobility and ubiquitous coverage are two crucial pillars for future networks [5], [14], [15], [16]. Obviously, for the telecommunication industry the radio frequency (RF) would be the best candidate to support the aforementioned factors. Although RF-based systems provide high capacity and reach, they are not cost efficient. In addition, they have some physical restrictions such as for the high data-rate links they have high power consumption [17]. In contrast, FSO communications can offer unlimited capacity (depend on the TX/RX) with license-free wireless spectrum domain. Also installation and development of this technique is very economic and fast. Thus, the composition of optical networks and FSO link should be very efficient and can support both flexibility and high-capacity in the fiber and wireless systems [18], [19].

In order to cope with the requirements of the next-generation networks, the identification and characterization of different technologies is required, to find how these technologies can be adopted to optical networks for the purpose of realizing integrated back-haul and front-haul nodes. The WDM is a future proof investment for LTE, LTE-evolution [20] and in optical metro and access networks have been widely considered in academia for many years and still is in the state of the art.

The most advanced technology for building the next-generation access network is fiber-to-the-home (FTTH), which is a residential communications infrastructure where connects a large number of subscribers to a central office. Basically, there are two major kinds of architectures for developing FTTH, the active optical network (AON) and the passive optical network (PON). In the AON or point-to-point network, each subscriber has his own dedicated fiber to the optical line terminal (OLT). In this kind of system, for transmitting a signal to specific users or to proper places, applies electrically powered switching equipment. PON allows point-to-multipoint fiber access networks relying on passive optical nodes and provides a high bit rate for a number of users with sharing OLT port and feeder fiber. In recent years, PON has been recognized as a cost-efficient and economical access network, because of providing high bandwidth demand with using the optimum amount of resources. Therefore, great attention was given to the implementation of cost-effective, flexible, reliable architectures for a different type of PON technologies and topologies.

Anyway, time-division multiplexing access (TDMA) has been the preferred technology in PON [7], [13]. TDM-PON applies the time-division multiplexing technique that shares a common wavelength between a set of optical network units (ONUs). TDM-PONs employ one wavelength for downstream side and another wavelength for upstream side. Several PON technologies such as Gigabit PON (GPON) and Ethernet PON (EPON), which are based on TDM and on-off-keying (OOK) modulation formats have been standardized by the ITU-T and the institute of electrical and electronics engineers (IEEE), respectively.

Furthermore, WDM technique has been presented as a solution, for higher data rate links, and at the same time supporting more users. WDM systems use wavelengths for multiple access to the shared optical infrastructure. They can provide dedicated wavelengths to each ONU corresponding to each user, establishing a point-to-point data link between the ONU and the OLT. In addition, it possesses benefits such as high flexibility in terms of protocol and transmission data rate. Although 10 Gbps ethernet PON (10GE-PON) and 10-Gigabit-capable PON (XG-PON) are still a solution by providing a single wavelength link, however, time and wavelength division multiplexing PON (TWDM-PON) is an alternative solution of the current TDMA of standard GPON for incoming access networks [21].

Generally, the intensity modulation/direct detection (IM/DD) systems are simples and offer low hardware cost and power consumption, which are critical for optical communications [13]. In IM/DD systems, photodiodes like PIN or avalanche photodiode (APD) with a trans-impedance amplifier (TIA) and good responsibility and sensitivity lead to envelop detection where all phase information is lost. The most applied modulation formats in IM/DD systems is OOK, also the higher order modulation beyond OOK such as 4-ary pulse-amplitude modulation (PAM-4) can be applied for higher bit rate [22]. PAM-4 is a new candidate for short reach and the direct detection systems which a lot of efforts also have been put nowadays in this modulation formats in order to increase the data rate using minimum requirements for electrical analog bandwidth. Basically, no DSP is involved in the IM/DD system. The IM/DD technology can be used for short reach applications, less than 100 km fiber and 100 Gbps. But when it employed for higher distance and higher data rate, faces some fundamental

impairments such as chromatic dispersion and discrete mode (DM) laser frequency chirp. Moreover, the receiver of direct detection technique is based on intensity function, and the information of the optical signal can only be encoded in one degree of freedom (DOF) per polarization, which provide poor SE. Extending this concept to a data rate and flexibility, ultra-dense wavelength division multiplexing (U-DWDM) PON based on coherent detection and both direct modulation and advanced modulation formats is the next unavoidable step and provides an opportunity [23], [24].

Optical coherent detection in short reach was introduced and demonstrated in 1980 [25]. The industrial version of Coherent U-DWDM PON technology emerged in 2009 by [26], proposing 1 Gbps per subscriber, by transmitting differential quadrature phase shift keying (DQPSK) modulation format. This has stemmed the study for the best compromise between performance and complexity using coherent U-DWDM PON network architecture. Several research groups have been studying several aspects of coherent U-DWDM PON networks such as optical modulation scheme [27], [28], pulse shaping [24], coexistence with other technologies in the market [29], [30], cost optimisation [31] and real-time signal processing [32]. Despite the tight technological requirements imposed by coherent transmission and reception, coherent U-DWDM offers a matured solution as well as meeting service requirements in terms of data rate, reach, energy consumption or dedicated and shared bandwidth, willing to become more competitive in the near future in terms of cost effectiveness [31]. For example in [29], a variable data rates from 150 Mbps to 10 Gbps and for up to 100 km distance and 1000 wavelengths was considered in a field trial demonstration. Besides new applications are reaching the user's premises such as television with augmented reality, which will request dedicated data rates up to approximately 10 Gbps per subscriber, opening the way for the deployment in the near future of Coherent U-DWDM PON technologies.

Generally, performance of the high baud rate optical coherent systems in the long-haul transmission link is reduced due to increasing CD and non-linearity. Recently the digital MSC multiplexing technique has been widely addressed in the long- haul optical networks. Specifically, in the MSC technique, the high baud rate single carrier is divided into closely spaced low baud rate subcarriers. With optimizing the symbol rate of subcarriers nonlinear propagation impairments is reduced. The MSC technique also enhances the robustness of the system against CD, which results efficiently improve the performance of optical systems, without increasing the number of transceivers, complexity and cost [33], [34], [35]. Therefore, combination of MSC technique with coherent detection is revealing to be an effective solution for the next-generation optical transmission systems [36].

In a nutshell, both coherent U-DWDM-PON and MSC technique have the similar structure. They are based on low baud rate signals. To support a high number of user, U-DWDM-PON can use several analogue carriers (optical lasers) with low bandwidth modulator and DAC or several digital carriers with high bandwidth modulator and DAC with only one analogue carrier. In the other side, MSC uses high bandwidth modulator and DAC with several digital carriers and one analogue carrier. U-DWDM-PON is implemented in optical metro and access networks for high number of user and lower bit rate per user, but MSC has application in long-haul to support more than 400 Gbps per line card. In that sense, it is necessary to identify the structure of both optical networks and implement a transmitter and a receiver based on dual polarization that can be flexible and can accommodate more than one modulation format in a smooth way.

2.2 Coherent Detection in Optical Networks

Optical coherent detection started writing its history in the mid 80's. Unlike direct detection systems, coherent detection with applying a local oscillator (LO) at the receiver as a reference, can recover full information of the optical field. It can exploit amplitude and phase of the light to carry information, which can provide a potential improvement in the receiver sensitivity [37]. Also, it can even access polarization states and allows to use different modulation formats such as phase shift keying (PSK), frequency shift keying (FSK), and QAM [38].

Although coherent receivers have access to full information of the signal and can restore in-phase and quadrature components and the state of the polarization, but also they are very sensitive to random variations in the phase and polarization of the incoming signal. Therefore, due to solving the issue related to the sensitive behaviour of coherent receivers, it would be clear that the configuration of coherent systems is more complicated than IM/DD systems [37].

Fig. 2.2 presents the fundamental concept of the coherent optical receiver, while SOPs of the transmitted signal and the LO assumed to be aligned. So the incoming optical signal can be written as [37]

$$E_S(t) = A_S(t)exp(j\omega_S t), \tag{2.1}$$

where $A_S(t)$ shows the complex amplitude of the incoming signal and ω_S is the angular frequency of the signal. Also, the electric field of the LO is

$$E_{LO}(t) = A_{LO}(t)exp(j\omega_{LO} t), \tag{2.2}$$

where $A_{LO}(t)$ represents the constant complex amplitude of the LO and ω_{LO} is the angular frequency of the LO signal. The complex amplitudes $A_S(t)$ is associated to the power of the signal P_S and $A_{LO}(t)$ is related to the LO powerP_{LO}, where $P_S = \frac{|A_S^2|}{2}$ and $P_{LO} = \frac{|A_{LO}^2|}{2}$.

The received signal in this configuration is combined with the LO signal by employing a 3-dB optical coupler, also called 180°, which results in 180° phase shift between two signals. After signal and LO are co-polarized, the electric fields E_1 and E_2 arrive on the upper and lower balanced photo-diodes and can be written as [37],

$$E_1 = \frac{1}{\sqrt{2}}(E_S + E_{LO}), \tag{2.3}$$

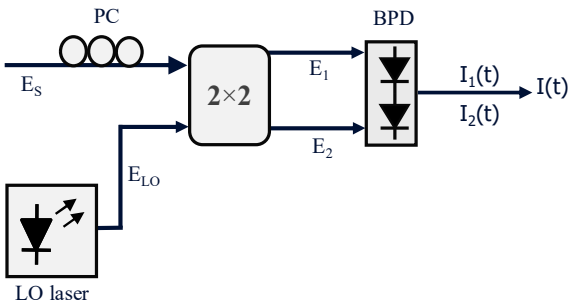

Figure 2.2: Fundamental concept of the coherent optical receiver. LO- local oscillator, PC- polarization controller, BPD- balanced photo-diode.

$$E_2 = \frac{1}{\sqrt{2}}(E_S - E_{LO}), \tag{2.4}$$

Then the output of photo-currents are given by

$$I_1 = \frac{R}{2}[P_S(t) + P_{LO} + 2\sqrt{P_S(t)P_{LO}}\cos(\omega_{IF}t + \theta_{Sig}(t) - \theta_{LO}(t))], \tag{2.5}$$

$$I_2 = \frac{R}{2}[P_S(t) + P_{LO} - 2\sqrt{P_S(t)P_{LO}}\cos(\omega_{IF}t + \theta_{Sig}(t) - \theta_{LO}(t))], \tag{2.6}$$

where ω_{IF} is given by $|\omega_S - \omega_{LO}|$, $\theta_{Sig}(t)$ and $\theta_{LO}(t)$ are the phases of the transmitted signal and the LO. In addition, R factor presents the responsitivity of the photo-diode, and is written as

$$R = \frac{e\eta}{\hbar\omega_S}, \tag{2.7}$$

where e is the electron charge, and η denotes the quantum efficiency of the photo-diode, and $\hbar$ shows Planck's constant. Finally, the output of the balanced photo-diode is written as

$$I_t = I_1(t) - I_2(t) = 2R\sqrt{P_S(t)P_{LO}}\cos(\omega_{IF}t + \theta_{Sig}(t) - \theta_{LO}(t))]. \tag{2.8}$$

Furthermore, it is worth to notice that only the beat between the signal and the LO is considered with balanced detection. The power of the LO is stable but the part of phases are randomly changed over the time [37].

2.2.1 Heterodyne Receivers

In the heterodyne detection the LO frequency, ω_{LO} is chosen to differ from the ω_S, in this case $|\omega_{IF}| \gg \omega_b/2$. Where ω_b is the modulation bandwidth of the optical carrier, which is determined by the symbol rate. As a consequence, $\omega_{IF} = (\omega_S - \omega_{LO})$. The signal phase is given as

$$\theta_s(t) = \theta_{Sig}(t) + \theta_{sn}(t), \tag{2.9}$$

where $\theta_s(t)$ denotes phase modulation and $\theta_{sn}(t)$ is the phase noise. The receiver output is given as

$$I(t) = 2R\sqrt{P_S(t)P_{LO}}\cos(\omega_{IF} + \theta_s(t) + \theta_n(t)). \tag{2.10}$$

The $\theta_n(t)$ is the total phase noise and can be written as

$$\theta_n(t) = \theta_{sn}(t) + \theta_{LO}(t), \tag{2.11}$$

The complex amplitude is written as

$$I_C(t) = R\sqrt{P_S(t)P_{LO}}exp[j(\theta_s(t) + \theta_n(t)], \tag{2.12}$$

In order to develop the heterodyne detected, the phase-locked loop (PLL) circuit at the IF stage is required. This electrical PLL circuit can remove the phase noise, which might be changed with time and also decode the symbol. Nowadays, heterodyne detection is considered as a potential solution for coherent WDM-PON and trades off receiver sensitivity for much greater simplicity of implementation. This receiver only needs automatic frequency control (AFC) of the local laser. Also, heterodyne comes at the cost of a 3-dB penalty over the respective homodyne (de-) modulation scheme [37].

2.2.2 Homodyne Receivers

The homodyne detection is a coherent detection technique, which corresponding to the case that the frequencies of the LO, ω_{LO} and incoming optical signal ω_S are directly extracted from the output of the photo-detector, in fact ω_{LO} is completely tuned with the received signal, therefore $\omega_{IF} = 0$. Herein, the receiver output is given as

$$I(t) = I_1(t) - I_2(t) = 2R\sqrt{P_S(t)P_{LO}}\cos\theta_{Sig}(t) - \theta_{LO}(t), \tag{2.13}$$

In order to decode the encoded data correctly, the optical phase-locked loop (OPLL) is needed, to lock the phase of the LO which can track frequency and phase of the received signal. Homodyne receivers offer 3 dB higher sensitivity, a simpler post-detection scheme and lower required receiver bandwidth comparing to heterodyne receivers. With looking to the previous equation, can be concluded that only the cosine component (the in-phase component with respect to the LO phase) is given. It shows that the quadrature component which comes from the sine component cannot be provided. This evidence proofs that extracting full information on the signal complex amplitude from this kind of homodyne receivers is not feasible.

The main motivation behind coherent detection during the 1980's was to improve the receiver sensitivity comparing with the direct-detection schemes, which was able to extend the transmission reach of lightwave communication links. However, coherent systems have been limited by high complexity and cost.

2.2.3 Phase Diversity Coherent Receivers

In order to detect both in-phase and quadrature components of complex signal in the homodyne receiver, another LO with 90° phase shifted using a 90° optical hybrid and also a 1:2 optical splitter to divide the signal into two paths are required. This kind of coherent receiver normally known as phase-diversity homodyne receiver or intradyne receiver [38].

Basically in the intradyne receivers, $\omega_{IF} \sim 0$ (typically <0.5 GHz). As the intermediate frequency ω_{IF} is close to zero, the exact phase of the signal after the ADC can be tracked in the digital domain and there is no need to employ an analog OPLL. Also, in intradyne detection, implementation of linear dispersion compensators (equalizers, digital filters) is feasible. Intradyne detection is now one of the most recent implementation of coherent receivers based on digital signal processing and attracts great attention. Digital intradyne detection is playing a great role in implementing both low and high baud rate signals (depend on application) and opens a new avenue for research on future ultra-high-speed and capacity transmission. Fig. 2.3 presents an architecture of a phase diversity coherent receivers. The electric fields incident on photodiodes are given as [39],

$$E_1 = \frac{1}{2}(E_S + E_{LO}), \tag{2.14}$$

$$E_2 = \frac{1}{2}(E_S - E_{LO}), \tag{2.15}$$

$$E_3 = \frac{1}{2}(E_S + jE_{LO}), \tag{2.16}$$

$$E_4 = \frac{1}{2}(E_S - jE_{LO}), \tag{2.17}$$

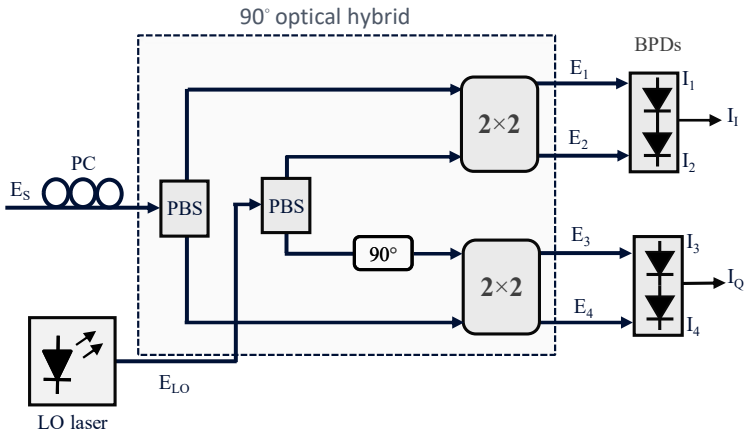

Figure 2.3: Schematic diagram of the phase-diversity homodyne receiver using a 90° optical hybrid. LO-local oscillator, PC- polarization controller, PBS- polarization beam splitter, BPD- balanced photo-diode.

and the output of photocurrents given by

$$I_I(t) = I_{I1}(t) - I_{I2}(t) = R\sqrt{P_S P_{LO}}\cos\left(\theta_{Sig}(t) - \theta_{LO}(t)\right), \tag{2.18}$$

$$I_Q(t) = I_{Q1}(t) - I_{Q2}(t) = R\sqrt{P_S(t) P_{LO}}\sin\left(\theta_{Sig}(t) - \theta_{LO}(t)\right). \tag{2.19}$$

The complex amplitude is written as

$$I_C(t) = I_I(t) + jI_Q(t) = R\sqrt{P_S(t) P_{LO}}exp[j(\theta_s(t) + \theta_n(t)], \tag{2.20}$$

where $\theta_n(t)$ is the total phase noise.

It is clear that using the heterodyne receiver also the full information on the optical signal can be detected. However, homodyne receiver has this advantage that can deliver the base-band signal directly after the photo-diode and it is more applicable compared to heterodyne receiver specially from a bandwidth point of view [39].

2.2.4 Polarization Diversity Coherent Receiver

Due to the random changes in the birefringence of the optical fibers, normally the polarization of a received signal is not aligned to the SOP of the LO. The difference between SOP of the incoming signal and LO effects on the receiver sensitivity. Polarization insensitive (PI) implementation of the receiver is one solution to control the SOP, but this approach can only apply to IM/DD technologies. One way to introduce PI to the coherent receiver is by implementing a polarization diversity (PD) scheme, which allows to separately recover the signal being split into both receiver polarizations. Therefore, two phase-diversity homodyne receivers are combined with the polarization diversity configuration, this configuration is known mostly as a full coherent detection system.

Full dual-polarization coherent receivers (homodyne and heterodyne detection) can support advanced modulation formats [37]. It allows accessing the full optical field of both polarizations. Although, this configuration provides very good spectral efficiency but it brings complexity. As Fig. 2.4 demonstrates, full coherent is based on two polarization beam splitter (PBS),

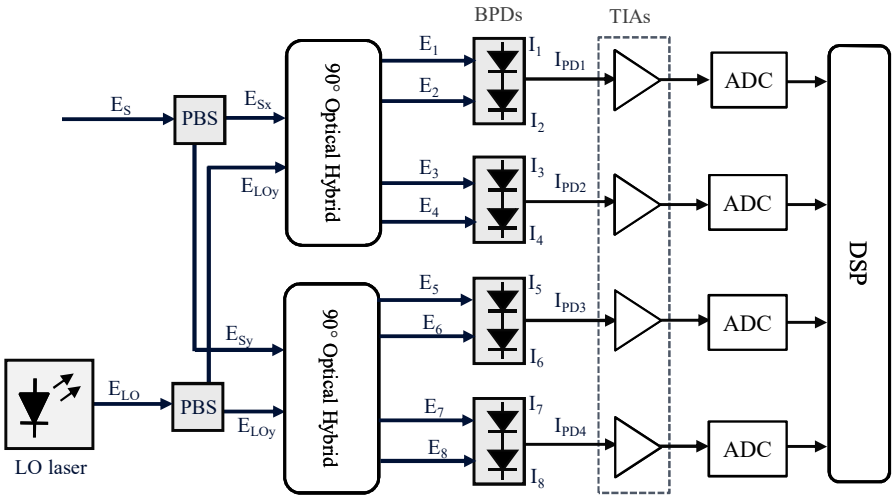

Figure 2.4: Configuration of full dual-polarization coherent receiver employing phase and polarization diversities. LO- local oscillator, PC- polarization controller, PBS- polarization beam splitter, BPD- balanced photo-diode, TIA- transmittance amplifier, ADC- analog-to-digital converter.

which split both incoming dual-polarization signal and LO into two orthogonal polarizations. Then in order to generate an in-phase and quadrature components for each polarization, two 90° optical hybrids are applied. Afterword, four signals are digitized using ADCs, then DSP is employed for signal demonstration. Of course, it can be used for OOK format, without DSP but with heterodyne detection and using RF multiplayer.

The received signal E_S, which has an arbitrary state of polarization, will be divided into two linear polarization components by a PBS. The $x-$ and $y-$polarization components after PBS can be given by [39],

$$\begin{bmatrix} E_{Sx} \\ E_{Sy} \end{bmatrix} = \begin{bmatrix} \sqrt{\alpha} A_S e^{j\delta} \\ \sqrt{1-\alpha} A_S \end{bmatrix} \exp(j\omega_s t), \tag{2.21}$$

where α denotes the power ratio of the two polarization components and δ the phase difference between polarizations. In addition, the $x-$ and $y-$polarization components, which are equally separated from the linearly polarized LO are given as [39],

$$\begin{bmatrix} E_{LOx} \\ E_{LOy} \end{bmatrix} = \frac{1}{\sqrt{2}} \begin{bmatrix} A_{LO} \\ A_{LO} \end{bmatrix} \exp(j\omega_{LO} t), \tag{2.22}$$

two 90° optical hybrids in Fig. 2.4 generate electric fields as

$$E_{1,2} = \frac{1}{2}(E_{Sx} \pm \frac{1}{\sqrt{2}} E_{LO}), \tag{2.23}$$

$$E_{3,4} = \frac{1}{2}(E_{Sx} \pm \frac{j}{\sqrt{2}} E_{LO}), \tag{2.24}$$

$$E_{5,6} = \frac{1}{2}(E_{Sy} \pm \frac{1}{\sqrt{2}} E_{LO}), \tag{2.25}$$

$$E_{7,8} = \frac{1}{2}(E_{Sy} \pm \frac{j}{\sqrt{2}} E_{LO}), \tag{2.26}$$

where E_{Sx} and E_{Sy} are the two-orthogonal received electric fields which were divided by PBS, corresponding to x and y polarization, and E_{LO} is the electric field of the local oscillator. The output of photocurrents are

$$I_{PD1}(t) = R\sqrt{\frac{\alpha P_S P_{LO}}{2}}\cos(\theta_S(t) - \theta_{LO}(t) + \delta), \tag{2.27}$$

$$I_{PD2}(t) = R\sqrt{\frac{\alpha P_S P_{LO}}{2}}\sin(\theta_S(t) - \theta_{LO}(t) + \delta), \tag{2.28}$$

$$I_{PD3}(t) = R\sqrt{\frac{1-\alpha P_S P_{LO}}{2}}\cos(\theta_S(t) - \theta_{LO}(t)), \tag{2.29}$$

$$I_{PD4}(t) = R\sqrt{\frac{1-\alpha P_S P_{LO}}{2}}\sin(\theta_S(t) - \theta_{LO}(t)), \tag{2.30}$$

where R is the photodiode responsibility, α is the power ratio between the two components of polarization, δ is the difference between respective phases, $\theta_S(t)$ and $\theta_{LO}(t)$ are phases of both signals. Then, the receiver can measure the complex amplitudes of two polarizations as

$$I_x(t) = I_{PD1}(t) + jI_{PD2}(t), \tag{2.31}$$

$$I_y(t) = I_{PD3}(t) + jI_{PD4}(t), \tag{2.32}$$

and finally, the output signals in two polarizations are

$$E_x(t) = I_x(t) + jQ_x(t), \tag{2.33}$$

$$E_y(t) = I_y(t) + jQ_y(t), \tag{2.34}$$

It is worth to notice that full coherent detection essentially doubles the cost of the receiver optics and additionally requires a hybrid integrated PBS, therefore cost for such a solution could be rather high. In this regard, some works investigated the polarization-independent coherent receivers [40], [41], [42], [43], [44]. Recently a PI coherent receiver for OOK modulation format, consisting of a PBS on the LO or on the incoming signal, a symmetric 3×3 optical coupler and three photodiodes has been proposed in COCONUT project [41].

2.2.5 Advanced Modulation Formats

Although OOK modulation format (non-return-to-zero (NRZ) or return to zero (RZ)) have been much-used format in direct-detection systems, there is a big gap for future optical networks, because of low spectral efficiency. Therefore, migration from traditional OOK formats to higher-order modulation with more bits per symbol, which provide higher symbol rates and higher capacity are required. Binary phase shift keying (BPSK) is the simplest form of PSK, which basically modulate at 1 bit per symbol. It applies two phases, divided by 180 degrees, compared to OOK that can be detected without the need for phase reference, and also offers 3 dB higher sensitivity [45], [46]. However, since coherent systems have access to all information of the optical field such as amplitude, phase, and polarization, give them

the possibility to employ high-order modulation formats. On the other hand in coherent systems, complex optical domain subsystems like polarization and phase-tracking, can be moved to the digital domain [47]. Meanwhile, coherent systems with enabling modulation in both I and Q components can usually employ multilevel modulation formats. Quadrature phase-shift keying (QPSK) is one of the multilevel modulation formats that has a four-point constellation differ in phase by $\pi/2$, and enabling the coding of two bits per symbol. The QPSK signal doubles the data rate while keeping the same bandwidth. Furthermore, with applying DP-QPSK, the spectral efficiency of the system can be doubled. The DP-QPSK is the most popular modulation format in the coherent systems due to its simplicity of implementation and good spectral efficiency. Moreover, since this modulation format can provide high power efficiency, can be employed in long-haul transmission systems [48].

In addition, Quadrature Amplitude Modulation (QAM) with employing both amplitude and phase components can present a high level of spectral efficiency, also it can adopted to coherent systems. In a QAM signal, two carriers shifted in phase by 90 degrees, yields In-phase or I signal, and the quadrature or Q signal. Since QAM formats can supports more bit per symbol, they can increase the efficiency of the system. Nevertheless, it is worth to notice that when higher order of the QAM are used, the probability of error may be enhanced, since the distance between the points in the constellation diagram will decrease. The most popular QAM formats in the coherent systems include 16QAM, 32QAM, 64QAM, and 128QAM. The 16-ary QAM , normally refers to the square implementation of the 16QAM, meanwhile other implementation of 16QAM exist like star-QAM, hexagonal 16QAM [49], [50]. In the 16QAM, four bits are represented by one symbol and each symbol is encoded by the Gray code, with the purpose of reducing the bit error. Meanwhile, the system performance and spectral efficiency can be double by using dual-polarization format [49], [51]. Fig. 2.5, presents constellation diagrams of OOK, BPSK, QPSK, 16QAM, 32QAM, and 64QAM modulation formats.

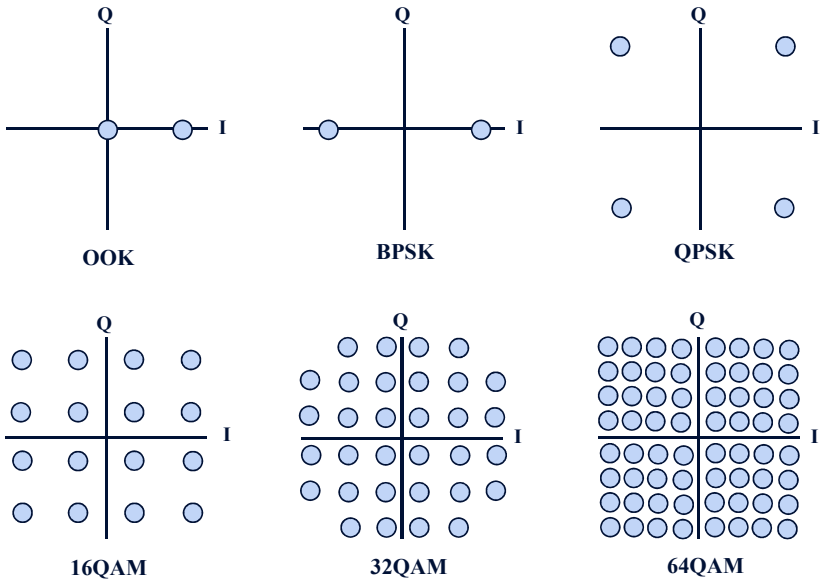

Figure 2.5: Constellation diagrams of various modulation formats.

2.2.6 Digital Signal Processing for the Coherent Receivers

The capacity of the optical systems can be enhanced by employing coherent detection technology together with powerful DSP [52]. A low complexity DSP, with enabling receivers to compensate time varying transmission impairments of advanced modulation format signals in the digital domain and employing advanced forward-error-correction codes, plays an important role in increasing system capacity. DSP techniques have some benefits comparing to the optical control methods, such as adaptive signal equalization and fast control response.

In a fully coherent system, after ADC units, which convert the analog current into the digital domain, the digital samples are fed into a DSP, in order to recover the transmitted symbols from the distorted received samples [47]. It applies many algorithms in the digital domain, such as phase and polarization tracking, thus some complex optical hardware implementation, such as the OPLL circuit are not required. Meanwhile, it enables to compensate and mitigate impairments arising due to fiber transmission. By employing suitable and accurate equalization algorithms, both linear and nonlinear impairments can be partially removed in the digital domain [53], [54], [55].

A structure of DSP subsystems of a full coherent receiver is shown in Fig. 2.6. The digitized I and Q components in both polarizations, I_x, Q_x, I_y and Q_y are fed to a DSP with several subsequence blocks. Digitized signals will be compensated against optical front-end faults, in the pre-processing stage. Afterward, fiber transmission impairments including linear and nonlinear impairments are compensated in the channel equalization block. Then the information of the incoming samples, such as timing, frequency and phase, will be adjusted in the clock and carrier recovery blocks. And finally, symbol identification and decoding will be applied in the last stage. In the following subsections, we briefly describe DSP algorithms that can be applied for compensating of the impairments in the optical fiber coherent communication systems.

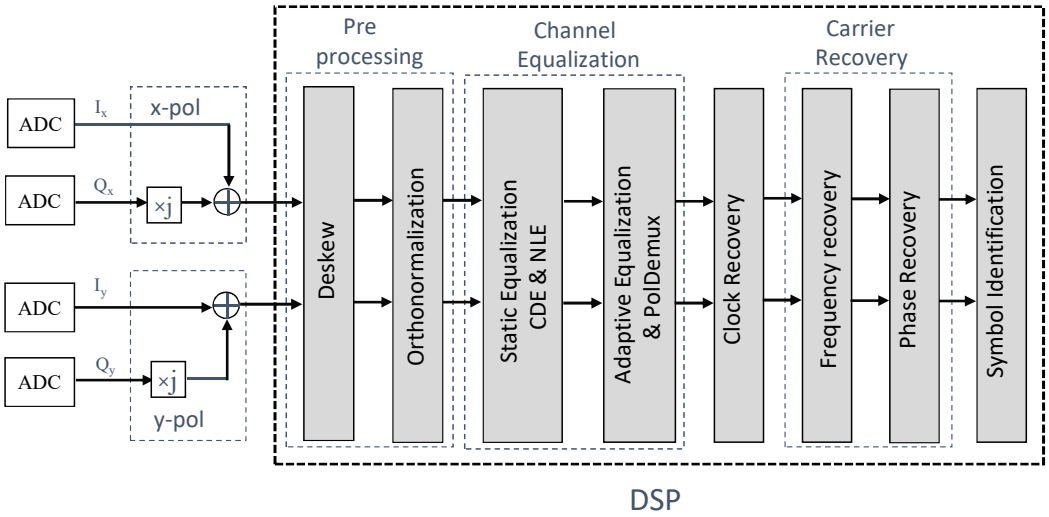

Figure 2.6: Post-detection digital signal processing subsystems employed by full coherent optical receiver.

2.2.6.1 Deskew and Orthogonalization

The I_x, Q_x, I_y, and Q_y signals, during modulation and demodulation travel in various optical paths, which may have different signal path lengths inside the receiver, therefore different delays may appear between them, which results in a time skew. In fact, this temporal misalignment occurs due to optical path dissension between the quadratures of each polarization tributary.

This timing mismatches can be digitally compensated using a deskew algorithm, which proposed and experimentally demonstrated in [56] to relax the skew requirement on coherent front-end. In addition, a blind adaptive 4×4 multiple-input multiple-output (MIMO) equalizer, with the possibility to compensate in-phase and quadrature timing skew up to half of the symbol period in the presence of Nyquist filtering, was demonstrated in [57]. Meanwhile, in [58], a novel adaptive finite-impulse-response (FIR) filter configuration, which allows adjusting any imbalance between the I and Q channels in the coherent optical receivers, was suggested.

On the other hand, quadrature imbalance also may cause by imperfections of the optical hybrid and responsivity mismatch between the balanced photodiode in the coherent systems, resulting in I and Q output signals if the 90° optical hybrids lose their orthogonality [59]. The detrimental effect of quadrature imbalance must be estimated and corrected by orthonormalization methods such as the widely used Gram-Schmidt algorithm [60]. Also, adaptive compensation of the quadrature imbalance can also be applied by CMA [59].

This kind of imperfection must clearly be compensated since it may have an effect on the next DSP stages, which resulting degradation of the system performance and capacity of the communication systems.

2.2.6.2 Static Equalization

The optical signal in the fiber may be distorted from some impairments which limit optical transmission distance and capacity. In fact, linear and nonlinear impairments are appeared during signal propagation and can destroy the received signal. These impairments can be partially removed and compensated in the digital domain. The static equalization stage is employed in the DSP in order to remove deterministic effects, such as chromatic dispersion (CD) and also nonlinear impairments (NI).

The CD is one of the most important linear impairments. It is mainly due to the changing the refractive index of the fiber core, which consequently different wavelengths of light have different speeds, therefore, each wavelength arrives in the receiver at different times [61]. Due to the statistic behaviour of CD, linear filtering can be implemented with the inverse transfer function of the fiber. In practice, CD equalizer (CDE), can be implemented in time-domain using FIR and infinite impulse response (IIR) filters or in frequency-domain, by reversing the CD transfer function [47], [62], [63]. In the time-domain implementation, the Wiener filter theory is used as a common solution to achieve the optimum FIR filter coefficients [53]. However, the static equalizer can also be implemented in frequency-domain, this implementation of the CDE is more computationally effective than static equalizer in time-domain. Specially for a link with large channel memory, it is a very effective solution in terms of complexity [64].

Some data-aided and blind adaptive CD equalization approaches have been introduced in the last few years. The most related methods are data-aided time-domain least mean square (LMS) adaptive filters [65], frequency-domain equalization with blind time-domain

adaptation [66] and blind frequency-domain estimation and compensation [67]. Also [68] suggested that for the small amount of accumulated dispersion, the time domain method is practical, but in the case that the transmission distance increased and consequently the amount of accumulated dispersion is also increased, the frequency domain method is desired [68].

On the other hand, nonlinear impairments in the optical fiber rise with increasing data rates, reach, the number of wavelengths and higher optical power. These impairments in the optical network must be considered as a critical issue due to the system degradation, since long haul systems apply high power lasers to transmit optical pulses over long spans in order to overcome attenuation. Inter-channel nonlinear effects in WDM systems are generated by the nonlinear coupling of signal frequency components which were placed inside the bandwidth of the WDM channel [69]. Additionally, nonlinear impairments in fibers, may also occur due to change in the refractive index of the medium. The power dependence of the refractive index is responsible for the Kerr-effect [69]. In fact, intra-channel nonlinear impairments arise due to its high launched power and are the effect of the interaction of signal pulses within a single channel. It is worth to notice, higher optical power causes the optical signal propagation in the nonlinear regime and resulting signal to noise ratio (SNR) degradation base on Shannon‘s limit [70]. The most known nonlinear impairments include self-phase modulation (SPM), cross-phase modulation (XPM) and four-wave mixing (FWM).

Applying nonlinear compensation in coherent systems can significantly increase the fundamental capacity limit of fiber transmission. Nonlinear equalization (NLE) technique to predict and equalize nonlinear effects is an active and important research topic in the optical community [71]. In this regard, the nonlinear Schrodinger equation (NLSE) is a well known nonlinear partial differential equation (PDE), which characterizes the evolution of the electric field in the optical fiber. Meanwhile, the digital backward propagation (DBP) with employing the split-step Fourier (SSF) method is used to simulate nonlinear transmission in optical fibers [72].

It is the most common algorithm for solving the NLSE and analyzing the signal propagation in the fiber due to its easy implementation and speed compared to other methods. In contrast to the DBP method, a frequency-domain Volterra series transfer function (VSTF) is another potential numerical method to solve scalar NLSE [73], [74], although its performance is limited by its computational complexity.

2.2.6.3 Adaptive Equalization

As previously mentioned, the full coherent receiver with applying polarization diversity structure can detect the complex signal of each polarization. Normally in an ideal standard single-mode (SSM) fiber with perfect cylindrical symmetry, both orthogonal polarization modes have the same refractive indexes, and both components move with the same velocity over fixed polarization axes. But in practice, real fiber exhibits some residual modal birefringence, which causes a propagation constant mismatch between the two polarization axes. As a consequence, the modal birefringence and the orientation of the respective polarization axes tend to change randomly along the fiber length, causing polarization-dependent effects such as polarization mode dispersion (PMD) and polarization-dependent loss (PDL) [75], [76]. Indeed, PMD is a form of a dispersion in the fiber because of unequal velocities of two orthogonal SOP, which causes dispersion of the optical pulse.

The dynamic equalization stage is employed in the DSP, to compensate for time-varying transmission impairments such as PMD and polarization crosstalk. It is also used to remove

residual amounts of the deterministic effect that may have not been compensated by the static equalization stage. For dual-polarization transmission systems, polarization demultiplexing (PolDemux) can also be implemented within this stage, in order to separate the two incoming polarization. As shown in Fig. 2.7, this stage includes two main parts, the filtering part and adaptive algorithm. The filtering part includes 4 FIR filters, which are connected in a butterfly structure and taps weights of each FIR filter are updated dynamically using an adaptation algorithm. One of the most popular and practical adaptive equalization algorithm is the CMA, which uses constant modulus characteristic of the phase-modulated signal to compensate distortions by finding the point that cost function is minimum.

The adaptive equalizer can be either applied with data-aided methods such as LMS method or using fully blind methods, like the CMA. The CMA is one of the most popular techniques to perform blind equalization and digital signal PolDemux in optical communications because of its simplicity, robustness, and immunity to phase noise [77], [78]. Meanwhile, for multi-level modulation formats such as 16QAM, radius directed equalizer (RDE) and the decision directed least mean square (DD-LMS) algorithms have been introduced to enhance equalizer performance [79]. Also recently, a three-dimensional (3-D) Stokes space-based PolDemux technique was proposed as a low complexity and format transparent algorithm [80], which is the main topic of this thesis and will be more discussed in the next chapter.

2.2.6.4 Clock Recovery

Typically, in a coherent system, since there is no direct synchronization between transmitters and receivers and because of some imperfections in ADCs, there is always some differences between the received data clock and the ADC sampling rate. Therefore, in a DSP subsystem, a clock recovery algorithm is required in order to recover the transmitter clock and apply symbol decision at proper sampling instants.

The clock recovery stage includes two parts: timing error detector (TED) and signal equalization. TED is corresponding to determine the error between the transmitter and

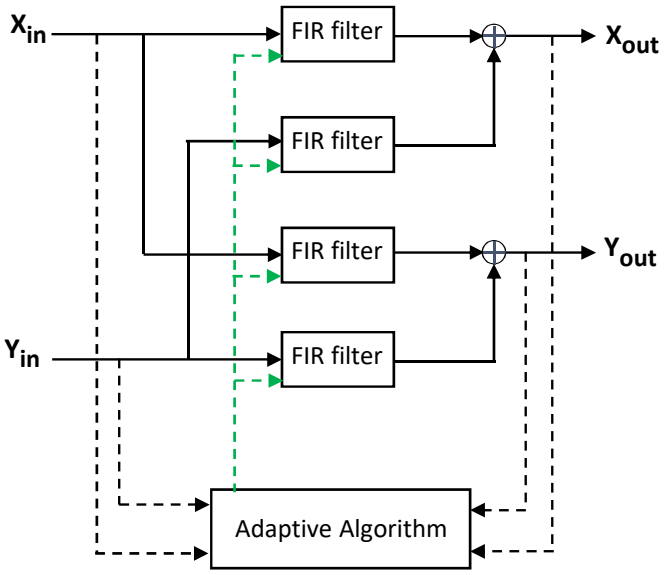

Figure 2.7: Main structure of an adaptive equalization with 4 FIR filters.

receiver clocks. Signal equalization matches the sampling instant of the received signal to the instant. Some algorithms have been proposed for estimating the timing error, such as Gardner, early-late gate, and Mueller and Muller algorithms [81], [82]. Recovering of the clock is performed by re-interpolating the signal according to a time basis of a timing error detection method. The Gardner algorithm is the most commonly used timing error detector, because of its high performance and simplicity [81], [83]. This stage can be located in different parts of the DSP subsystem. Also, it is worth to notice that the clock recovery stage is used for real-time scenarios since the transmitter and receiver are not synchronized by hardware and data are taken over hours. In the optical laboratory and in the case of offline experiments, clocks of transmitter and receiver are locked by hardware, usually with a using direct cable between them.

2.2.6.5 Carrier Recovery

In intradyne receiver and free-running laser as the LO, normally a frequency offset between the transmitter laser and the LO exists. This frequency offset is down-converted the received signal to an intermediate frequency ω_{IF}, instead of the base-band, which results in a complex rotation of the received signal constellation. The intermediate frequency is given by $\omega_{IF} = (\omega_S - \omega_{LO})$, where ω_S and ω_{LO} are angular frequencies of the signal and LO respectively. In addition, the transmitter and the LO lasers have phase noise, which is often due to non-zero lasers linewidth and is related to the time that phase of the laser is stable. Thus, the digital carrier recovery stage in the DSP is needed to estimate and compensate the residual intermediate frequency and laser phase noise from the received signal.

Carrier recovery includes two independent blocks, frequency recovery and phase recovery. The frequency recovery block aims to estimate the frequency offset between the optical received signal and the LO and to transfer the received signal into the baseband. The two most well-known classification methods for frequency estimation are differential phase methods based on Viterbi and Viterbi algorithm and spectral methods. Differential phase methods are implemented in the time domain, then each symbol is measured with its former, allowing to estimate the frequency shift between two consecutive symbols [84]. Spectral methods employ a Fourier transform of the signal over some time slot to estimate the frequency offset [85]. Herein, estimation is performed by applying a M^{th} power non-linearity and then detecting the maximum power in the Fourier transform of the recovered signal. The differential phase methods based on the Viterbi and Viterbi algorithm is a very common method for frequency estimation, due to providing efficient processing procedure and hardware-efficient solution, which also prevents the frequency-time domain transitions.

Carrier phase estimation is employed in the DSP to average out phase noise due to the varying relative phase of the transmitter and LO lasers, because of their non-zero laser linewidth. Some feed-forward and feed-backward algorithms have been widely considered to estimate and eliminate the phase noise[51, 86]. The feed-forward Viterbi and Viterbi algorithm is considered as a common solution for phase offset recovery [86]. Blind phase search (BPS) is another well-know carrier phase estimation method, which can present good laser linewidth tolerance and can provide parallel implementation [51]. Although Viterbi and Viterbi algorithm provides good performance for QPSK format, it is challenging to adapt it for advanced modulation formats, since some constellation points may be discarded. There are some modification of this algorithm that can support high level modulation formats [87]. Furthermore, the decision-directed digital phase-locked loop (DD-PLL) algorithm is a suitable

solution for a wide range of MQAM formats [88].

2.2.6.6 Symbol Identification and Decoding

Finally, after clock recovery and carrier phase estimation, the received symbols stream is forwarded to the symbol demapping and decoding block to retrieve the transmitted symbols. Then the forward error correction (FEC) is required, which is able to decrease the probability of error at the cost of some bit overhead. In fact, FEC is a process for controlling errors, by encoding the signal with extra error detection and correction overhead information. Typically there are two major categories of FEC, hard-decision FEC of 3.8×10^{-3} (with 7% overhead) and the soft-decision FEC of 1.5×10^{-2} (around 20% overhead) [89], [90]. In the hard-decision FEC, a firm decision is made based on the incoming signal and provides a single bit of information, a 1 or a 0. While the soft-decision FEC utilizes additional data bits and presents a confidence factor indicating how far the signal is above or below the threshold crossing. Although implementing the FEC, allows to reduce the error probability, but due to the redundant bits added to the original signal, complexity and power consumption may be increased.

2.3 Laboratory Facilities

In this section two important laboratory-based setups, which were improved and used in this thesis, as optical fiber recirculating loop test-bed and a laboratory-based free-space optical communication system will be described.

2.3.1 Recirculating Loop

Beside metro and access networks, in recent years, investigating and studying long haul communication systems in order to develop both transoceanic and terrestrial communication system, has a great interest. However, establishing such a long transition system is very expensive. A recirculating loop is an instrument in the optical laboratories for simulating and analyzing long-distance optical transmission systems [91]. This technique was developed for evaluating the transmission performance of both ultra-long reach submarine systems and terrestrial fiber-optic systems without actually using many spans of fibers and a large number of optical amplifiers [92]. However, the capacity and reach of optical fiber can be limited by some impairments such as CD and PMD as linear effects and SPM as nonlinear effects. In this regard, applying a digital nonlinear equalizer technique is crustal to eliminate impacts of the nonlinearity in long transmission systems, which has been commonly implemented through digital backward propagation split-step Fourier method [93], [94].

In this subsection, we present implementation details for the recirculating loop technique and discuss experimental issues related to this technique. In addition, by considering a nonlinear compensation method, we demonstrate the result of transmitted 100 Gbps DP-QPSK signal over 8000 km of SSM fiber, by keeping the bit error ratio (BER) below the FEC threshold.

2.3.1.1 Timing management in the Loop

A fiber-optic recirculating loop is implemented in the optical communication laboratories in order to emulate the transmission performance of a long-haul system by reusing an optical

data signal through a modest length amplifier chain. It uses several erbium-doped fiber amplifier (EDFA)s after each span of fiber and applies a controlled optical switch which allows the optical signal from a transmitter to pass through an optical system many times [91]. Two controlled optical switches are applied for recirculating technique, in which the timing management of these optical switches must be taken into account. The switching states and timing control of these two optical switches are shown in detail in Fig. 2.8 and Fig. 2.9.

In order to describe the recirculating loop operation, it is useful to define the loop time. The loop time or roundtrip time is the time that the optical signal takes to travel through the fiber spans within the loop, being defined as $\tau = nL/c$, where n is the refractive index of the fiber, L is the length of the fiber and c is the speed of light [91], [92]. In this regard, the repetition rates of the optical switches must be a function of the loop time. The number of signal recirculation within the optical loop is controlled by three electrical signals, corresponding to the following three fundamental operation states:

1. Loading state: In this state two switches are held in loading condition for at least one loop time. Therefore this allows the optical signal to fill up the entire transmission

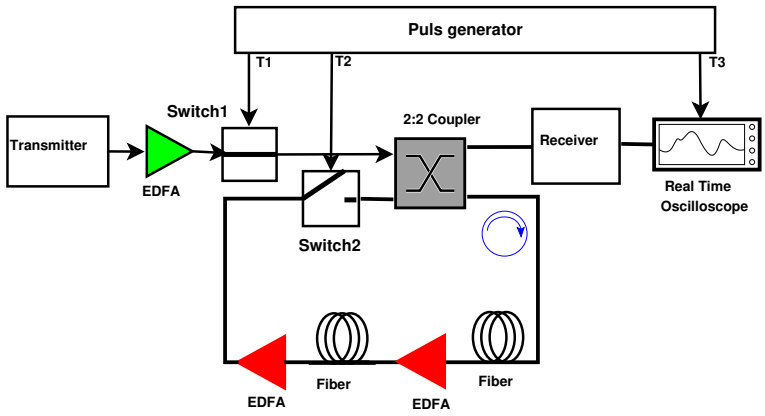

a)

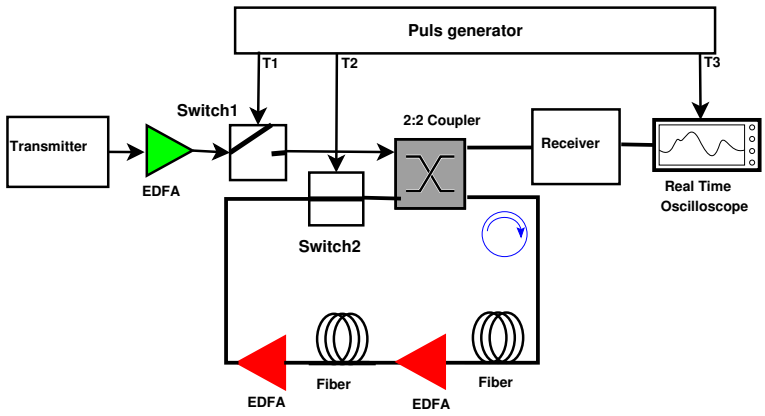

b)

Figure 2.8: Two states of controlled optical switch setting: a) loading state, b) looping state.

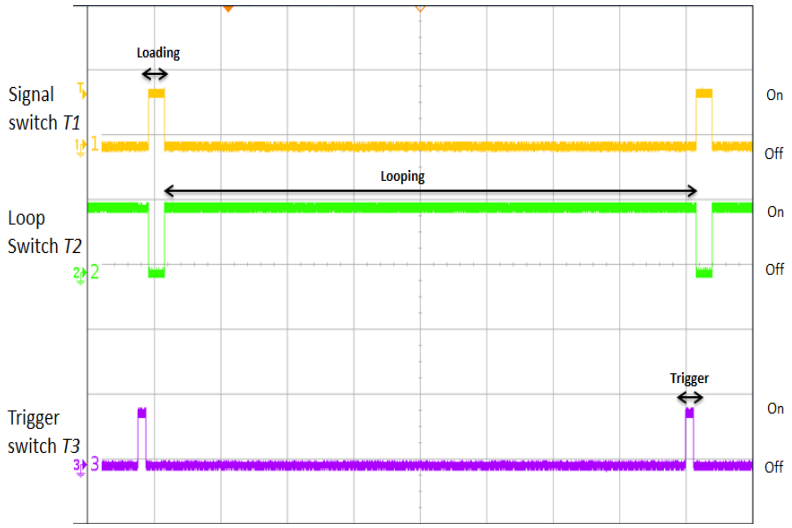

Figure 2.9: Timing control diagram for recirculating loop experiment. Time unit is normalized by loop time τ.

system through the signal switch-1 and the fiber coupler. In the loading state, the control pulse T1 is in the high level to turn on the signal switch and T2 should be in the low level to turn off the loop switch, as can be seen in Fig. 2.8 (a) .

2. Looping state: This state may start when the loop is fully loaded with the optical signal. In this state, T1 is in the low level to turn off the signal switch, whereas T2 is in the high level to turn on the loop switch, it can be observed in Fig. 2.8 (b). Then, the optical signal is allowed to circulate in the loop for a specified number of revolutions. The duration of a looping state can be estimated by $\triangle T = \tau \times N$, where N is the loop number and τ is the roundtrip time for each loop.

3. Trigger time: After each loop, a portion of the optical signal is coupled to the receiver with the 2×2 coupler. The BER for each loop is measured only at the end of the looping state. With tuning the pulse generator, T3 is created to deliver to the oscilloscope only during the BERT gating time window.

In this loop experiment, we use a two-span fiber-optic system with 80 km of optical fiber in each span (160 km in total), so that the roundtrip time for each loop is given by

$$\tau = \frac{n \times L}{c} = \frac{1.5 \times 160 \times 10^3}{3 \times 10^8} = 800 \ \mu\text{s},$$

where n=1.5 is refractive index in the fiber. In order to guarantee that the optical signal is fully loaded into the loop, the time window of loading state should be between 800 μs and 1600 μs. In this test we set the loading time to

$$\triangle t_1 = 1200 \ \mu\text{s}.$$

The time window of looping time depends on the number of loops, for example for 50 loops it equals to

$$\triangle t_2 = \tau \times N = 800 \times 50 = 40000 \ \mu\text{s}.$$

The switch repetition period can be chosen as

$$\triangle t = \triangle t_1 + \triangle t_2 = 41200\ \mu\text{s}.$$

The trigger time, is the time that information can be captured by the oscilloscope. This time should be after loading state and during the looping state, in the desired length. In trigger time, the margin of 100 μs should be used due to the rise and fall time of the signal and loop switches

$$\triangle t_3 = \tau - 100\mu s - 100\mu s = 600\ \mu\text{s}.$$

In fact, the captured data is obtained over a time-window that is much shorter than the roundtrip time.

2.3.1.2 Optical Gain Adjustment in the Loop

In long-haul transmission systems, power managing is one of the essential issues that must be considered. In this case for system stability consideration, it is necessary to adjust optical gain. In order to overcome the loss of optical fibers and other optical components, optical amplifiers are crucial components in long-distance transmission systems. In the recirculating loop technique an optical signal travels through the loop for a number of circulations and the input power of each loop must be equal. Therefore optical amplifiers in the loop have the responsibility to adjust optical gain in order to exactly compensate for the losses in the system, including coupling losses and fiber attenuation.

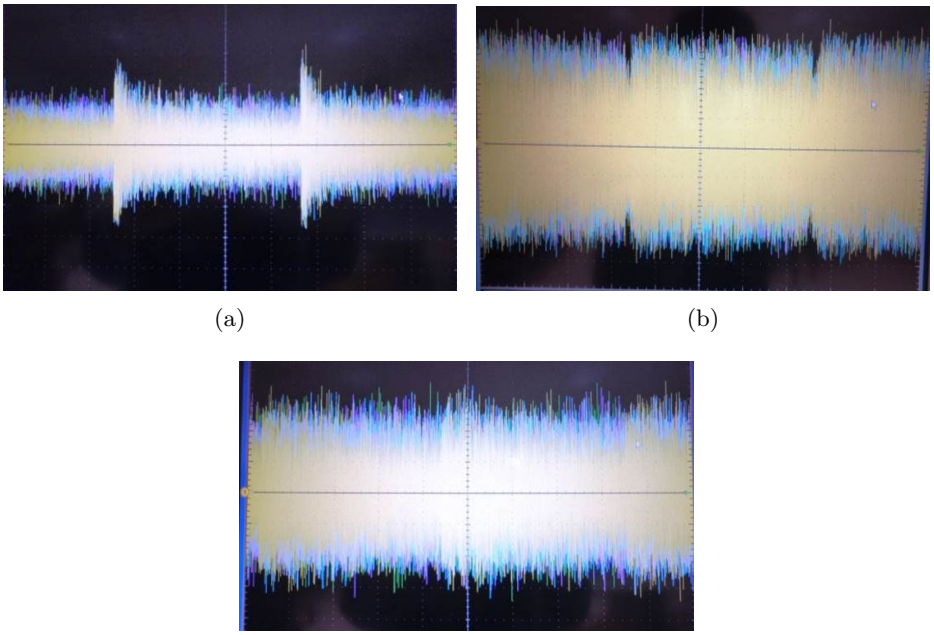

(a) (b)

(c)

Figure 2.10: Optical gain adjustment for a) loop gain smaller than unity, b) loop gain higher than unity, c) loop gain exactly compensates the losses.

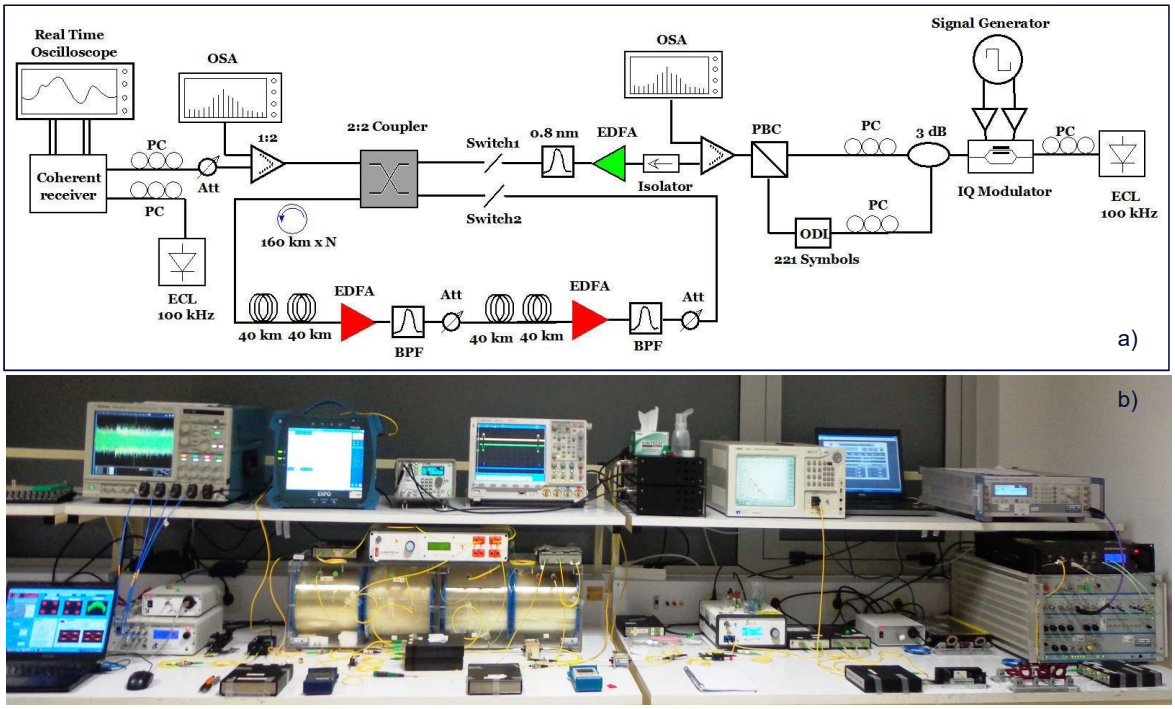

Figure 2.11: a) Diagram of the experimental setup for long haul transmission using the recirculating loop. ECL: external cavity laser, PC: polarization controller, PBC: polarization beam combiner, ODL: optical delay line, OSA: optical spectrum analyzer, EDFA- erbium doped fiber amplifier, BPF: band pass filter, Att: attenuator. b) Developed setup for long haul transmission using the recirculating loop in the optical laboratory.

In the recirculating loop, an EDFA is used after each span in order to compensate the fiber loss. Also a variable optical attenuator (VOA) is added after each EDFA for adjusting the loop gain. As we have DP-QPSK, an easy way to adjust the loop gain is to use balanced detector electrical output inside the coherent receiver, which is connected directly to the oscilloscope. If the gain of each loop is smaller than the accumulated losses, the electrical signal displayed on the oscilloscope decreases with each consecutive loop circulation, as shown in Fig. 2.10(a). Also if the gain of each loop is higher than the accumulated losses, the waveform on the oscilloscope will increase, as shown in Fig. 2.10(b). The correct gain calibration is obtained when there is no optical power change from one loop circulation to the next loop, which the optical gain exactly compensates for the loss, as shown in Fig. 2.10(c).

2.3.1.3 Experimental Setup and Results

The proposed experimental setup for recirculating loop technique is presented in Fig. 2.11 (a). At the transmitter side, the light from a 100 kHz linewidth external cavity laser (ECL) was fed to the QPSK modulator, which was driven by a BPG 121000B, producing a 25 Gbaud QPSK signal ($2^{15} - 1$ pseudo random binary sequence (PRBS)) in continuous mode operation. The signal was modulated by an IQ modulator and then it must be separated into two polarizations. In this case, we can use an optical delay line (ODL), (221 symbols delayed) for decorrelation purposes and multiplex in polarization to have a dual-polarization 100 Gbps DP-QPSK signal. This ODL enables to decorrelate the information contained in the X and Y

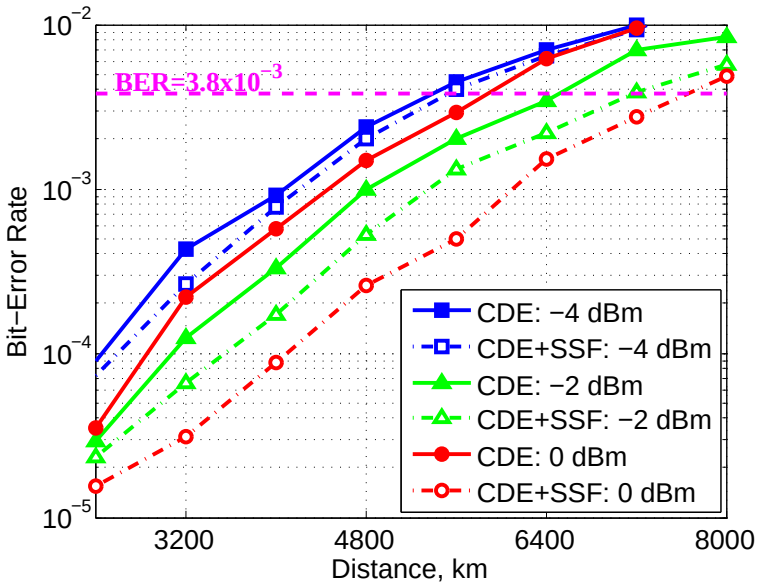

Figure 2.12: Measured BER for -4 dBm, -2 dBm, 0 dBm optical powers versus different distance; CDE+SSF: CDE includes nonlinear equalizer, with applying BP-SSF method.

polarization. After passing the signal into one coupler and an optical isolator, the launch power in recirculating loop was set by an EDFA and a VOA prior to the optical switch (Gooch and Housego acousto-optic modulator: 26027-2-1.55-LTD-FO) driven by a digital driver (NEOS N21027-1DS) and controlled by a pulse/delay generator (BNC 575).

The modulated signal was passed through the first switch and splits into two parts by a 2×2 coupler. One output from the coupler is sent to the coherent receiver and the other output is sent to a recirculating loop consisting of four 40 km SSM fiber spans with 16.75-ps/nm/km dispersion. The average span loss for each two 40 km series span was 16 dB that was amplified by EDFA. After each EDFA one band pass filter (BPF) with 100 GHz bandwidth was used to remove the out-of-band amplified spontaneous emission (ASE) noise from the amplifiers. The signal launch power in each span was controlled with VOA after BPF. At the receiver side, the DP-QPSK signal is coherently detected with the ECL local oscillator (linewidth < 100 kHz) using a 90° optical hybrid. The electrical signals after balanced photodetectors were converted to a digital form using a 50 GSa/s real-time oscilloscope with analog bandwidth around 20 GHz (Tektronix DPO72004B). After the coherent receiver, the 100 Gbps signal was processed offline using MATLAB and included. Moreover, BER evaluation was performed by direct error counting over 2^{17} bits. The real scenario for implementing a long haul transmission system using a recirculating loop in the optical laboratory can be also shown in Fig. 2.11 (b).

We assessed the performance of the transmission system with BER measurement, by studying the effect of power per channel versus different distance. The DSP includes CDE with/without nonlinear equalizer. For this study, we apply the back propagation split-step Fourier (BP-SSF) method for nonlinear compensation caused by self-phase modulation. The BER measurement and maximum signal reach after DSP, including CDE with/without SSF are shown in Fig. 2.12 and Fig. 2.13, for a wide set of input powers and propagation distances. The results in Fig. 2.12, are corresponding to the optical powers of -4 dBm, -2 dBm and 0 dBm. It can be observed that for -4 dBm the maximum reach with only CDE is limited to 5200 km.

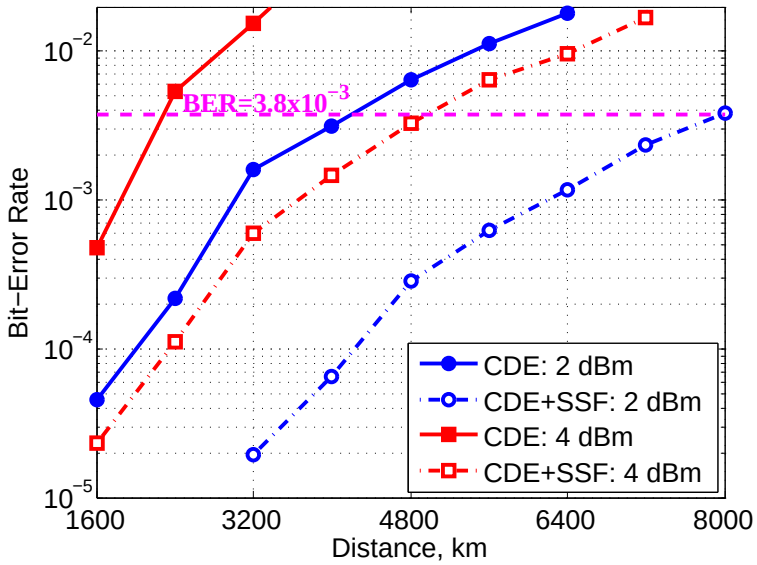

Figure 2.13: Measured BER for 2 dBm and 4 dBm optical powers versus different distance; CDE+SSF: CDE includes nonlinear equalizer, with applying BP-SSF method.

In this power, the BER measurement with and without applying the SSF method are almost the same. In this case, the fiber response will converge to the linear propagation regime. For 0 dBm power, we have more OSNR, but as shown in Fig. 2.12 there is a gap between using and not using SSF in propagation distance corresponding to BER=3.8×10^{-3} due to the impact of nonlinearities. Considering NLE with SSF method, the maximum transmission reach is extended to 7500 km at an input power of 0 dBm.

Fig. 2.13 indicates the BER dependence on the launched powers 2 dBm and 4 dBm, applying CDE and SSF. As shown in this figure with 4 dBm optical power, the impact of nonlinearity in fiber due to SPM, is limiting the transmission length to 2200 km that with nonlinear compensation this distance can be increased to 5000 km. Also, this figure shows that the optimum power for higher distance is 2 dBm. In this power we have optimum OSNR as well as SSF method work very well and compensates SPM nonlinearity in the fiber. As it is observed, 8000 km reach was achieved for this power by applying nonlinear equalizer. The BER for different powers and distances were calculated and the experimental results further show that DP-QPSK is one of the potential candidates for transoceanic communications. Furthermore, with applying the split-step Fourier method for NLE, we demonstrated a 35% and 60% increase in maximum reach relatively to CDE only for 0 dBm and 2 dBm optical powers, respectively. As a result, 8000 km reach was achieved for the 100 Gbps DP-QPSK signal using chromatic dispersion equalizer with nonlinear equalizer based on the BP-SSF method.

2.3.2 Free Space Optical links

One interesting economic solution for providing high-speed connections, can be offered by FSO, it can address the bandwidth requirements of the future optical systems [95], [96]. FSO is a broadband access technology, refers to the straight forward deployment transmission system, which uses light sources to propagate the light between two points [95]. Indeed, in

this technology instead of establishing fiber optical link, light is transmitted in a narrow beam through the atmosphere. Meanwhile, FSO links have attracted great attention within the research community as a temporary, fast and economic solution for the network resiliency without restriction in bandwidth and kind of the network configuration [97]. It can provide very high bit rates, full-duplex transmission, high transmission security, besides very fast installation, and license-free operation [98]. FSO can be applied as an alternative technology for optical fiber networks, in certain areas where the deployment of the optical fiber is not possible or fiber optic cables is impractical.

Another application of FSO links is the prompt network recovery after any disconnection in the network, civil conflicts or natural disaster. Also it can be used as a backup link, in order to recover and reconfigure the network very fast. In addition, the FSO can be employed for inter-building connections such as point-to-point or multipoint links as well as for temporary installation of events. In addition, FSO connections are proposed to support front haul and back-haul for wireless cellular networks, and besides for data centers connection [99], [18]. Fig. 2.14, depicts a general architecture of hybrid optical-wireless system deployed for access networks.

Meanwhile, it should be mentioned that the stability of the FSO links are highly dependent on atmospheric factors and local weather conditions [100], [19]. In fact, since FSO for making links between transmitter and receiver employs air as an interface, any atmospheric variations result to change in the refractive index of air along the transmitting path, which effect on the system performance [101]. Therefore atmospheric factors must be considered before establishing FSO links. Meanwhile, in order to provide bandwidth requirements of the high capacity networks, the dispersive nature of the FSO channel has to be addressed.

In our laboratory, we study and investigate the possibility of implementing a hybrid optical network by installing outdoor FSO link inside the U-DWDM communication system. The

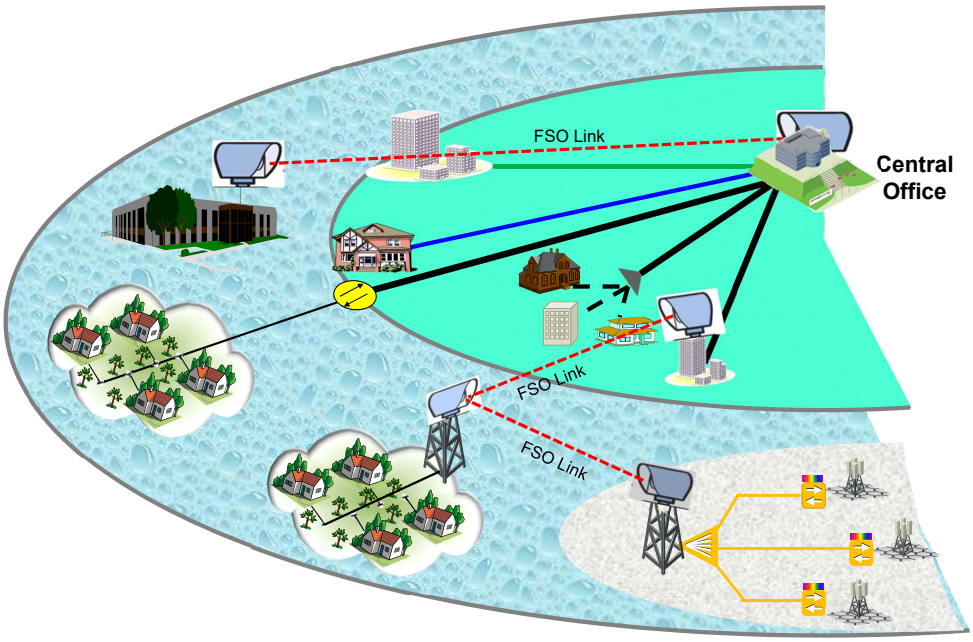

Figure 2.14: General architecture of free space optical system deployed for access networks.

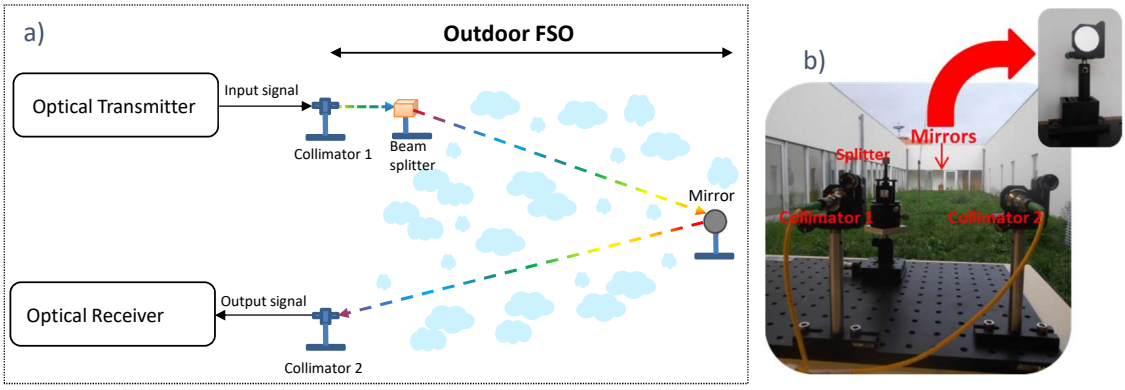

Figure 2.15: FSO experimental system.

54 m FSO link in this study includes two fiber collimators and a polarization independence beam splitter and a concave mirror. Fig. 2.15 depicts the outdoor FSO experimental setup which we used in this work. The weather conditions were at a temperature of 10°C, wind: 12 km/h, and humidity: 73% [96]. Collimator lenses are employed at the end of the fiber in order to convert the optical signal and transmit it through the air, then the collimated beam passes through the outdoor FSO channel. The transmission link length has 27 m long, but with applying a mirror and reflecting transmitted beam, the overall transmission distance will be doubled, 54 m. The reflected beam is sent to the second collimator at the receiver and then guided to the coherent receiver.

This experimental setup for FSO link, widely used in chapter 4 of this thesis, for validating the performance of a U-DWDM system with support to hybrid optical-wireless links enabled by polarization demultiplexing technique, implemented in off-line and real-time operations.

2.4 Final Remarks

The purpose of this chapter has been to provide a short review of next-generation optical networks and their requirements. The technologies that have been proposed to be as a candidate for next-generation optical systems, were also described. In addition, the fundamental concept of coherent optical communication systems was provided. Different type of coherent systems was also discussed. Impairments in the coherent systems as an important issue due to the system degradation in optical communication were briefly explained. The commonly DSP algorithms, which employed by high-speed coherent transmission systems to compensate time-varying transmission impairments, were reviewed.

We presented the details of the recirculating loop and discussed the main issues related to this technique such as loop timing and power management. We have experimentally demonstrated a 100 Gbps DP-QPSK over a transmission system with 8000 km of SSM fiber and EDFA amplification. Finally, a laboratory-based free space optical communication system, which used in this thesis was briefly discussed.

Bibliography

[1] N. Suzuki, H. Miura, K. Matsuda, R. Matsumoto, and K. Motoshima, "100 Gbps to 1 Tbps based coherent passive optical network technology," *Journal of Lightwave Technology*, vol. 36, no. 8, pp. 1485–1491, Apr 2018.

[2] Cisco, "Cisco visual networking index: Forecast and methodology 2017-2022," Tech. Rep., 2017.

[3] A. Oliva, X. C. Perez, A. Azcorra, A. Giglio, F. Cavaliere, D. Tiegelbekkers, J. Lessmann, T. Haustein, A. Mourad, and P. Iovanna, "Xhaul: Toward an integrated fronthaul/backhaul architecture in 5G networks," *IEEE Wireless Communications*, vol. 22, no. 5, pp. 32–40, 2015.

[4] E. commission, "The EU explained: digital agenda for Europe, year=2017,."

[5] J. Kani, M. Yoshino, K. Asaka, H. Ujikawa, T. Yamada, K. Nishimoto, K. Suzuki, and A. Otaka, "Flexible access system architecture (FASA) to support diverse requirements and agile service creation," *Journal of Lightwave Technology*, vol. 36, no. 8, pp. 1510–1515, Apr 2018.

[6] M. Fiorani, B. Skubic, J. Martensson, L. Valcarenghi, P. Castoldi, L. Wosinska, and P. Monti, "On the design of 5G transport networks," *Photonic network communications*, vol. 30, no. 3, pp. 403–415, 2015.

[7] C. Knittle, "IEEE 100G-EPON," in *Proc. Optical Fiber Communication Conf. and Exposition (OFC)*, 2016, pp. Th1I–6.

[8] I. M. S. G. C. L. K. Roberts, Q. Zhuge, "Beyond 100 Gbps: capacity, flexibility, and network optimization," *Journal of Optical Communications and Networking*, vol. 9, no. 4, pp. C12–C24, 2017.

[9] "IEEE 5G and beyond technology roadmap," *White paper*, 2017.

[10] M. Ruffini, "Multi-Dimensional convergence in future 5G networks," *Journal of Lightwave Technology*, vol. 35, no. 3, pp. 535–549, Feb 2017.

[11] M. Ruffini, "Metro-Access network convergence," in *Proc. Optical Fiber Communication Conf. and Exposition (OFC)*, 2016, paper Th4B–1.

[12] K. Roberts and C. Laperle, "Flexible transceivers," in *Proc. Optical Fiber Communication Conf. and Exposition (OFC)*, 2012, paper We.3.A.3.

[13] P. Vetter, "Next generation optical access technologies," in *Proc. European Conf. and Exhibition on Optical Communication (ECOC)*. Optical Society of America, 2012, paper Tu.3.G.1.

[14] T. Pfeiffer, "Next generation mobile fronthaul architectures," in *Proc. Optical Fiber Communication Conf. and Exposition (OFC)*. Optical Society of America, 2015, paper M2J–7.

[15] J. Kani, J. Terada, K. Suzuki, and A. Otaka, "Solutions for future mobile fronthaul and access-network convergence," *Journal of Lightwave Technology*, vol. 35, no. 3, pp. 527–534, 2017.

[16] B. Blanco, J. R. Fajardo, I. Giannoulakis, E. Kafetzakis, S. Peng, J. Perez-Romero, I. Trajkovska, P. Khodashenas, L. Goratti, M. Paolino *et al.*, "Technology pillars in the architecture of future 5G mobile networks: NFV, MEC and SDN," *Computer Standards and Interfaces*, vol. 54, pp. 216–228, 2017.

[17] H. Kaushal and G. Kaddoum, "Optical communication in space: challenges and mitigation techniques," *IEEE communications surveys and tutorials*, vol. 19, no. 1, pp. 57–96, 2017.

[18] A. Shahpari, R. Ferreira, V. Ribeiro, Z. Vujicic, A. Tavares, S. Ziaie, A. Sousa, F. P. Guiomar, M. Lima, A. N. Pinto, and A. L. Teixeira, "Free space optics hybrid PTMP advanced modulation bidirectional PON," in *Proc. European Conf. on Optical Communication (ECOC)*. IEEE, 2014, pp. 1–3.

[19] A. Shahpari, R. Ferreira, V. Ribeiro, A. Sousa, S. Ziaie, A. Tavares, Z. Vujicic, F. P. Guiomar, J. D. Reis, A. N. Pinto, and A. Teixeira, "Coherent ultra-dense wavelength division multiplexing passive optical networks," *Optical Fiber Technology, Elsevier*, vol. 26, pp. 100–107, December 2015.

[20] D. Hillerkuss and J. Leuthold, "Software-defined transceivers for dynamic access networks," in *Proc. Optical Fiber Communication Conf. and Exposition (OFC)*, 2015, paper Tu2E.4.

[21] K. Grobe and J. P. Elbers, "PON in adolescence: from TDMA to WDM-PON," *IEEE Communications Magazine*, vol. 46, no. 1, 2008.

[22] Z. Vujicic, A. Shahpari, B. Neto, N. Pavlovic, A. Almeida, A. Tavares, M. Ribeiro, S. Ziaie, R. Ferreira, R. Bastos, and A. L. Teixeira, "Considerations on performance, cost and power consumption of candidate 100G-EPON architectures," in *Proc. 18th International Conf. on Transparent Optical Networks (ICTON)*, ser. We. D1.1, 2016, pp. 1–6.

[23] R. Ferreira, J. D. Rei, S. M. Rossi, S. B. Amado, A. Shahpari, N. Gonzalez, J. R. Oliveira, A. N. Pinto, and A. L. Teixeira, "Demonstration of nyquist UDWDM-PON with digital signal processing in real-time," in *Proc. Optical Fiber Communication Conf. and Exposition (OFC)*, 2015, paper Th3I–4.

[24] J. D. Reis, A. Shahpari, R. M. Ferreira, S. Ziaie, D. M. Neves, M. Lima, and A. L. Teixeira, "Terabit+ (192x10 Gb/s) nyquist shaped UDWDM coherent PON with upstream and downstream over a 12.8 nm band," *Journal of Lightwave Technology*, vol. 32, no. 4, pp. 729–735, Feb. 2014.

[25] E. J. Bachus, R. Braun, W. Eutin, E. Grossmann, H. Foisel, K. Heimes, and B. Strebel, "Coherent optical-fibre subscriber line," *Electronics Letters*, vol. 21, no. 25, pp. 1203–1205, 1985.

[26] H. Rohde, S. Smolorz, E. Gottwald, and K. Kloppe, "Next generation optical access: 1 Gbps for everyone," in *Proc. 35th European Conf. Optical Communication (ECOC)*. IEEE, 2009, paper 10.5.5.

[27] D. Lavery, R. Maher, D. S.Millar, B. C. Thomsen, P. Bayvel, and S. J. Savory, "Digital coherent receivers for long-reach optical access networks," *Journal of Lightwave Technology*, vol. 31, no. 4, pp. 609–620, 2013.

[28] D. Lavery, C. Behrens, and S. J. Savory, "A comparison of modulation formats for passive optical networks," *Optics Express*, vol. 19, no. 26, pp. B836–B841, 2011.

[29] H. Rohde, E. Gottwald, A. Teixeira, J. D. Reis, A. Shahpari, K. Pulverer, and J. S. Wey, "Coherent ultra dense WDM technology for next generation optical metro and access networks," *Journal of Lightwave Technology*, vol. 32, no. 10, pp. 2041–2052, May 2014.

[30] A. Shahpari, R. S. Luís, V. Ribeiro, J. D. Reis, R. M. Ferreira, J. M. D. Mendinueta, Z. Vujicic, B. J. Puttnam, M. Lima, N. Wada, and A. Teixeira, "Spectrally efficient enhanced-performance bidirectional coherent PON with laserless 10 Gb/s ONU," *Journal of Optical Communications and Networking (JOCN)*, vol. 7, no. 3, pp. A403–A413, 2015.

[31] I. N. Cano, A. Lerin, V. Polo, and J. Prat, "Direct phase modulation DFBs for cost-effective ONU transmitter in UDWDM PONs," *IEEE Photonics Technology Letters*, vol. 26, no. 10, pp. 973–975, 2014.

[32] R. M. Ferreira, A. Shahpari, S. Amado, P. Costa, F. P. Guiomar, A. N. Pinto, and A. L. Teixeira, "Impact of TWDM on optional real-time QPSK WDM channels," in *European Conf. on Optical Communication (ECOC)*. IEEE, 2014, pp. 1–3.

[33] P. Poggiolini, Y. Jiang, A. Carena, G. Bosco, and F. Forghieri, "Analytical results on system maximum reach increase through symbol rate optimization," in *Proc. Optical Fiber Communication Conf. and Exposition (OFC)*. Optical Society of America, 2015, pp. Th3D–6.

[34] A. Nespola, L. Bertignono, G. Bosco, A. Carena, Y. Jiang, S. Bilal, P. Poggiolini, S. Abrate, and F. Forghieri, "Experimental demonstration of fiber nonlinearity mitigation in a WDM multi-subcarrier coherent optical system," in *European Conf. on Optical Communication (ECOC)*. IEEE, 2015, pp. 1–3.

[35] F. P. Guiomar and A. Carena, "Achieving fine bit-rate granularity with hybrid subcarrier modulation," in *Signal Processing in Photonic Communications*. Optical Society of America, 2016, paper SpW3F–2.

[36] M. Qiu, Q. Zhuge, X. Xu, M. Chagnon, M. Morsy-Osman, and D. V. Plant, "Subcarrier multiplexing using DACs for fiber nonlinearity mitigation in coherent optical communication systems," in *Proc. Optical Fiber Communication Conf. and Exposition (OFC)*. Optical Society of America, 2014, paper Tu3J.2.

[37] K. Kikuchi, "Fundamentals of coherent optical fiber communications," *Journal of Lightwave Technology*, vol. 34, no. 1, pp. 157–179, 2016.

[38] K. Kikuchi and S. Tsukamot, "Evaluation of sensitivity of the digital coherent receiver," *Journal of Lightwave Technology*, vol. 26, no. 13, pp. 1817–1822, 2008.

[39] K. Kikuchi, "Coherent optical communications: Historical perspectives and future directions," in *High Spectral Density Optical Communication Technologies*. Springer, 2010, pp. 11–49.

[40] J. Prat, I. Cano, M. Presi, I. Tomkos, D. Klonidis, R. B. G. Vall-llosera, R. Pous, G. Papastergiou, A. Rafel *et al.*, "Technologies for cost-effective UDWDM-PONs," *Journal of Lightwave Technology*, vol. 34, no. 2, pp. 783–791, 2016.

[41] E. Ciaramella, "Polarization-independent receivers for low-cost coherent OOK systems," *IEEE Photonics Technology Letters*, vol. 26, no. 6, pp. 548–551, 2014.

[42] I. Cano, J. C. Velásquez, and J. Prat, "7.5 Gb/s direct DFB phase modulation with 8-DPSK for 6.25 GHz spaced coherent UDWDM-PONs," in *Proc. Optical Fiber Communication Conf. and Exposition (OFC)*. IEEE, 2016, paper M3C.4.

[43] M. Artiglia, R. Corsini, M. Presi, F. Bottoni, G. Cossu, and E. Ciaramella, "Coherent systems for low-cost 10 Gb/s optical access networks," *Journal of Lightwave Technology*, vol. 33, no. 15, pp. 3338–3344, 2015.

[44] J. Tabares, V. Polo, and J. Prat, "Polarization-independent heterodyne dpsk receiver based on 3× 3 coupler for cost-effective udWDM-PON," in *Proc. Optical Fiber Communication Conf. and Exposition (OFC)*, 2017, paper Th1K.3.

[45] C. Xu, X. Liu, and X. Wei, "Differential phase-shift keying for high spectral efficiency optical transmissions," *IEEE Journal of Selected Topics in Quantum Electronics*, vol. 10, no. 2, pp. 281–293, 2004.

[46] M. Rohde, C. Caspar, N. Heimes, M. Konitzer, E.-J. Bachus, and N. Hanik, "Robustness of DPSK direct detection transmission format in standard fibre wdm systems," *Electronics Letters*, vol. 36, no. 17, pp. 1483–1484, 2000.

[47] S. J. Savory, "Digital coherent optical receivers: algorithms and subsystems," *Selected Topics in Quantum Electronics, IEEE Journal of*, vol. 16, no. 5, pp. 1164–1179, 2010.

[48] M. Seimetz, M. Noelle, and E. Patzak, "Optical systems with high-order DPSK and star QAM modulation based on interferometric direct detection," *Journal of Lightwave Technology*, vol. 25, no. 6, pp. 1515–1530, 2007.

[49] L. Beygi, E. Agrell, and M. Karlsson, "Optimization of 16-point ring constellations in the presence of nonlinear phase noise," in *Proc. Optical Fiber Communication Conf. and Exposition (OFC)*. IEEE, 2011, paper OThO4.

[50] C. R. Doerr, L. Zhang, P. Winzer, and A. H. Gnauck, "28-Gbaud InP square or hexagonal 16-QAM modulator," in *Proc. Optical Fiber Communication Conf. and Exposition (OFC)*. Optical Society of America, 2011, paper OMU2.

[51] T. Pfau, S. Hoffmann, and R. Noé, "Hardware-efficient coherent digital receiver concept with feedforward carrier recovery for M-QAM constellations," *Journal of Lightwave Technology*, vol. 27, no. 8, pp. 989–999, 2009.

[52] R. Ferreira, J. D. Rei, S. M. Rossi, S. B. Amado, A. Shahpari, N. Gonzalez, J. R. Oliveira, A. N. Pinto, and A. L. Teixeira, "Coherent nyquist UDWDM-PON with digital signal processing in real-time," *Journal of Lightwave Technology*, vol. 34, no. 2, pp. 826–833, 2016.

[53] E. Ip and J. M. Kahn, "Digital equalization of chromatic dispersion and polarization mode dispersion," *Journal of Lightwave Technology*, vol. 25, no. 8, pp. 2033–2043, 2007.

[54] S. J. Savory, "Digital filters for coherent optical receivers," *Optics Express*, vol. 16, no. 2, pp. 804–817, 2008.

[55] X. Li, X. Chen, G. Goldfarb, E. Mateo, I. Kim, F. Yaman, and G. Li, "Electronic post-compensation of wdm transmission impairments using coherent detection and digital signal processing," *Optics Express*, vol. 16, no. 2, pp. 880–888, 2008.

[56] T. Tanimura, S. Oda, T. Tanaka, T. Hoshida, Z. Tao, and J. C. Rasmussen, "A simple digital skew compensator for coherent receiver," in *Proc. 35th European Conf. Optical Communication (ECOC)*, 2009, paper 7.3.2.

[57] M. Paskov, D. Lavery, and S. J. Savory, "Blind equalization of receiver in-phase/quadrature skew in the presence of nyquist filtering," *IEEE Photonics Technology Letters*, vol. 25, no. 24, pp. 2446–2449, 2013.

[58] M. S. Faruk and K. Kikuchi, "Compensation for in-phase/quadrature imbalance in coherent-receiver front end for optical quadrature amplitude modulation," *IEEE Photonics Journal*, vol. 5, no. 2, pp. 7 800 110–7 800 110, 2013.

[59] C. S. Petrou, A. Vgenis, I. Roudas, and L. Raptis, "Quadrature imbalance compensation for PDM QPSK coherent optical systems," *IEEE Photonics Technology Letters*, vol. 21, no. 24, pp. 1876–1878, 2009.

[60] I. Fatadin, S. J. Savory, and D. Ives, "Compensation of quadrature imbalance in an optical QPSK coherent receiver," *IEEE Photonics Technology Letters*, vol. 20, no. 20, pp. 1733–1735, 2008.

[61] S. J. Savory, G. Gavioli, R. I. Killey, and P. Bayvel, "Electronic compensation of chromatic dispersion using a digital coherent receiver," *Optics Express*, vol. 15, no. 5, pp. 2120–2126, 2007.

[62] G. Goldfarb and G. Li, "Chromatic dispersion compensation using digital iir filtering with coherent detection," *IEEE Photonics Technology Letters*, vol. 19, no. 13, pp. 969–971, 2007.

[63] B. Spinnler, "Equalizer design and complexity for digital coherent receivers," *Journal of Selected Topics in Quantum Electronics*, vol. 16, no. 5, pp. 1180–1192, 2010.

[64] R. Kudo, T. Kobayashi, K. Ishihara, Y. Takatori, A. Sano, and Y. Miyamoto, "Coherent optical single carrier transmission using overlap frequency domain equalization for long-haul optical systems," *Journal of Lightwave Technology*, vol. 27, no. 16, pp. 3721–3728, 2009.

[65] T. Xu, G. Jacobsen, S. Popov, J. Li, E. Vanin, K. Wang, A. T. Friberg, and Y. Zhang, "Chromatic dispersion compensation in coherent transmission system using digital filters," *Optics Express*, vol. 18, no. 15, pp. 16 243–16 257, Jul 2010.

[66] D. Wang, C. Lu, A. P. T. Lau, and S. He, "Adaptive chromatic dispersion compensation for coherent communication systems using delay-tap sampling technique," *IEEE Photonics Technology Letters*, vol. 23, no. 14, pp. 1016–1018, 2011.

[67] F. N. Hauske, C. Xie, Z. Zhang, C. Li, L. Li, and Q. Xiong, "Frequency domain chromatic dispersion estimation," in *Proc. Optical Fiber Communication Conf. and Exposition (OFC)*, 2010, paper JThA11.

[68] M. Kuschnerov, F. N. Hauske, K. Piyawanno, B. Spinnler, M. S. Alfiad, A. Napoli, and B. Lankl, "DSP for coherent single-carrier receivers," *Journal of Lightwave Technology*, vol. 27, no. 16, pp. 3614–3622, 2009.

[69] G. P. Agrawal, "Nonlinear fiber optics (academic press, New York, USA)," 2007.

[70] G. Bosco, R. Cigliutti, A. Nespola, A. Carena, V. Curri, F. Forghieri, Y. Yamamoto, T. Sasaki, Y. Jiang, and P. Poggiolini, "Experimental investigation of nonlinear interference accumulation in uncompensated links," *IEEE Photonics Technology Letters*, vol. 24, no. 14, pp. 1230–1232, 2012.

[71] J. C. Cartledge, F. P. Guiomar, F. R. Kschischang, G. Liga, and M. P. Yankov, "Digital signal processing for fiber nonlinearities," *Optics Express*, vol. 25, no. 3, pp. 1916–1936, 2017.

[72] E. Ip and J. M. Kahn, "Compensation of dispersion and nonlinear impairments using digital backpropagation," *Journal of Lightwave Technology*, vol. 26, no. 20, pp. 3416–3425, 2008.

[73] F. P. Guiomar, J. D. Reis, A. Carena, G. Bosco, A. L. Teixeira, and A. N. Pinto, "Experimental demonstration of a frequency-domain Volterra series nonlinear equalizer in polarization-multiplexed transmission," *Optics Express*, vol. 21, no. 1, pp. 276–288, 2013.

[74] F. P. Guiomar, J. D. Reis, A. L. Teixeira, and A. N. Pinto, "Mitigation of intra-channel nonlinearities using a frequency-domain Volterra series equalizer," *Optics Express*, vol. 20, no. 2, pp. 1360–1369, Jan 2012.

[75] N. J. Muga and A. N. Pinto, "Digital PDL compensation in 3D Stokes space," *Journal of Lightwave Technology*, vol. 31, no. 13, pp. 2122–2130, 2013.

[76] J. P. Gordon and H. Kogelnik, "PMD fundamentals: Polarization mode dispersion in optical fibers," *Proceedings of the National Academy of Sciences*, vol. 97, no. 9, pp. 4541–4550, 2000.

[77] F. P. Guiomar, S. B. Amado, A. Carena, G. Bosco, A. Nespola, A. L. Teixeira, and A. N. Pinto, "Fully blind linear and nonlinear equalization for 100G PM-64QAM optical systems," *Journal of Lightwave Technology*, vol. 33, no. 7, pp. 1265–1274, Apr 2015.

[78] S. J. Savory, G. Gavioli, E. Torrengo, and P. Poggiolini, "Impact of interchannel nonlinearities on a split-step intrachannel nonlinear equalizer," vol. 22, no. 10, pp. 673–675, 2010.

[79] I. Fatadin, D. Ives, and S. J. Savory, "Blind equalization and carrier phase recovery in a 16-QAM optical coherent system," *Journal of lightwave technology*, vol. 27, no. 15, pp. 3042–3049, 2009.

[80] N. J. Muga and A. N. Pinto, "Adaptive 3-D Stokes space-based polarization demultiplexing algorithm," *Journal of Lightwave Technology*, vol. 32, no. 19, pp. 3290–3298, Oct. 2014.

[81] F. Gardner, "A BPSK/QPSK timing-error detector for sampled receivers," *IEEE Transactions on communications*, vol. 34, no. 5, pp. 423–429, 1986.

[82] L. Litwin, "Matched filtering and timing recovery in digital receivers," *RF design*, vol. 24, no. 9, pp. 32–49, 2001.

[83] X. Zhou and X. Chen, "Parallel implementation of all-digital timing recovery for high-speed and real-time optical coherent receivers," *Optics Express*, vol. 19, no. 10, pp. 9282–9295, 2011.

[84] A. Leven, N. Kaneda, U.-V. Koc, and Y.-K. Chen, "Frequency estimation in intradyne reception," *IEEE Photonics Technology Letters*, vol. 19, no. 6, pp. 366–368, 2007.

[85] Y. Liu, Y. Peng, S. Wang, and Z. Chen, "Improved fft-based frequency offset estimation algorithm for coherent optical systems," *IEEE Photonics Technology Letters*, vol. 26, no. 6, pp. 613–616, 2014.

[86] A. Viterbi, "Nonlinear estimation of PSK-modulated carrier phase with application to burst digital transmission," *IEEE Transactions on Information Theory*, vol. 29, no. 4, pp. 543–551, July 1983.

[87] I. Fatadin, D. Ives, and S. J. Savory, "Laser linewidth tolerance for 16-QAM coherent optical systems using QPSK partitioning," *IEEE Photonics Technology Letters*, vol. 22, no. 9, pp. 631–633, 2010.

[88] G. Picchi and G. Prati, "Blind equalization and carrier recovery using a" stop-and-go" decision-directed algorithm," *IEEE Transactions on Communications*, vol. 35, no. 9, pp. 877–887, 1987.

[89] G. Tzimpragos, C. Kachris, I. B. Djordjevic, M. Cvijetic, D. Soudris, and I. Tomkos, "A survey on FEC codes for 100 G and beyond optical networks," *IEEE Communications Surveys Tutorials*, vol. 18, no. 1, pp. 209–221, Firstquarter 2016.

[90] F. Chang, K. Onohara, and T. Mizuochi, "Forward error correction for 100 G transport networks," *IEEE Commun. Mag*, vol. 48, no. 3, pp. S48–S55, March 2010.

[91] N. S. Bergano and C. Davidson, "Circulating loop transmission experiments for the study of long-haul transmission systems using erbium-doped fiber amplifiers," *Journal of Lightwave Technology*, vol. 13, no. 5, pp. 879–888, 1995.

[92] R. Hui and M. O'Sullivan, *Fiber optic measurement techniques.* Elsevier Academic Press, 2009.

[93] F. P. Guiomar and A. N. Pinto, "Optimizing the nonlinear operator in backward propagation," in *Proc. International Conf. on Computer as a Tool (EUROCON)*, 2011.

[94] S. Ziaie, F. P. Guiomar, R. M. Ferreira, A. Shahpari, A. Teixeira, and A. N. Pinto, "100 Gbps DP-QPSK transmission over 8000 km of standard single mode fiber using recirculating loop technique," in *Proc. 10th Conf. on Telecommunications (Conftele)*, 2015, p. paper CD.

[95] M. Matsumoto, K. Osawa, S. Hotta, and K. Wakamori, "Innovative tracking system for next generation fso systems under massive earthquakes," in *Proc. International Conf. on Optical Network Design and Modeling (ONDM).* IEEE, 2015, pp. 233–238.

[96] A. N. Sousa, I. A. Alimi, R. M. Ferreira, A. Shahpari, M. Lima, P. P. Monteiro, and A. L. Teixeira, "Real-time dual-polarization transmission based on hybrid optical wireless communications," *Optical Fiber Technology, Elsevier*, vol. 40, pp. 114–117, 2018.

[97] E. Ciaramella, Y. Arimoto, G. Contestabile, M. Presi, A. D'Errico, V. Guarino, and M. Matsumoto, "1.28 Terabit/s (32x40 Gbit/s) WDM transmission system for free space optical communications," *IEEE Journal on selected areas in communications*, vol. 27, no. 9, pp. 1639–1645, 2009.

[98] M. A. Khalighi and M. Uysal, "Survey on free space optical communication: A communication theory perspective," *IEEE Communications Surveys Tutorials*, vol. 16, no. 4, pp. 2231–2258, Fourthquarter 2014.

[99] G. Cossu, A. Khalid, P. Choudhury, R. Corsini, and E. Ciaramella, "3.4 gbit/s visible optical wireless transmission based on RGB LED," *Optics Express*, vol. 20, no. 26, pp. B501–B506, 2012.

[100] I. Sugino, "Disaster recovery and the R&D policy in Japan's telecommunication," *Proc. Optical Fiber Communication Conf. and Exposition (OFC)*, March 2012.

[101] L. Yang, M. O. Hasna, and X. Gao, "Performance of mixed RF/FSO with variable gain over generalized atmospheric turbulence channels," *IEEE Journal on Selected Areas in Communications*, vol. 33, no. 9, pp. 1913–1924, Sep. 2015.

Chapter 3

Polarization Demultiplexing

Coherent technologies together with Nyquist pulse shaped multi-level modulation formats and digital signal processing, lead to high aggregated capacity per fiber for elastic optical networks. Furthermore, the spectral efficiency can be doubled by employing dual-polarization. Therefore, analysis of polarization effects in the optical communication systems and a detailed description of fibre birefringence as well as a robust tool to represent the SOP of a light wave are required. Recently, a three-dimensional Stokes space-based PolDemux technique was proposed as a low complexity and format transparent algorithm. Despite the promising results achieved with this PolDemux technique, a versification of its applicability for optical metro and access networks is still required.

In section 3.1, we review the polarization representation of the light wave in the Jones and Stokes Formalism. Then in section 3.2, we briefly consider polarization demultiplexing techniques and present the adaptive Stokes PolDemux algorithm. Then in section 3.3, performance of the adaptive Stokes algorithm will be evaluated in terms of several factors specially convergence speed and complexity of the algorithm. We also experimentally assess and validate the adaptive Stokes PolDemux algorithm targeting its application to optical metro and access networks based on DP-QPSK and DP-16QAM modulation formats. And finally the main conclusions of this chapter are summarized in section 3.4.

3.1 Polarization in the Optical Fiber

Polarization is a fundamental property of the light wave, and one of the potential gains of coherent detection technology over the direct detection is extracting the information of the polarization of the signal [1].

3.1.1 Polarization Representation

Basically, the light beam is an electromagnetic wave, which is characterized by its polarization, wavelength, and intensity. A polarized light that has propagated in z-direction has two linear polarized components in the x and y directions [2].

$$E_x(z,t) = E_{0x}\cos(\tau + \phi_x), \tag{3.1}$$

$$E_y(z,t) = E_{0y}\cos(\tau + \phi_y), \tag{3.2}$$

Table 3.1: Jones vector of the fundamental SOPs.

State of polarization	Jones Vector
Linear horizontal	$\begin{bmatrix}1\\0\end{bmatrix}$
Linear Vertical	$\begin{bmatrix}0\\1\end{bmatrix}$
Linear 45°	$\frac{1}{\sqrt{2}}\begin{bmatrix}1\\1\end{bmatrix}$
Linear -45°	$\frac{1}{\sqrt{2}}\begin{bmatrix}1\\-1\end{bmatrix}$
Right circular	$\frac{1}{\sqrt{2}}\begin{bmatrix}1\\j\end{bmatrix}$
Left circular	$\frac{1}{\sqrt{2}}\begin{bmatrix}1\\-j\end{bmatrix}$

where E_{0x} and E_{0y} present the real maximum amplitudes of the electric field. In addition, ϕ_x and ϕ_y are the phases and $\tau = \omega t - kz$ represents the propagation of the signal component along the z-direction.

3.1.1.1 Jones Formalism

Full information of a polarized light wave can be presented by the amplitude and phase of both components of the electric field vector in the plane of polarization [3]. A suitable method for representing polarization vectors is using the Jones vector, which includes the horizontal and vertical complex components of the electric vector. This vector describes the SOP of completely polarized light, and the light wave can be represented using this concept as [4],

$$\begin{bmatrix}E_x\\E_y\end{bmatrix} = \begin{bmatrix}E_{0x}e^{j\phi_x}\\E_{0y}e^{j\phi_y}\end{bmatrix}, \tag{3.3}$$

where E_{0x} and E_{0y} are the amplitudes of x and y polarization, ϕ_x and ϕ_y are the phases, and $j = \sqrt{-1}$.

The most common SOPs used to describe the basis of the Jones vectors are linear horizontal polarization (LHP) and linear vertical polarization (LVP), in addition, linear polarization at +45°, linear polarization at -45°, the left circular polarization (LCP) and the right circular polarization (RCP) can also be considered. Table 3.1 denotes the Jones vectors related to the fundamental SOPs [4], [5].

The Jones matrix uses to describe the relationship between both output and input Jones vectors and can be written as,

$$\begin{bmatrix} E_{x,out} \\ E_{y,out} \end{bmatrix} = \begin{bmatrix} J_{xx} & J_{xy} \\ J_{yx} & J_{yy} \end{bmatrix} \begin{bmatrix} E_{x,in} \\ E_{y,in} \end{bmatrix}. \tag{3.4}$$

The Jones matrix has different forms for the retarder, rotator and polarizer [4], [2] as follows

- Retarder (wave plate)

  The Jones matrices for a wave plate ($E_{0x} = E_{0y} = 1$) includes a phase shift of $\frac{\phi}{2}$ and $-\frac{\phi}{2}$, along x (fast), and y (slow axis, respectively) and is defined by

$$\begin{bmatrix} e^{\frac{j\phi}{2}} & 0 \\ 0 & e^{\frac{-j\phi}{2}} \end{bmatrix}. \tag{3.5}$$

- Rotator

  When the rotation angle is α, then Jones matrix can be written as,

$$\begin{bmatrix} \cos\alpha & \sin\alpha \\ -\sin\alpha & \cos\alpha \end{bmatrix}. \tag{3.6}$$

- Polarizer

  For a linear polarizer, the Jones matrix is defined by

$$\begin{bmatrix} p_x & 0 \\ 0 & p_y \end{bmatrix}. \tag{3.7}$$

  The p_x and p_y are transmission factors for the x and y axes, respectively. For complete transmission, $p_x = p_y = 1$, whereas for complete attenuations these factors will be $p_x = p_y = 0$.

Table 3.2 presents Jones matrix for different optical elements [4], [5].

3.1.1.2 Stokes Formalism

The light polarization behavior also can be described in terms of physical observables [6], [7], and four Stokes polarization parameters. Unlike Jones vectors, the Stokes parameters are real and can describe both full or partially polarized light. Stokes parameter is written as,

$$\mathbf{S} = \begin{bmatrix} S_0 \\ S_1 \\ S_2 \\ S_3 \end{bmatrix} = \begin{bmatrix} E_{0x}^2 + E_{0y}^2 \\ E_{0x}^2 - E_{0y}^2 \\ 2E_{0x}E_{0y}\cos(\phi) \\ 2E_{0x}E_{0y}\sin(\phi) \end{bmatrix}, \tag{3.8}$$

where E_{0x}, E_{0y} denote real maximum amplitudes and $\phi = \phi_y - \phi_x$ represents the phase difference.

As can be concluded from this formula, the S_0 parameter defines the total powers of the light and the S_1 parameter shows the difference between the powers of the LHP and the

Table 3.2: Jones matrix for different optical element.

Optical element	Jones Matrix
Linear horizontal polarizer	$\begin{bmatrix} 1 & 0 \\ 0 & 0 \end{bmatrix}$
Linear Vertical polarizer	$\begin{bmatrix} 0 & 0 \\ 0 & 1 \end{bmatrix}$
Linear polarizer at 45°	$\frac{1}{2}\begin{bmatrix} 1 & 1 \\ 1 & 1 \end{bmatrix}$
Linear polarizer at -45°	$\frac{1}{2}\begin{bmatrix} 1 & -1 \\ -1 & 1 \end{bmatrix}$
Quarter-wave plate, fast axis vertical	$e^{\frac{j\phi}{4}}\begin{bmatrix} 1 & 0 \\ 0 & -j \end{bmatrix}$
Quarter-wave plate, fast axis horizontal	$e^{\frac{-j\phi}{4}}\begin{bmatrix} 1 & 0 \\ 0 & j \end{bmatrix}$
Circular polarizer, right handed	$\frac{1}{2}\begin{bmatrix} 1 & j \\ -j & 1 \end{bmatrix}$
Circular polarizer, left handed	$\frac{1}{2}\begin{bmatrix} 1 & -j \\ j & 1 \end{bmatrix}$

LVP light. Also, the difference in the powers of the linearly 45° polarized light and linearly -45° polarized light can be represented by S_2 parameter. In addition, S_3 parameter denotes the difference in the powers of the RCP light and the LCP light. The Stokes vector can be represented by the last three parameters [8],

$$\vec{S} = \begin{bmatrix} S_1 \\ S_2 \\ S_3 \end{bmatrix}, \tag{3.9}$$

It can be observed that the intensity of the polarized component of the light beam is specified by the length of the Stokes vector. If a fully polarized light has been propagated, the length of the Stokes vector is S_0 parameter. As mentioned before, the Stokes representation can describe partially polarized and unpolarized light. The degree of polarization (DOP) can be concluded from the Stokes parameters, as [4],

$$DOP = \frac{\sqrt{S_1^2 + S_2^2 + S_3^2}}{S_0}, \tag{3.10}$$

Table 3.3: Stokes vectors related to the fundamental SOPs.

State of polarization	Stokes space
Linear horizontal	$\begin{bmatrix} 1 \\ 0 \\ 0 \end{bmatrix}$
Linear Vertical	$\begin{bmatrix} -1 \\ 0 \\ 0 \end{bmatrix}$
Linear 45°	$\begin{bmatrix} 0 \\ 1 \\ 0 \end{bmatrix}$
Linear -45°	$\begin{bmatrix} 0 \\ -1 \\ 0 \end{bmatrix}$
Right circular	$\begin{bmatrix} 0 \\ 0 \\ 1 \end{bmatrix}$
Left circular	$\begin{bmatrix} 0 \\ 0 \\ -1 \end{bmatrix}$

the value of 0 is for unpolarized light and 1 is for totally polarized light. Also, the degree of linear polarization (DOLP) and degree of circular polarization (DOCP) can be defined as,

$$DOLP = \frac{\sqrt{S_1^2 + S_2^2}}{S_0}, \tag{3.11}$$

$$DOCP = \frac{S_3}{S_0}, \tag{3.12}$$

The SOP of the light is specified by the normalized Stokes vector, S_1/S_0, S_2/S_0 and S_3/S_0, which have values between -1 and 1. Some Stokes vectors corresponding to the fundamental SOPs are represented in Table 3.3.

The all possible normalized Stokes vectors form the surface of a unit sphere known as the Poincaré sphere [9], are represented in Fig. 3.1.

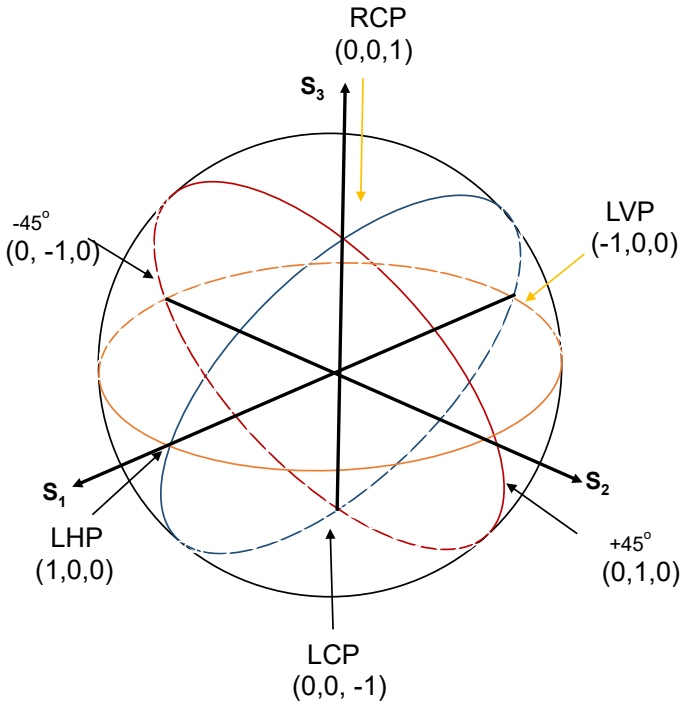

Figure 3.1: The Stokes space representation of fundamental SOPs in the Poincaré sphere.

3.1.2 Evolution of SOP in Optical Systems

The polarization of a signal after passing through a deployed fiber is random, and its SOP may change on a millisecond time-scale [10], [11]. In the real implementation of the optical fiber, the SOP of the signal especially in standard single-mode fiber can change during signal propagation. In reality, the core of the SSM fiber is not perfectly circular and some phenomena can create birefringence in the fiber. However, external birefringence such as vibration in the street, external stress, physical bending, changing temperature and also the core and cladding asymmetry significantly contributes to polarization effects.

The SSM fiber is interested in optical communication systems, since higher bandwidth, reach and transmission speed can be supported by it comparing to multimode fibers, meanwhile, it presents lower signal interruption [12]. Furthermore, a SSM fiber can support two orthogonal polarization modes, by employing dual orthogonal SOPs, the SE of the fiber-optic communication systems can be doubled [13]. However coherent systems, when employing dual-polarization signals are more sensitive to polarization effects such as random polarization rotation, PMD and PDL [14], [15]. In addition, since PMD and CD in the high-speed communication systems, are the main sources of the signal distortion and pulse spreading and also have a cumulative effect as a function of the fiber length [16], several methods and techniques have been proposed to compensate these impairments. Such as employing powerful DSP stages or deploying orthogonal frequency-division multiplexing (OFDM) in the optical systems [17].

3.2 Polarization Demultiplexing

During signal propagation in the fiber, SOP rotations is changing randomly and two polarization components are mixed. Therefore, a polarization demultiplexing stage is required in the DSP, in order to reverse the mixing of two polarization components [18]. Different PolDemux algorithms have been suggested for coherent systems, such as CMA, decision-directed least mean square (DD-LMS), recursive least square (RLS), radius directed equalization (RDE) and adaptive Stokes algorithm. The polarization multiplexed signal at the receiver after propagation in the optical fiber can be presented by the Jones matrix[19]:

$$\begin{bmatrix} E_x \\ E_y \end{bmatrix} = \begin{bmatrix} \sqrt{\alpha}\exp(j\delta) & -\sqrt{1-\alpha} \\ \sqrt{1-\alpha} & \sqrt{\alpha}\exp(-j\delta) \end{bmatrix} \begin{bmatrix} E_{in,x} \\ E_{in,y} \end{bmatrix}, \tag{3.13}$$

where $E_{in,x}$ and $E_{in,y}$ are original signals in two polarizations x and y, and E_x and E_y are received signal. Also, α is the power splitting ratio and δ is the phase difference between two polarizations. The CMA is one of the most popular techniques to perform blind equalization and digital signal PolDemux in optical communications because of its simplicity, robustness and immunity to phase noise [20], [21], [22]. However, the CMA presents a moderate convergence speed and a singularity problem [22], [23], [24], which can be solved at expenses of increased computational complexity [25], [18], [26]. A modified CMA method was proposed in [18], which uses the Stokes space to define the initial coefficients of the filter. In this case, the singularity problem can be eliminated and the convergence speed is improved. In [26], an algorithm based on error signals evaluated in the Stokes space was proposed to update the values of a butterfly equalizer taps. This was experimentally demonstrated in a DP-16QAM Nyquist-WDM system with multi-span transmission over three types of fiber [27].

Although the CMA is an attractive solution for constant amplitude formats, its extension to multi-level QAM modulation requires a RDE strategy, which is modulation format dependent and may require several cascaded training stages for proper pre-convergence [21], [28]. In addition, this class of PolDemux algorithms generally suffers from the well-known problem of singularity, resulting in the loss of information on one polarization [29]. To circumvent these limitations, 3-D adaptive Stokes space PolDemux algorithm was proposed as a format transparent and low-complexity technique, which is singularity-free and provides faster convergence [13], [30], [31].

In [30], the Stokes parameters are calculated for each signal sample in order to continuously obtain the best fitting plane. The demultiplexing transformation matrix is defined using the information of the normal vector of the best fitting plane and then applied to the signal in order to reverse the mixing of the two orthogonal polarization components. A PolDemux method based on the Stokes space technique for coherent DP-orthogonal frequency division multiplexing (DP-OFDM) systems was proposed in [32]. For each DP-OFDM subcarrier, the OFDM signal is digitally converted to the frequency domain, enabling PolDemux without training sequences [32]. The PDL compensation techniques were also proposed based on rotations and translations of the signal samples in the Stokes space [14], [33]. In [13], a Stokes space-based PolDemux of an endless time-varying SOP signal was obtained by applying an adaptive estimation of the inverse rotation matrix, based on calculating the best normal to the plane through a geometrical algorithm. It has been shown through numerical simulations that this adaptive Stokes algorithm can improve the convergence speed and scalability to higher-level M-ary signals with reduced computational requirements, comparing with the CMA [13].

3.2.1 CMA algorithm

Polarization demultiplexing in the coherent receiver, can be achieved by using a two-by-two matrix controlled by CMA. It is a blind algorithm and was proposed initially by Godard [34]. Initially, it can perform polarization demultiplexing and simultaneously equalizes residual CD, PMD and PDL. It has been adopted in coherent optical systems, particularly in the case that constellation of the modulation format has constant modulus, such as QPSK format. Nonetheless, this algorithm can efficiently be employed when advanced modulation formats are applied [35]. The singularity problem may happen in the CMA due to the blinding update of the weight, while both equalized signals converge to the same output [36]. The main architecture of this algorithm is shown in Fig. 3.2.

The filter parameters are updated based on a gradient descent method [22]. For each received normalized digital sample x_{in} and y_{in} (in the two polarizations, x and y), the CMA will produce digital signal samples x_{out} and y_{out} by applying a set of FIR filters, as follows,

$$\begin{bmatrix} x_{out} \\ y_{out} \end{bmatrix} = \begin{bmatrix} h_{xx} & h_{xy} \\ h_{yx} & h_{yy} \end{bmatrix} \begin{bmatrix} x_{in} \\ y_{in} \end{bmatrix}, \tag{3.14}$$

where h_{xx}, h_{xy}, h_{yx}, and h_{yy} are the coefficients of the adaptive filter. These coefficient are updated sample by sample according to [37], [22]

$$h_{xx}(k+1) = h_{xx}(k) + \mu\varepsilon_x(k)x_{out}(k)x_{in}^*(k), \tag{3.15}$$

$$h_{xy}(k+1) = h_{xy}(k) + \mu\varepsilon_x(k)x_{out}(k)y_{in}^*(k), \tag{3.16}$$

$$h_{yx}(k+1) = h_{yx}(k) + \mu\varepsilon_y(k)y_{out}(k)x_{in}^*(k), \tag{3.17}$$

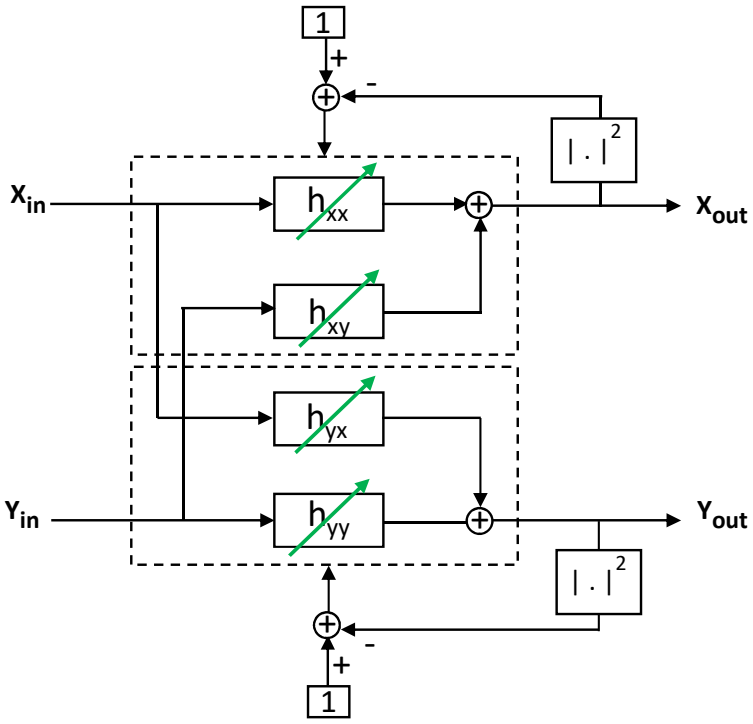

Figure 3.2: The main structure of CMA based on FIR-filters in the butterfly configuration.

$$h_{yy}(k+1) = h_{yy}(k) + \mu\varepsilon_y(k)y_{out}(k)y_{in}^{*}(k), \tag{3.18}$$

where k is the sample number, x_{in}^{*} and y_{in}^{*} denote the complex conjugate of x_{in} and y_{in}, respectively, and μ is the step-size parameter, which sets the amplitude of the error signal used for the update of the FIR filter taps. The CMA attempts to minimize the modulus cost functions given by

$$\varepsilon_x = 1 - |x_{out}|^2, \tag{3.19}$$

$$\varepsilon_y = 1 - |y_{out}|^2, \tag{3.20}$$

which in fact measure the distance of the received point to the unit circle.

3.2.2 RDE Algorithm

Basically, for multi-level modulation formats, which the modulus of the constellation is not constant, such as 16QAM, the CMA algorithm may not present the optimum performance, since the error cannot converge to zero [38], [39]. The CMA can adopt to the RDE algorithm, where RDE uses the same mathematical procedure as CMA, but for updating the equalizer weights, it measures the error between the output of the equalizer and the nearest constellation radius. Therefore, RDE presents better performance and convergence speed for the QAM signal compared to the CMA algorithm [40], [38]. The error function in RDE is given by

$$\varepsilon_x = R_x - |x_{out}|^2, \tag{3.21}$$

$$\varepsilon_y = R_y - |y_{out}|^2, \tag{3.22}$$

where R_x and R_y are the radius of the nearest constellation symbol for each equalizer output.

3.2.3 DD-LMS Algorithm

Another adaptive algorithm that can be applied in the coherent optical systems and perform polarization demultiplexing is DD-LMS. The DD-LMS is one of the common least square algorithms, which is based on the gradient descent method and is used to update the weight coefficient of adaptive filters. This algorithm provides very good tracking besides stability and low computational complexity [41]. Unlike the CMA algorithm, which tries to minimize the modulus cost function by measuring the distance between the received signal point and the unit circle corresponding to the constellation points, typically the DD-LMS algorithm uses constellation point as a reference and calculate the distance between the equalizer output and desired signal. In fact, firstly a blind adaptive equalizer is employed then the filtered outputs are delivered to the directed-decision unit. It is worth to notice that that DD-LMS is very sensitive to phase fluctuation, thus phase and frequency estimation must be performed before or during the DD-LMS algorithm. The error function in the DD-LMS is calculated as follows [36],

$$\varepsilon_x = R_x - x_{out}, \tag{3.23}$$

$$\varepsilon_y = R_y - y_{out}, \tag{3.24}$$

where R_x and R_y show referenced signal, which can measured by,

$$R_x = \exp(j\theta_x)d_x, \tag{3.25}$$

$$R_y = \exp(j\theta_y)d_y, \tag{3.26}$$

where d_x and d_y terms stand for decision signals or training signals, and θ_x and θ_y are estimated phase after frequency and carrier estimation stage. The coefficients of the adaptive filter are updated as follow,

$$h_{xx}(k+1) = h_{xx}(k) + \mu\varepsilon_x(k)x_{in}^*(k), \tag{3.27}$$

$$h_{xy}(k+1) = h_{xy}(k) + \mu\varepsilon_x(k)y_{in}^*(k), \tag{3.28}$$

$$h_{yx}(k+1) = h_{yx}(k) + \mu\varepsilon_y(k)x_{in}^*(k), \tag{3.29}$$

$$h_{yy}(k+1) = h_{yy}(k) + \mu\varepsilon_y(k)y_{in}^*(k), \tag{3.30}$$

where k shows the number of sample sequence, x_{in}^* and y_{in}^* are the complex conjugate of x_{in} and y_{in}, respectively. Also, μ denotes the step-size parameter, which must be optimized to have better convergence speed and consequently better performance.

Although CMA and DD-LMS are both based on the gradient descent method and have almost same mathematical performing, but in the DD-LMS, the equalizer outputs firstly must pass through frequency and carrier phase recovery and then be fed to decision block, thus DD-LMS has higher feedback latency compared to CMA, which can calculate error directly from filter outputs [39].

3.2.4 Adaptive Stokes Algorithm

Recently, a 3-D Stokes space-based PolDemux technique was proposed as low complexity and format transparent algorithm [13]. The Stokes space-based techniques operation principle comprises the calculation of the Stokes parameters for each received orthogonal complex optical fields, which are used to compute a best-fitting plane in the 3D Stokes space. Therefore, the transformation matrix is calculated using the normal vector of such plane to reverse the mixing of the two orthogonal polarization components [13], [42].

Fig. 3.3 represents the stages of calculating the adaptive Stokes algorithm. For each received orthogonal complex optical fields the Stokes parameters are calculated and used to compute the best fitting plane to each sample in the 3D Stokes space [13], [30]. By adjusting the normal vector of the plane for each sample, $\hat{n}(k)$, we can calculate the inverse transmission matrix $\mathbf{F}(\hat{n}(k))$, which help to revers the mixing of the two orthogonal polarization components. The inverse SOP rotation matrix can be calculated by [30]

$$\mathbf{F} = \begin{bmatrix} \cos(p)\exp(jq/2) & \sin(p)\exp(-jq/2) \\ -\sin(p)\exp(jq/2) & \cos(p)\exp(-jq/2) \end{bmatrix}, \tag{3.31}$$

with

$$p = 1/2\text{atan}(a, (b^2 + c^2)^{1/2}), \tag{3.32}$$

and

$$q = \text{atan}(b, c), \tag{3.33}$$

where a, b and c represent the normal vector components, $\hat{n}(k) = (a, b, c)^T$ in the Stokes space. Due to the assumptions of the Stokes space-based PolDemux technique, namely that the optical fiber is relatively well approximated by a unitary matrix, only two entries of the matrix $\mathbf{F}$ are independent, i.e. $f_{yy} = f_{xx}^*$ and $f_{yx} = -f_{xy}^*$, with

$$f_{xx} = \cos(p)\exp(jq/2), \tag{3.34}$$

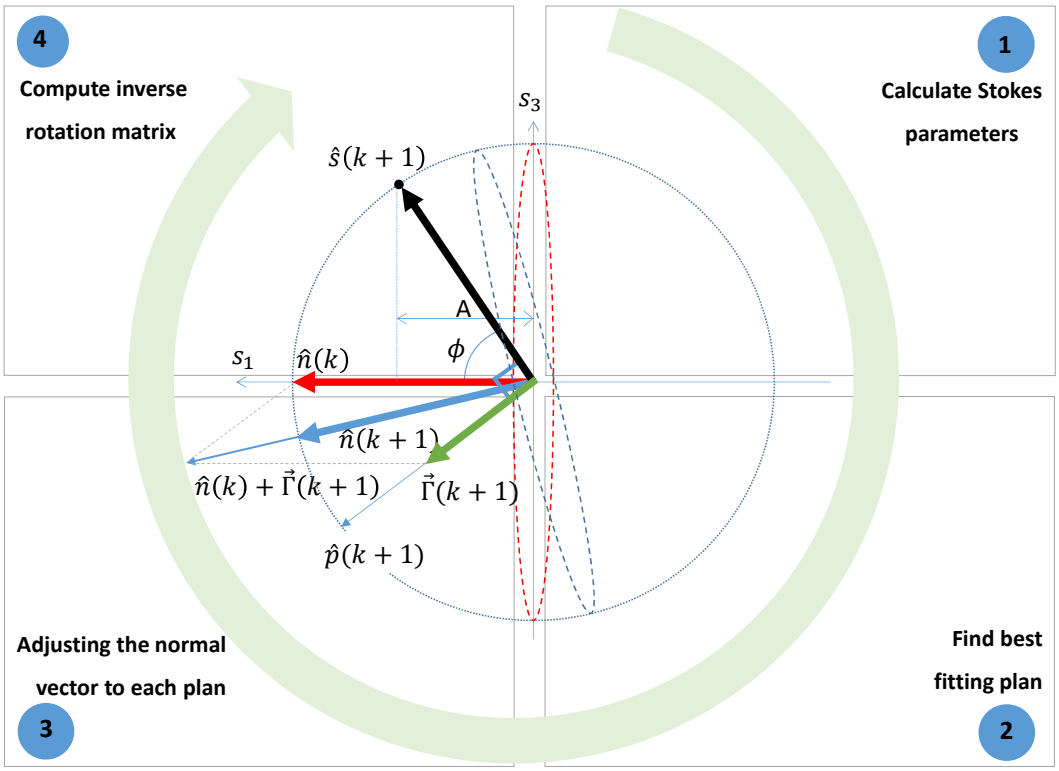

Figure 3.3: Schematic representation of the different vectors of the adaptive Stokes PolDemux algorithm in the "s_2 – s_3" plan [13].

and

$$f_{xy} = \sin(p)\exp(-jq/2), \tag{3.35}$$

this leads to the avoidance of the singularity problem [30].

Note that at the receiver side, if the two orthogonal states of polarization are aligned with the $\hat{x}$ and $\hat{y}$ axis, the symmetry plane is "s_2 – s_3" and the normal vector takes the value $(1,0,0)^T$ [30]. The adaptive Stokes method proposed in [13] uses the Stokes vector of each sample, $\hat{s}(k+1)$, to continuously compute the normal $\hat{n}(k+1)$. To update the normal vector $\hat{n}(k+1)$, the following equation is applied sample by sample

$$\hat{n}(k+1) = \frac{\hat{n}(k)+\vec{\Gamma}(k+1)}{\left\|\hat{n}(k)+\vec{\Gamma}(k+1)\right\|}, \tag{3.36}$$

where $\vec{\Gamma}(k+1)$ is a vector lying in the 3D Stokes plane and the direction of $\vec{\Gamma}(k+1)$ is perpendicular to $\hat{s}(k+1)$,

$$\vec{\Gamma}(k+1) = \mu A[\hat{s}(k+1)\times\hat{n}(k)]\times\hat{s}(k+1), \tag{3.37}$$

where μ is the step-size parameter and $A = \left|\hat{s}(k)\cdot\hat{n}(k)\right|$, [13], which is used to smooth the variation of the vector.

Also Fig. 3.4, depicts data conversion, comprising four ADC and DSP subsystems including adaptive equalization and Stokes PolDemux algorithm architecture in the coherent system.

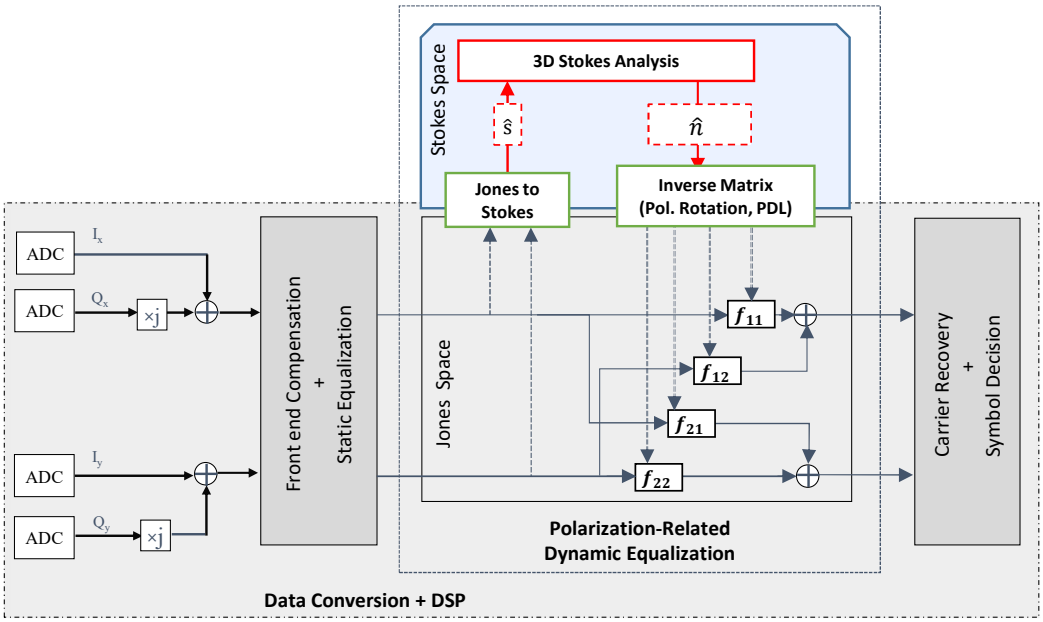

Figure 3.4: Data conversion and DSP subsystems including adaptive equalization and Stokes PolDemux algorithm architecture.

3.3 Validation of the Adaptive Stokes Algorithm

It is worth noticing that the geometrical nature of the adaptive Stokes method imposes memory-less (single tap) processing, at least in its current version. Notice that since the adaptive Stokes algorithm does not account for memory effects, it cannot equalize CD and/or PMD. On the other hand, it is well known that CD does not affect the effectiveness of the Stokes space-based PolDemux, in contrast with PMD [14]. The application of this method to long-haul transmission requires, in principle, some form of PMD compensation. Therefore, in this work we restrict the application of the adaptive Stokes method for metro and access network scenarios where the impact of PMD can be neglected. For these systems, we experimentally compare the performance and convergence speed of the adaptive Stokes and CMA methods. Due to the negligible memory effects experienced by the optical signal, the CMA method can be applied with a single-tap FIR filter, thereby reducing the computational effort while still guaranteeing high accuracy for PolDemux [43].

After the PolDemux technique, the local oscillator frequency offset is compensated with a 4th-power spectral method [44]. Carrier phase recovery is implemented by the Viterbi and Viterbi algorithm for QPSK signal [45] and by the QPSK-partitioning strategy for 16QAM signal [46]. Meanwhile, the BER evaluation is performed by direct error counting over 2^{18} bits.

The experimental setup for the validation of the adaptive Stokes algorithm is presented in Fig. 3.5. Initially, at the transmitter, the light from a 100 kHz ECL at 1549.32 nm was injected in an IQ modulator (IQM) driven by a 12 GSa/s arbitrary waveform generator (AWG), producing a 3.125 Gbaud QPSK or 16-QAM signal ($2^{15} - 1$ PRBS). The IQM driving electrical signal was digitally filtered by a raised-cosine filter with 0.1 roll-off factor. In order to test the U-DWDM scenario, at the transmitter, 3 ECLs are coupled together using an optical coupler. The channel spacing between the three lasers was set to 6.25 GHz for both

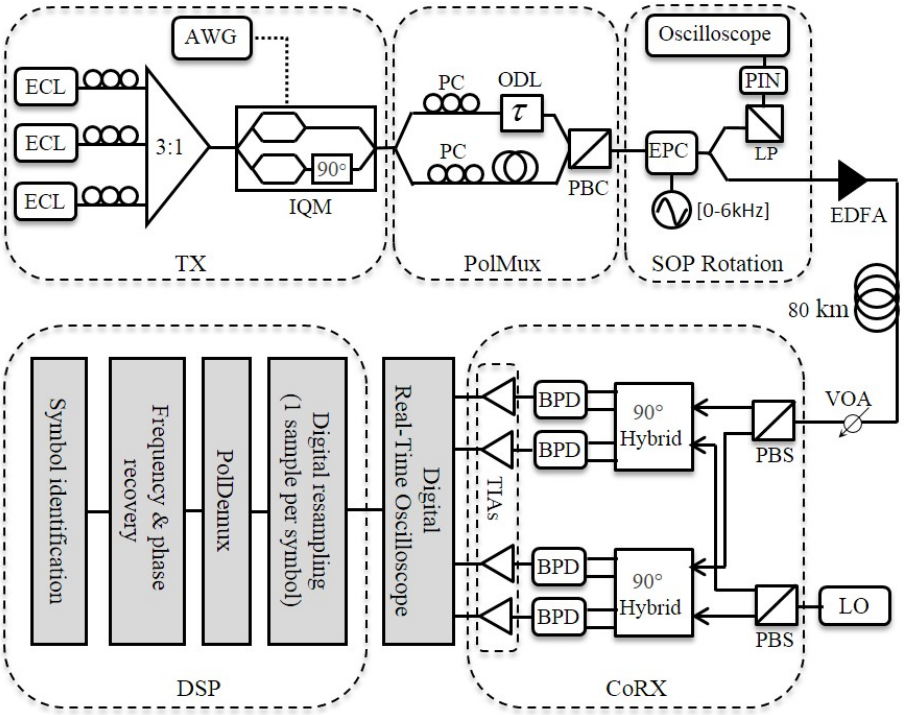

Figure 3.5: Experimental setup for the validation of the adaptive Stokes algorithm. ECL- external cavity laser, AWG- arbitrary waveform generator, IQM- IQ modulator, PC- polarization controller, ODL- optical delay line, PBC/S- polarization beam combiner/splitter, EPC- electrical polarization controller, LP- linear polarizer, EDFA- erbium doped fiber amplifier, VOA- variable optical attenuator, CoRX- coherent receiver, LO- local oscillator, BPD- balanced photo-diode, TIA- transmittance amplifier.

DP-QPSK and DP-16QAM signals. The launch power per channel was set to -3 dBm and -5 dBm for DP-QPSK and DP-16QAM signals, respectively. The DP signal is generated in the optical domain, using an ODL with 69 symbols of delay and a polarization beam combiner (PBC), generating a 12.5 Gbps DP-QPSK or a 25 Gbps DP-16QAM optical signal. To test the potential use of the Stokes algorithm, an electrical polarization controller (EPC) was inserted before the fiber. The EPC has 1 dB insertion loss and is able to change the SOP with a frequency up to 6 kHz. Note that, this 6 kHz polarization rotation is selected due to the limitation of the EPC available in the laboratory. Nevertheless this frequency should be high enough to emulate the kind of perturbations that installed fibers may suffer in the field. Using a coupler after the EPC, one part of the signal was used to monitor the changes of SOP. After the EPC, the signal is transmitted over 80 km of standard single-mode fiber.

At the receiver side, detection was performed using an integrated phase- and polarization-diverse coherent receiver (CoRX). An ECL with 100 kHz linewidth and optical power of 13 dBm was used as a local oscillator. After the CoRX a 50 GSa/s real-time oscilloscope is used to convert the signal into the digital domain.

In order to investigate the impact of fast SOP changes on the performance of the adaptive Stokes algorithm, we begin the analysis by considering a constant polarization rotation of 6 kHz. Initially, experiments are undertaken for 1-channel DP-QPSK and DP-16QAM Nyquist signals at 3.125 Gbaud, in a back-to-back (BTB) scenario.

3.3.1 Optimization of the Step-Size

In order to find the best performance point for the CMA and the adaptive Stokes algorithm, we start by optimizing the step-size parameter μ for both methods, at received optical powers of -42 dBm and -34 dBm for DP-QPSK and DP-16QAM signals, respectively. These received optical powers are near the hard-decision FEC threshold of 3.8×10^{-3} [47] for both modulation formats (see Fig. 3.11).

The μ parameter in the CMA controls the convergence speed of the algorithm [22]. In the adaptive Stokes technique, the step-size is used to adjust the weight of each sample into the orientation change of the normal vector in the 3D Stokes space[13]. Fig. 3.6(a) and Fig. 3.6(b) present BER as a function of the different step-size values for 12.5 Gbps DP-QPSK, and 25 Gbps DP-16QAM signals, respectively, with 6 kHz polarization rotation. The CMA achieved its best performance with a step-size of $\mu = 0.003$, for both modulation formats. For step-sizes higher than 0.003, the performance of the CMA decreases slowly up to the value

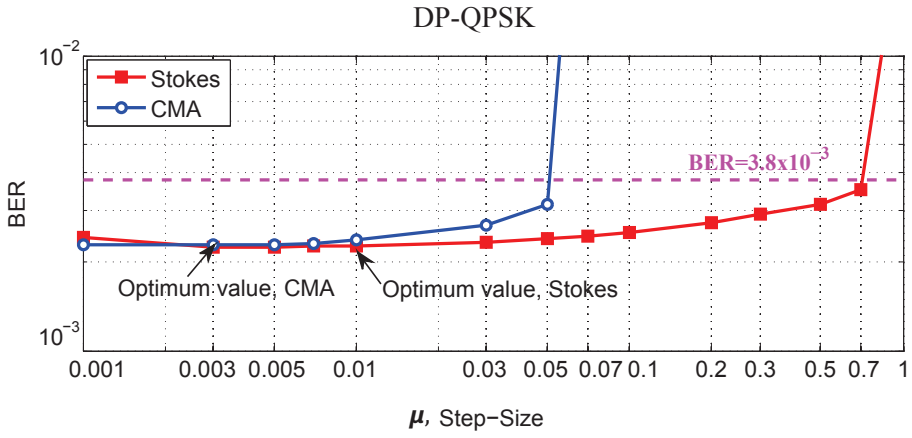

Figure 3.6: Optimization of the step-size parameter for the CMA and the adaptive Stokes algorithm for (a) 12.5 Gbps DP-QPSK with -42 dBm optical power and (b) 25 Gbps DP-16QAM signal with -34 dBm optical power, with 6 kHz polarization rotation. x and y axes are presented in logarithmic scale.

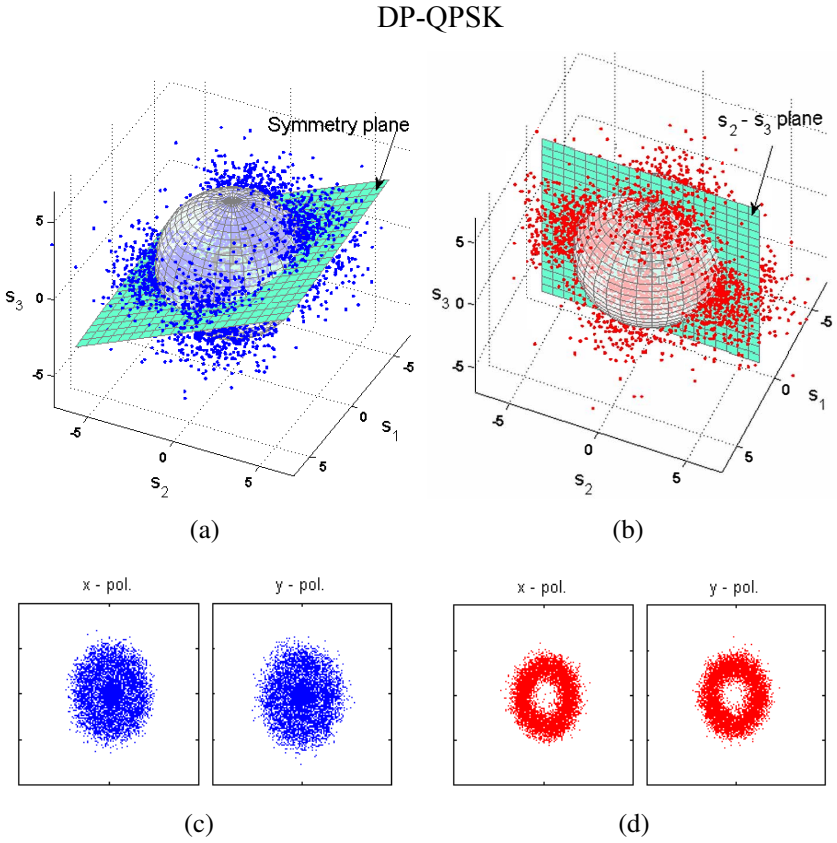

Figure 3.7: Stokes representation in Poincaré sphere for DP-QPSK signal considering a constant frequency rotation of 6 kHz, (a) Stokes space before PolDemux, (b) Stokes space after PolDemux, (c) constellation diagrams before PolDemux, (d) constellation diagrams after PolDemux. In (a) and (b) two symmetry planes are also presented. These results are represented using 6000 samples.

0.05 for DP-QPSK and 0.03 for DP-16QAM. On the other hand, the best performance of the adaptive Stokes is achieved at the value 0.01 for both modulation formats. For step-sizes higher than 0.01, the adaptive Stokes algorithm continues to work with minimal penalty, whereas the BER starts to rise sharply at μ values of 0.7 and 0.07, for DP-QPSK and DP-16QAM, respectively. Therefore, we choose $\mu = 0.003$ for the CMA and $\mu = 0.01$ for the adaptive Stokes algorithm.

Fig. 3.7 illustrates the polarization of the signal samples on the Stokes space, before and after applying the adaptive Stokes PolDemux algorithm, at -42 dBm for a DP-QPSK signal that experienced a constant frequency SOP rotation (6 kHz). Before PolDemux, the four clusters of points have a symmetry plane, also represented in Fig. 3.7(a), misaligned with the plane "$s_2 - s_3$". The normal to such symmetry plane was used into the computation of the inverse matrix (3.31), which was therefore applied to each signal sample. As shown in Fig. 3.7(b), the set of points representing the signal samples SOP after PolDemux have now the plane "$s_2 - s_3$" as the symmetry plane. The constellation diagrams for both x- and y-polarizations, see Fig. 3.7(c) and Fig. 3.7(d), corroborate the accurate accomplishment of the signal PolDemux. Likewise, Fig. 3.8 illustrates the polarization of the signal samples on the Stokes space (at -34 dBm), before and after applying the adaptive Stokes PolDemux

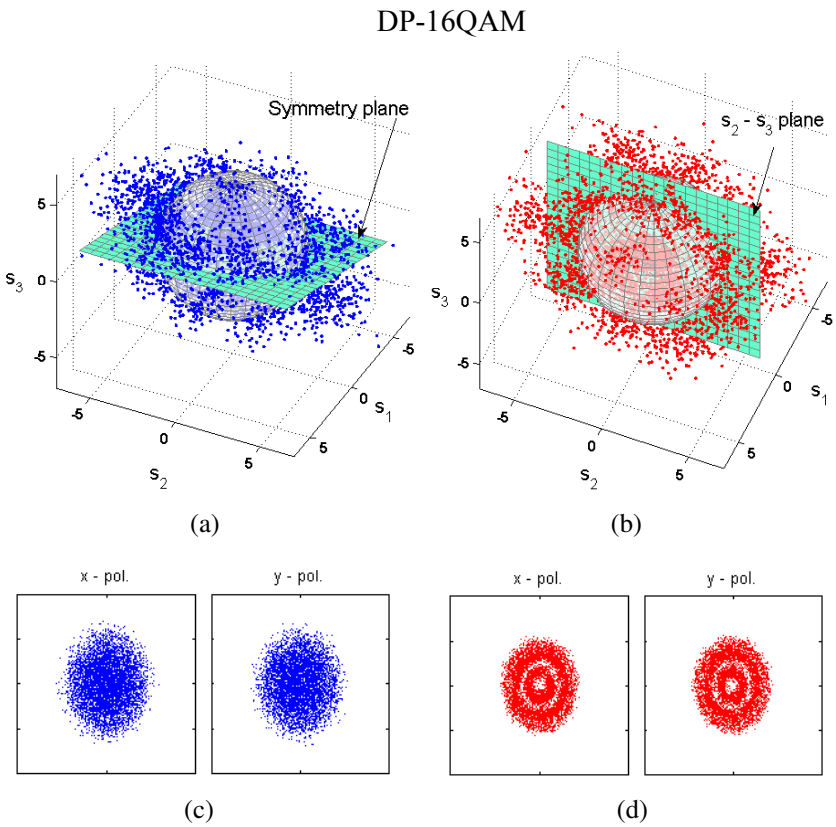

Figure 3.8: Stokes representation in Poincaré sphere for DP-16QAM signal considering a constant frequency rotation of 6 kHz, (a) Stokes space before PolDemux, (b) Stokes space after PolDemux, (c) constellation diagrams before PolDemux, (d) constellation diagrams after PolDemux. In (a) and (b) two symmetry planes are also presented. These results are represented using 6000 samples.

algorithm, for the DP-16QAM signal that experienced a constant frequency SOP rotation (6 kHz). Results also show a realignment of the symmetry plane after PolDemux, even if the number of clusters representing the signal samples SOP are now larger when compared with the DP-QPSK case.

3.3.2 Convergence Speed

In order to compare the convergence speeds of both techniques, we considered the evolution of the inverse matrix entries considering different step-sizes. Fig. 3.9 shows the evolution of the absolute value of the filter coefficients in the inverse matrix, given by (3.14) and (3.31), as a function of the number of received samples for both algorithms. Results correspond to the 12.5 Gbps DP-QPSK signal, considering the same polarization rotation (6 kHz) for different step-size values. Fig. 3.9(a) and Fig. 3.9(b) show the convergence of the CMA and Stokes to the solution and the insets of Fig. 3.9(a) and Fig. 3.9 represent the solutions of both algorithms after convergence.

By increasing the μ parameter, an increment of the noise level is visible in the inset of Fig. 3.9(a) for $\mu = 0.05$, whereas the Stokes algorithm with $\mu = 0.1$ is able to achieve a good tracking with low noise level. The difference of convergence speed for the two algorithms can be

observed by inspection of Fig. 3.9(a) and Fig. 3.9(b). The convergence of the adaptive Stokes algorithm is substantially quicker than that of CMA in their best performance point ($\mu = 0.003$ for CMA and $\mu = 0.01$ for Stokes), i.e. the Stokes algorithm needs a shorter training sequence in order to achieve a stable performance. Note that, although the CMA convergence can also be accelerated by increasing the μ value over 0.003, this comes at the expense of a performance degradation, as evidenced in Fig. 3.6. In contrast, the Stokes algorithm is able to run with a

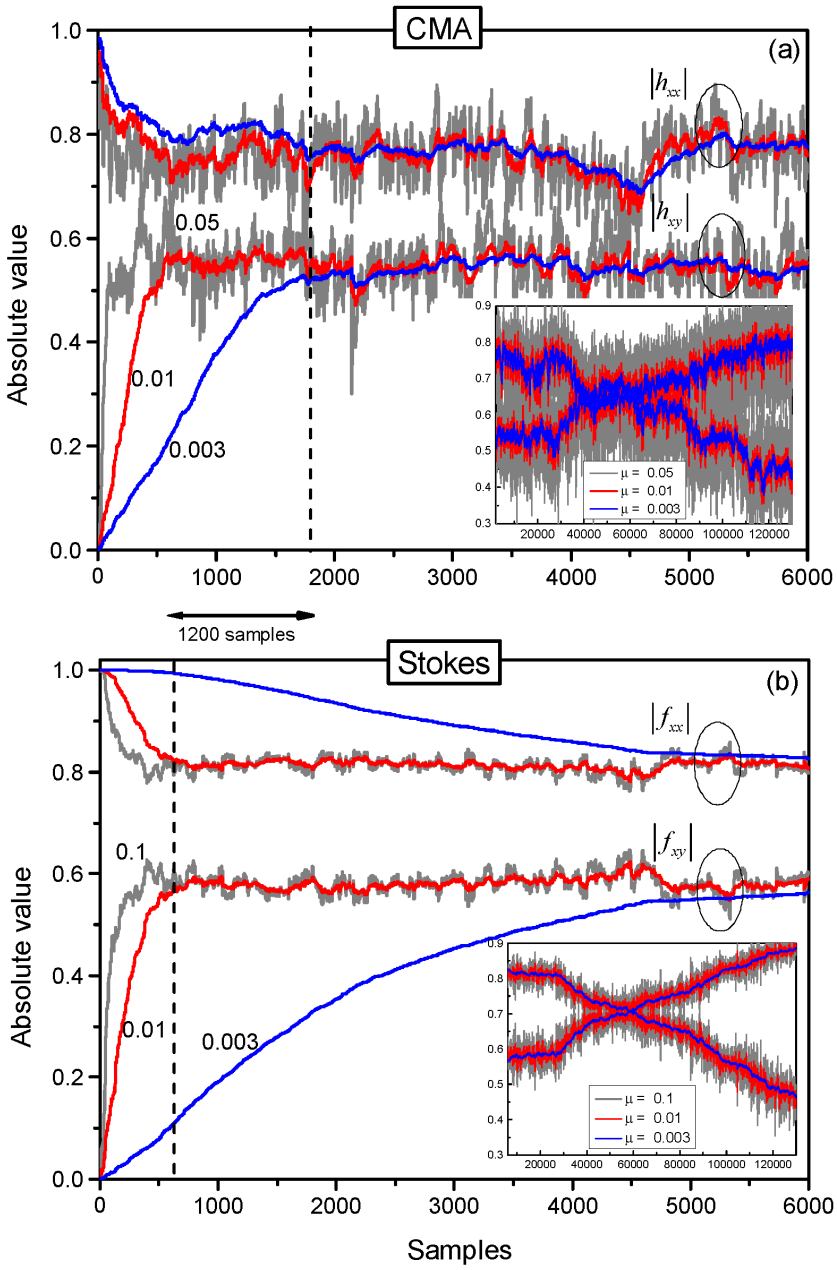

Figure 3.9: Evolution of the absolute value of the filter coefficients for 12.5 Gbps DP-QPSK, (a) CMA, (b) adaptive Stokes algorithm. Dashed lines represent the number of required samples that each algorithm needs to converge.

step-size within the range [0.001 - 0.1] without incurring any substantial performance penalty. Moreover, it is observed that for the DP-QPSK signal, the CMA needs about 1800 samples in order to achieve a stable performance while the adaptive Stokes algorithm needs only 600 samples to converge. In addition, Fig. 3.10(a) and Fig. 3.10(b) depict the absolute value of the filter coefficients in the inverse matrix, given by (3.14) and (3.31), as a function of the number of received samples for the 25 Gbps DP-16QAM signal with the same polarization

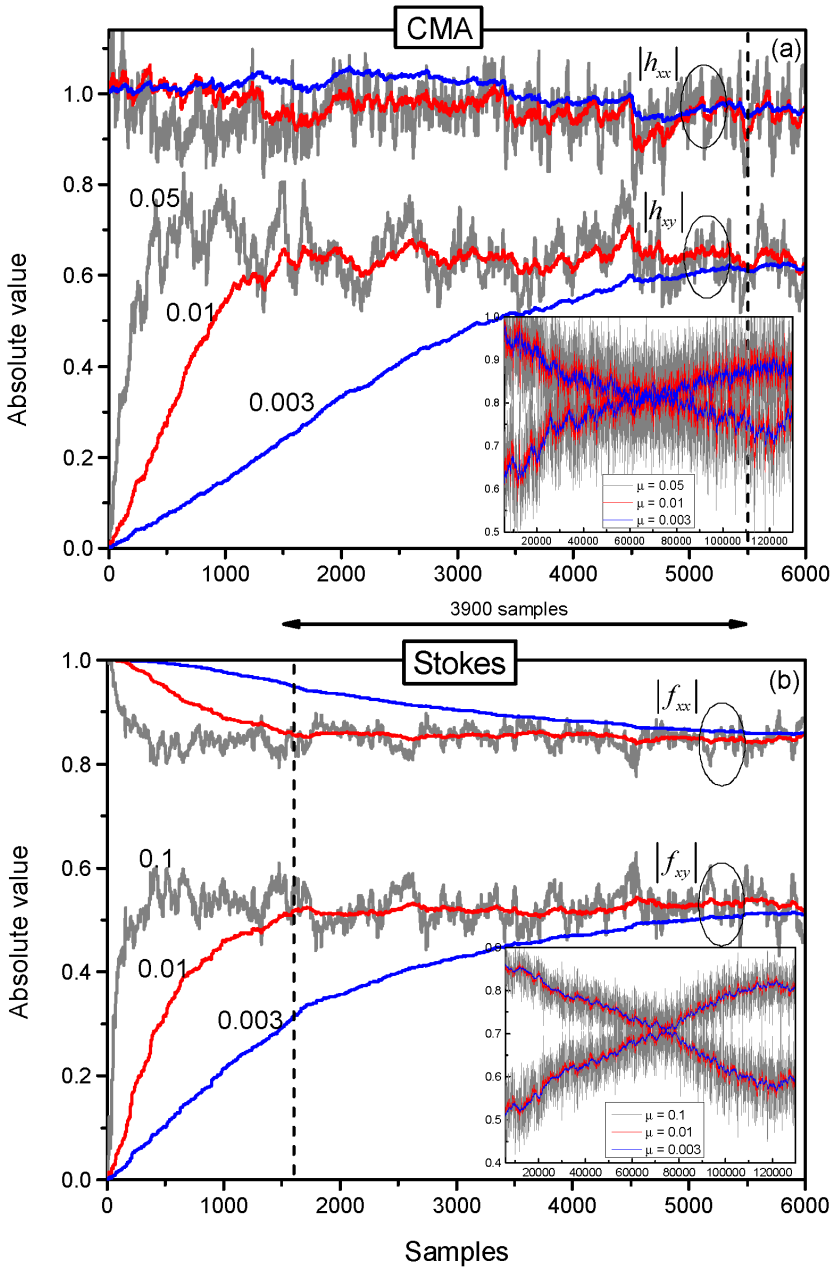

Figure 3.10: Evolution of the absolute value of the filter coefficients for 25 Gbps DP-16QAM, (a) CMA, (b) adaptive Stokes algorithm. Dashed lines represent the number of required samples that each algorithm needs to converge.

rotation (6 kHz) and for different step-size values.

Similarly, for the DP-16QAM signal the adaptive Stokes algorithm also requires a shorter training sequence in order to achieve a stable performance comparing with the CMA. Indeed, Fig. 3.10 shows that the CMA needs more than 5500 samples whereas the adaptive Stokes needs only 1600 samples.

3.3.3 Performance Comparison of CMA and Adaptive Stokes

Experiments in this subsection compare the performance of the adaptive Stokes algorithm and CMA as a function of the input power at the coherent receiver, thus testing the impact of PolDemux subsystem on the receiver sensitivity. Fig. 3.11 shows the results of these experimental investigations for DP-QPSK and DP-16QAM Nyquist signals at 3.125 Gbaud on a BTB scenario in terms of BER vs. received optical power with induced SOP rotation of 6 kHz. For different received optical powers, both algorithms present identical performance for DP-QPSK and DP-16QAM signals. The results indicate that for the DP-QPSK signal, the BER exceeds the hard-decision FEC threshold of 3.8×10^{-3} at a received optical power of -43 dBm and exceeds the soft-decision FEC threshold of 1.5×10^{-2} [48] at -44.5 dBm. In turn, a sensitivity of -34 dBm was achieved for the DP-16QAM signal. The effective data rates of 10 Gbps and 20 Gbps per channel, are achieved up to -44 dBm and -36 dBm for DP-QPSK and DP-16QAM respectively, considering the 1.5×10^{-2} threshold. In addition, the insets of Fig. 3.11 present the constellation diagrams of the adaptive Stokes algorithm for -42 dBm and -34 dBm optical power, respectively.

In order to assess the performance of the adaptive Stokes algorithm in more realistic scenarios, we continued our experiments by measuring the receiver sensitivity for 3-channels

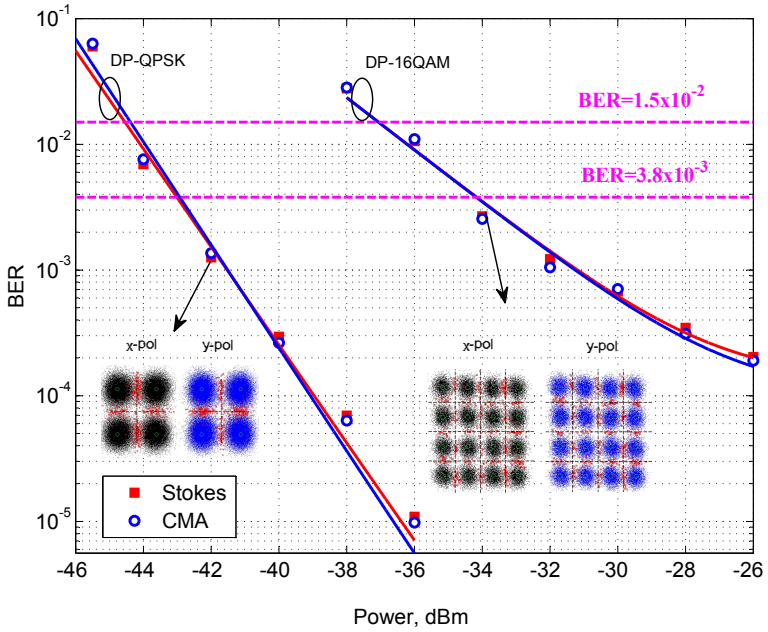

Figure 3.11: BER performance versus received optical power for 12.5 Gbps DP-QPSK and 25 Gbps DP-16QAM in the BTB scenario considering a constant frequency rotation of 6 kHz for the CMA and the adaptive Stokes algorithms. Insets show the constellation diagrams for the adaptive Stokes algorithm at a received optical power near the FEC threshold of 3.8×10^{-3}.

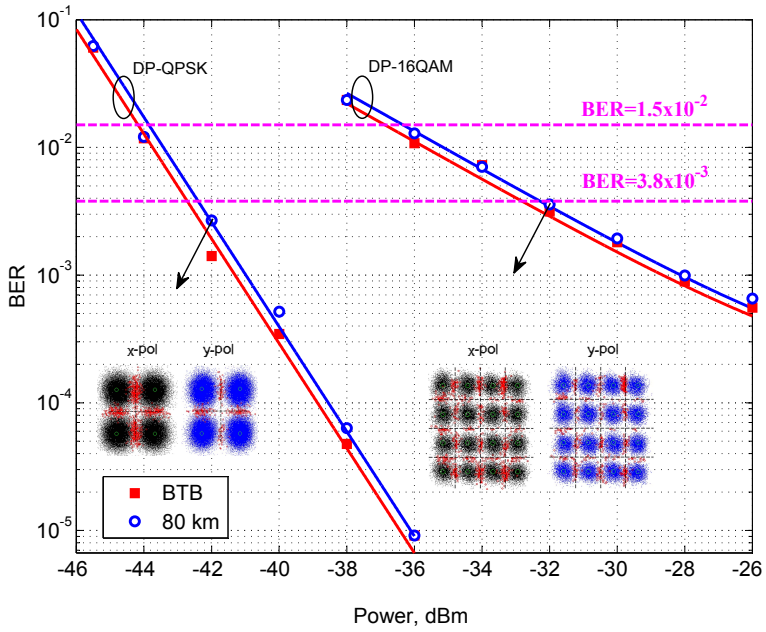

Figure 3.12: Measured BER for the central channel of 3-channels 12.5 Gbps DP-QPSK and 25 Gbps DP-16QAM using the adaptive Stokes algorithm for BTB and 80 km of fiber length. Insets show the constellation diagrams for the adaptive Stokes algorithm near the FEC threshold of 3.8×10^{-3}, after 80 km of SSM fiber.

DP-QPSK and DP-16QAM Nyquist UDWDM systems at 3.125 Gbaud with 6.25 GHz channel spacing. These analyses are considered for BTB and 80 km of SSM fiber transmission, using the EPC in the scrambler mode. Note that, since the adaptive Stokes method is sensitive to PMD, the experimental setup in this chapter is restricted to narrow bandwidth and short distance scenarios, in order to reduce the impact of such effect in the optical signal. Fig. 3.12, presents the impact of decreased transmission power on the receiver sensitivity for 3-channels 12.5 Gbps DP-QPSK and 25 Gbps DP-16QAM signals in a BTB and transmission scenario. The insets of Fig. 3.12, present constellation diagrams of the adaptive Stokes algorithm after 80 km of fiber length, for -42 dBm and -32 dBm received optical powers. The total power penalty is negligible between the BTB and transmission scenarios. A sensitivity penalty below 0.5 dB can be observed at the BER of 3.8×10^{-3}, when using 80 km of SSM fiber compared to the BTB scenario for 3-channels.

In addition, Fig. 3.13(a) and Fig. 3.13(b) show the spectra of the 3-channel signal for 3.125 Gbaud DP-QPSK, and DP-16QAM with 6.25 GHz channel spacing that were obtained by an optical spectrum analyzer (OSA) with a 100 MHz resolution, before the fiber.

3.4 Final remarks

In this chapter we discussed about polarization representation of the light and review its representation in the Jones and Stokes Formalism. Different polarization demultiplexing techniques, CMA and adaptive Stokes algorithm, for reversing the mixing of polarization components in the DSP, were explained. Then we experimentally validated the adaptive Stokes algorithm considering DP-QPSK and DP-16QAM modulation formats. The performance and

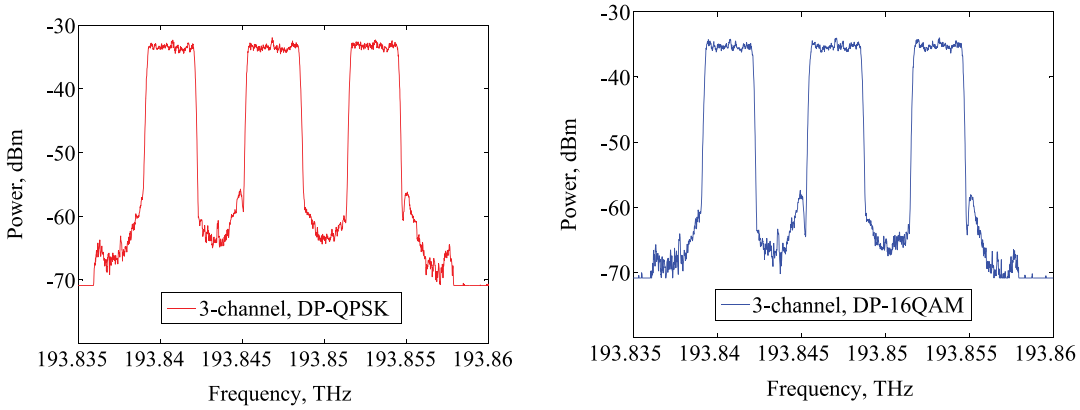

Figure 3.13: The measured optical spectra (resolution 100 MHz) are shown for (a) 3-channels, DP-QPSK and (b) 3-channels, DP-16QAM.

convergence speed of the adaptive Stokes technique were compared with conventional CMA for 1-channel DP-QPSK and DP-16QAM Nyquist signals at 3.125 Gbaud, with constant frequency SOP rotation (6 kHz) in a back-to-back scenario. Despite both algorithms can achieve identical performance by properly adjusting their step-size, the convergence of the adaptive Stokes algorithm has been found to be approximately three times quicker than that of CMA. Due to the transparency of this technique, we demonstrated that the Stokes PolDemux is a suitable solution for metro and access networks with flexible transceivers based on higher-level M-ary signals.

Bibliography

[1] K. Kikuchi, "Fundamentals of coherent optical fiber communications," *Journal of Lightwave Technology*, vol. 34, no. 1, pp. 157–179, 2016.

[2] E. Collett, "Polarized light. fundamentals and applications," *Optical Engineering, New York: Dekker*, 1992.

[3] R. C. Jones, "A new calculus for the treatment of optical systems. I. description and discussion of the calculus," *Journal of the Optical Society of America*, vol. 31, no. 7, pp. 488–493, 1941.

[4] K. Perlicki, "Polarization effects in optical fiber links," in *Book: Advances in Optical Fiber Technology: Fundamental Optical Phenomena and Applications*. InTech, 2015.

[5] A. Fymat, "Jones matrix representation of optical instruments. I: beam splitters," *Applied optics*, vol. 10, no. 11, pp. 2499–2505, 1971.

[6] G. G. Stokes, "On the composition and resolution of streams of polarized light from different sources," *Transactions of the Cambridge Philosophical Society*, vol. 9, p. 399, 1851.

[7] N. J. Muga, "Polarization effects in fiber-optic communication systems," Ph.D. dissertation, Universidade de Aveiro (Portugal), 2011.

[8] S. G. Evangelides, L. F. Mollenauer, J. P. Gordon, and N. S. Bergano, "Polarization multiplexing with solitons," *Journal of Lightwave Technology*, vol. 10, no. 1, pp. 28–35, 1992.

[9] J. N. Damask, *Polarization optics in telecommunications*. Springer Science & Business Media, 2004, vol. 101.

[10] M. Karlsson, J. Brentel, and P. A. Andrekson, "Long-term measurement of PMD and polarization drift in installed fibers," *Journal of Lightwave Technology*, vol. 18, no. 7, p. 941, 2000.

[11] G. Xavier, G. V. de Faria, G. Temporão, and J. Von der Weid, "Full polarization control for fiber optical quantum communication systems using polarization encoding," *Optics Express*, vol. 16, no. 3, pp. 1867–1873, 2008.

[12] C. white paper, "Limitations of transmission distances over multimode fiber," Tech. Rep., 2008.

[13] N. J. Muga and A. N. Pinto, "Adaptive 3-D Stokes space-based polarization demultiplexing algorithm," *Journal of Lightwave Technology*, vol. 32, no. 19, pp. 3290–3298, 2014.

[14] N. J. Muga and A. N. Pinto, "Digital PDL compensation in 3D Stokes space," *Journal of Lightwave Technology*, vol. 31, no. 13, pp. 2122–2130, 2013.

[15] J. P. Gordon and H. Kogelnik, "PMD fundamentals: Polarization mode dispersion in optical fibers," *Proceedings of the National Academy of Sciences*, vol. 97, no. 9, pp. 4541–4550, 2000.

[16] G. Foschini and C. Poole, "Statistical theory of polarization dispersion in single mode fibers," *Journal of Lightwave Technology*, vol. 9, no. 11, pp. 1439–1456, 1991.

[17] W. Shieh, X. Yi, Y. Ma, and Y. Tang, "Theoretical and experimental study on PMD-supported transmission using polarization diversity in coherent optical OFDM systems," *Optics Express*, vol. 15, no. 16, pp. 9936–9947, 2007.

[18] Z. Yu, X. Yi, J. Zhang, M. Deng, H. Zhang, and K. Qiu, "Modified constant modulus algorithm with polarization demultiplexing in Stokes space in optical coherent receiver," *Journal of Lightwave Technology*, vol. 31, no. 19, pp. 3203–3209, Oct. 2013.

[19] K. Kikuchi, "Coherent optical communications: Historical perspectives and future directions," in *High Spectral Density Optical Communication Technologies*. Springer, 2010, pp. 11–49.

[20] I. Roudas, A. Vgenis, C. S. Petrou, D. Toumpakaris, J. Hurley, M. Sauer, J. Downie, Y. Mauro, and S. Raghavan, "Optimal polarization demultiplexing for coherent optical communications systems," *Journal of Lightwave Technology*, vol. 28, no. 7, pp. 1121–1134, 2010.

[21] F. P. Guiomar, S. B. Amado, A. Carena, G. Bosco, A. Nespola, A. L. Teixeira, and A. N. Pinto, "Fully blind linear and nonlinear equalization for 100G PM-64QAM optical systems," *Journal of Lightwave Technology*, vol. 33, no. 7, pp. 1265–1274, Apr 2015.

[22] S. J. Savory, G. Gavioli, E. Torrengo, and P. Poggiolini, "Impact of interchannel nonlinearities on a split-step intrachannel nonlinear equalizer," vol. 22, no. 10, pp. 673–675, 2010.

[23] B. C. Thomsen, R. Maher, D. S. Millar, and S. J. Savory, "Burst mode receiver for 112 Gb/s DP-QPSK with parallel DSP," *Optics Express*, vol. 19, no. 26, pp. B770–B776, Dec. 2011.

[24] H. Zhang, Z. Tao, L. Liu, S. Oda, T. Hoshida, and J. Rasmussen, "Polarization demultiplexing based on independent component analysis in optical coherent receivers," in *Proc. European Conf. on Optical Communication (ECOC)*, Sept 2008, pp. 1–2.

[25] A. Vgenis, C. Petrou, C. Papadias, I. Roudas, and L. Raptis, "Nonsingular constant modulus equalizer for PDM-QPSK coherent optical receivers," *Photonics Technology Letters*, vol. 22, no. 1, pp. 45–47, Jan. 2010.

[26] G. Bosco, M. Visintin, P. Poggiolini, and F. Forghieri, "A novel update algorithm in Stokes space for adaptive equalization in coherent receivers," in *Proc. Optical Fiber Communication Conf. and Exposition (OFC)*, 2014, paper Th3E.6.

[27] G. Bosco, M. Visintin, P. Poggiolini, A. Nespola, M. Huchard, and F. Forghieri, "Experimental demonstration of a novel update algorithm in Stokes space for adaptive equalization in coherent receivers," in *Proc. European Conf. on Optical Communication (ECOC)*, Sep. 2014, paper Tu.3.3.6.

[28] D. Lavery, M. Paskov, R. Maher, S. J. Savory, and P. Bayvel, "Modified radius directed equaliser for high order QAM," pp. 1–3, Sep. 2015.

[29] S. J. Savory, "Digital coherent optical receivers: algorithms and subsystems," *Selected Topics in Quantum Electronics, IEEE Journal of*, vol. 16, no. 5, pp. 1164–1179, 2010.

[30] B. Szafraniec, B. Nebendahl, and T. Marshall, "Polarization demultiplexing in Stokes space," *Optics Express*, vol. 18, no. 17, pp. 17 928–17 939, Aug. 2010.

[31] S. Ziaie, N. J. Muga, F. P. Guiomar, G. M. Fernandes, R. M. Ferreira, A. Shahpari, A. L. Teixeira, and A. N. Pinto, "Experimental assessment of the adaptive Stokes space-based polarization demultiplexing for optical metro and access networks," *Journal of Lightwave Technology*, vol. 33, no. 23, pp. 4968–4974, December 2015.

[32] Z. Yu, X. Yi, Q. Yang, M. Luo, J. Zhang, L. Chen, and K. Qiu, "Polarization demultiplexing in Stokes space for coherent optical PDM-OFDM," *Optics Express*, vol. 21, no. 3, pp. 3885–3890, Feb. 2013.

[33] Z. Yu, X. Yi, J. Zhang, D. Zhao, and K. Qiu, "Experimental demonstration of polarization-dependent loss monitoring and compensation in Stokes space for coherent optical PDM-OFDM," *Journal of Lightwave Technology*, vol. 32, no. 23, pp. 4528–4533, Dec 2014.

[34] D. Godard, "Self-recovering equalization and carrier tracking in two-dimensional data communication systems," *Communications, IEEE Transactions on*, vol. 28, no. 11, pp. 1867 – 1875, 1980.

[35] R. Johnson, P. Schniter, T. J. Endres, J. D. Behm, D. R. Brown, and R. A. Casas, "Blind equalization using the constant modulus criterion: A review," *Proceedings of the IEEE*, vol. 86, no. 10, pp. 1927–1950, 1998.

[36] S. J. Savory, "Digital filters for coherent optical receivers," *Optics Express*, vol. 16, no. 2, pp. 804–817, 2008.

[37] K. Kikuchi, "Performance analyses of polarization demultiplexing based on constant-modulus algorithm in digital coherent optical receivers," *Optics Express*, vol. 19, no. 10, pp. 9868–9880, May 2011.

[38] I. Fatadin, D. Ives, and S. J. Savory, "Blind equalization and carrier phase recovery in a 16-QAM optical coherent system," *Journal of lightwave technology*, vol. 27, no. 15, pp. 3042–3049, 2009.

[39] M. S. Faruk and S. J. Savory, "Digital signal processing for coherent transceivers employing multilevel formats," *Journal of Lightwave Technology*, vol. 35, no. 5, pp. 1125–1141, 2017.

[40] M. J. Ready and R. P. Gooch, "Blind equalization based on radius directed adaptation," pp. 1699–1702, 1990.

[41] S. S. Haykin, B. Widrow, and B. Widrow, *Least-mean-square adaptive filters*. Wiley Online Library, 2003, vol. 31.

[42] N. J. Muga, F. P. Guiomar, and A. N. Pinto, "Stokes space based digital PolDemux for polarization switched-QPSK signals," *Proc. Conf. on Lasers and Electro-Optics (CLEO)*, 2013.

[43] C. Kottke, J. K. Fischer, R. Elschner, F. Frey, J. Hilt, C. Schubert, D. Schmidt, Z. Wu, and B. Lankl, "Coherent UDWDM PON with joint subcarrier reception at OLT," *Optics Express*, vol. 22, no. 14, Jul. 2014.

[44] S. Hoffmann, S. Bhandare, T. Pfau, O. Adamczyk, C. Wordehoff, R. Peveling, M. Porrmann, and R. Noe, "Frequency and phase estimation for coherent QPSK transmission with unlocked DFB lasers," *Photonics Technology Letters*, vol. 20, no. 18, pp. 1569–1571, Sep 2008.

[45] A. Viterbi, "Nonlinear estimation of PSK-modulated carrier phase with application to burst digital transmission," *IEEE Transactions on Information Theory*, vol. 29, no. 4, pp. 543–551, July 1983.

[46] I. Fatadin and S. J. Savory, "DSP techniques for 16-QAM coherent optical systems," in *Photonics Society Summer Topical Meeting Series, 2010 IEEE*, ser. MA4.2, 2010, pp. 22 –23.

[47] "Forward error correction for high bit-rate DWDM submarine systems," *ITU-T Rec. G.975.1*, Feb. 2004.

[48] F. Chang, K. Onohara, and T. Mizuochi, "Forward error correction for 100 G transport networks," *IEEE Commun. Mag*, vol. 48, no. 3, pp. S48–S55, March 2010.

Chapter 4

Coherent U-DWDM Based on Adaptive Stokes

In order to ensure commercial viability and reduce cost per bit, optical metro and access networks should follow the path of simple and robust solutions using advanced optical components and systems. In addition, flexibility and spectral efficiency beside of optimization of the network concept are the most important keys for the design of these optical networks which enable these technologies for software defined networking architectures. Furthermore, resiliency and dynamic power range in last mile optical networks should be provided. Coherent U-DWDM using dual-polarization modulation formats can fully utilize the bandwidth and increase the transmission capacity-reach, while still guaranteeing sophisticated and high-performance transceivers.

In this chapter, we experimentally demonstrate a dual-polarization coherent U-DWDM system with support to optical-wireless link enabled by adaptive Stokes space PolDemux in off-line and real-time implementation. The resiliency of the adaptive Stokes PolDemux technique is evaluated in terms of nonlinearity and optical power budget as well as dynamic power range. In section 4.1, the performance of a flexible optical metro link based on Nyquist pulse shaping U-DWDM system and hybrid optical signals is evaluated. Then in section 4.2, we experimentally implement the adaptive Stokes technique over a bidirectional optical metro network. The real-time implementation of adaptive Stokes algorithm is depicted in section 4.3. Transceiver performance in terms of complexity and sensitivity also is evaluated in this section. And finally, the main conclusions of this chapter are summarized in section 4.4.

4.1 Flexible U-DWDM Systems

Optical metro networks are coming under increasing pressure from heterogeneous massive traffic growth as well as different types of end users to evolve from star configurations to ring category. A U-DWDM system can be an essential technology to upgrade current deployed PON infrastructures to the oncoming systems in order to support high number of users with several wavelength channels with a few channels spacing [1], [2]. Employing a coherent system, which provides very high wavelength selectivity, allows using such a dense spacing without highly elaborated wavelength filters.

On the other hand, using bidirectional mesh configurations as the one shown in Fig. 4.1, all-optical merged networks with different capacities, bandwidths and adaptive distances can

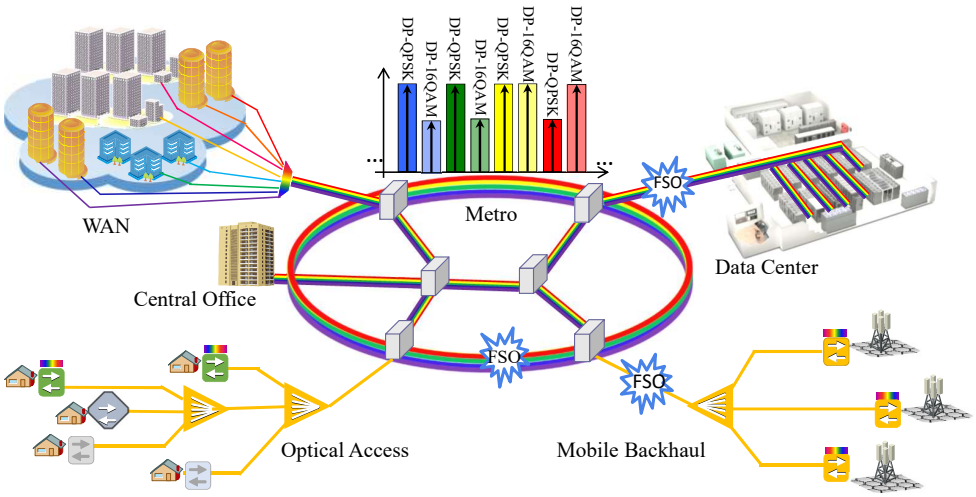

Figure 4.1: Exemplary topology of a flexible optical metro-access network.

be connected, enabling fast and efficient provisioning of high data rate optical paths. In this context, support to flexible grids and data rates, as well resiliency to high dynamic power range are increasingly important issues for the design of this kind of networks. Meanwhile, free space optics links have attracted great attention within the research community as a temporary, fast and cost-effective solution for the network resiliency without limitation in bandwidth and type of the network configuration [3], [4]. In addition, in optical metro networks based on mesh topology, any signal with different optical powers and modulation formats can be added to the system according to the load of the network. Therefore, the performance of high spectral efficiency systems in a flexible network should be characterized. It has been shown that coherent U-DWDM together with dual-polarization pulse shaped multi-level modulation formats and DSP enable high SE, excellent sensitivity and selectivity in optical metro and access networks [5], [6].

In this section, we evaluate the performance of a flexible optical link based on Nyquist pulse shaping U-DWDM (6.25 GHz ITU-T grid) implemented by DP modulation formats and DSP based on the adaptive Stokes PolDemux algorithm. The hybrid optical signals based on DP-QPSK and DP-16QAM modulation formats are transmitted over up to 80 km of SSM fiber plus 54 m outdoor FSO link, as well as field-deployed fiber. The system performance in terms of sensitivity and resilience to dynamic power range (DPR) is assessed by counting the BER.

Fig. 4.2, presents the experimental setup proposed to characterize a flexible hybrid bit rate and distribution system based on Nyquist shaping U-DWDM and the adaptive Stokes PolDemux method. At the transmitter, the light from a 100 kHz ECL was injected in a MZM driven by 12.5 GHz RF signals to generate multi-tones. Using a wavelength selective switch (WS), 5 flat channels were filtered and selected. These 5 tones were fed into an IQM, driven by a 12 GSa/s AWG, producing a 3.125 Gbaud QPSK or 16QAM signal (2^{15} PRBS) and digitally filtered by a raised-cosine filter with 0.1 roll-off factor. The signal was separated into two polarizations (69 symbols delayed for de-correlation purposes) using an ODL, and then multiplexed in polarization again by a polarization beam combiner, creating dual-polarization 12.5 and 25 Gbps DP-QPSK and DP-16QAM, respectively. Combining 4 ECL lasers with 12.5 GHz frequency spacing and feeding it to the second IQM driven by a 65 GSa/s AWG,

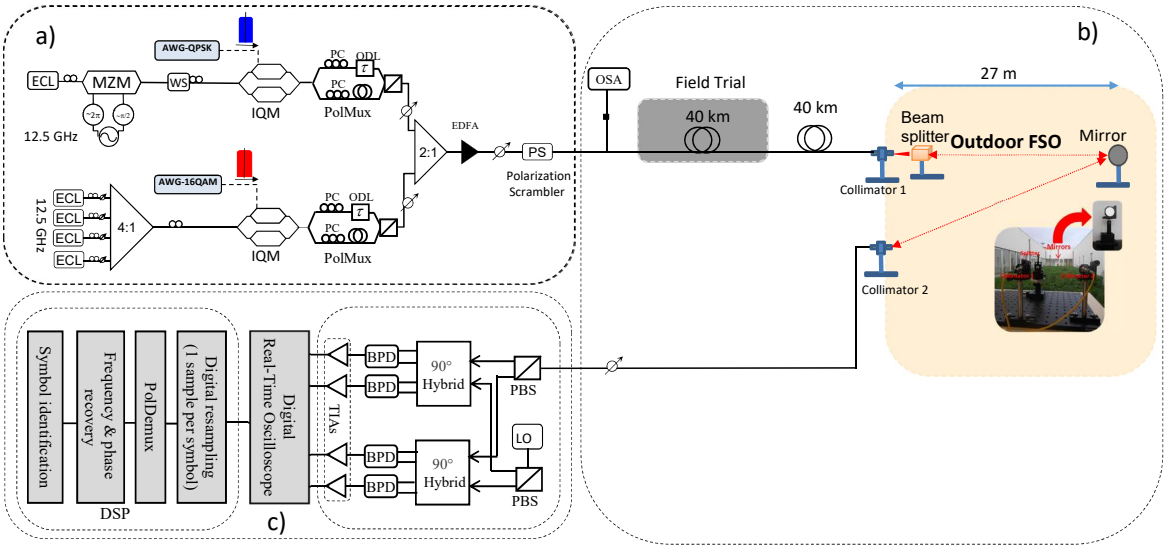

Figure 4.2: (a) Experimental setup for flexible transmission; (b) Transmission links including 80-km SSM fiber, Field trial link and FSO; (c) Coherent receiver and DSP subsystems.

4×3.125 Gbaud QPSK or 16QAM signals were generated. In the PolMux part, these signals were polarization multiplexed and then interleaved with the previous 5 channels by means of a coupler. The optical spectrum of these 9 channels at the input of the fiber is shown in Fig. 4.3. The launch power at the fiber input for 9 channels was set by an EDFA and a VOA prior to the polarization scrambler and the transmission link.

The transmission part was based on 80 km fiber, field trial plus 40 km fiber and 80 km plus FSO. We used installed fiber in Aveiro city, Portugal, plus 40 km of SSM fiber in the lab. The FSO link with total loss of 8 dB was based on 54 m outdoor optical wireless link that included two collimators, polarization independence beam splitter and concave mirror. Using a beam splitter we were able to divide the FSO link into two links. Note that we only analyze the straight direction as shown in Fig. 4.2 (b). At the receiver side, U-DWDM signals were detected using an integrated phase- and polarization-diverse coherent receiver followed by a 50 GSa/s real-time scope. An ECL with 13 dBm optical power and 100 kHz linewidth was

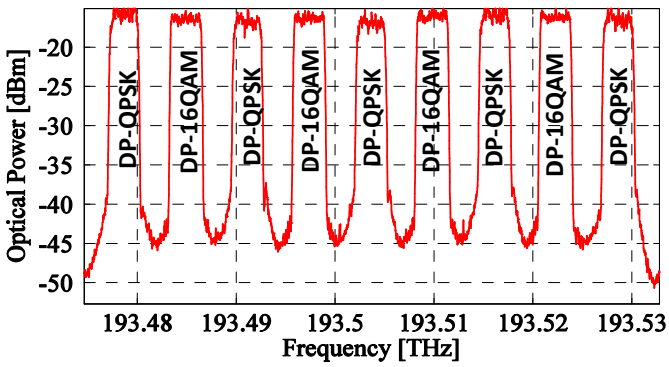

Figure 4.3: Spectrum of 3.125 Gbaud DP-QPSK and DP-16QAM U-DWDM channels with 6.25 GHz channel spacing.

Figure 4.4: Satellite view of the deployed SSM fiber between Instituto de Telecomunicações and two sites of Portugal Telecome in Aveiro, Portugal.

used as a local oscillator.

The DSP chain was implemented offline using MATLAB, and comprised digital resampling, PolDemux, and frequency and carrier phase recovery subsystems, as depicted in Fig. 4.2 (c). The electrical output signal was resampled to 1 sample per symbol. In order to accomplish a robust, flexible and format-transparent separation of the mixed signals transmitted in the two orthogonal polarizations, we used the adaptive Stokes space based PolDemux algorithm. By representing data in the Stokes space, the algorithm finds a best fitting plane, whose normal is then employed into the computation of the inverse polarization rotation matrix of the channel.

The installed fiber in Aveiro city, Portugal, which mentioned here as Field trial, is an optical connection with a total length of 8.4 km SSM fiber between Instituto de Telecomunicações

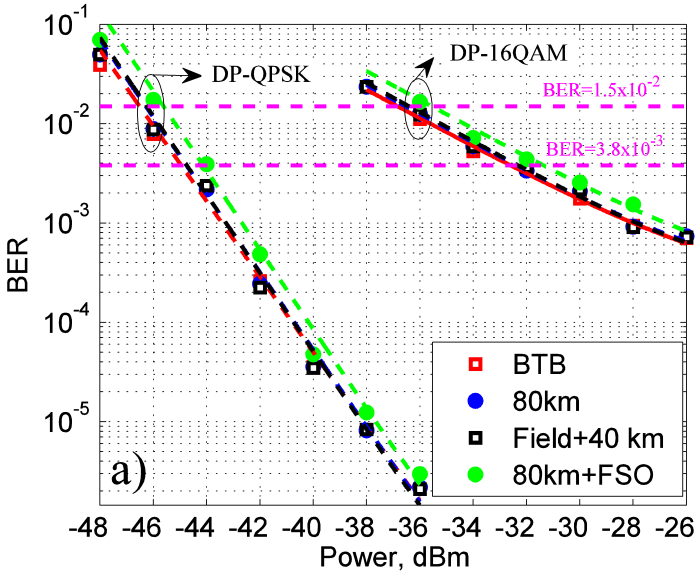

Figure 4.5: BER performance versus received optical power for 12.5 Gbps DP-QPSK and 25 Gbps DP-16QAM in the BTB, 80 km, 80 km plus FSO and field trial transmissions.

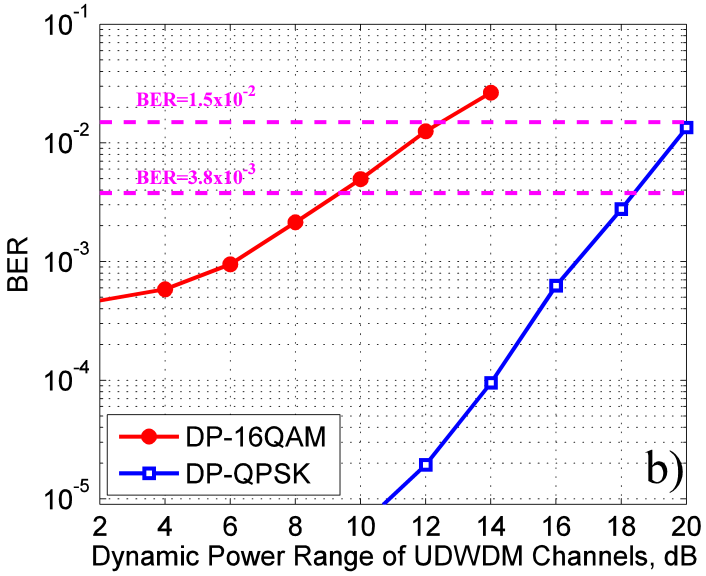

Figure 4.6: Measured BER for the central channel of U-DWDM channels vs. DPR in the input of 80 km fiber.

and two sites of Portugal Telecom, the satellite view can be seen in Fig. 4.4.

In order to verify and assess the performance of the adaptive Stokes algorithm, we measured BER as a function of the receiver input power per multi-channel for BTB, transmission scenarios over 80 km fiber, FSO links and field-trial, results can be seen in Fig. 4.5. The launched optical power per channel in the input of fiber was set to -5 dBm. Results show an acceptable -45 and -32 dBm sensitivity considering a FEC-compatible BER=3.8×10^{-3} for DP-QPSK and DP-16QAM channels, respectively. For the hybrid optical wireless scenario, due to fluctuation of optical power, we observed 1 dB penalty in receiver sensitivity. Using soft-decision FEC (1.5×10^{-2}), the receiver sensitivities of -46 and -36 dBm are achieved for 10 Gbps DP-QPSK and 20 Gbps DP-16QAM, respectively.

Fig. 4.6 depicts the DPR of the system, which characterizes the maximum power unbalance between adjacent channels. For this purpose, we fixed the transmitted optical power of DP-QPSK/ DP-16QAM channels and changed the launched power of the DP-16QAM/DP-QPSK signals. The difference between powers gives the DPR. Considering soft-decision FEC, the BER measurements present 20 and 12 dB DPR between channels for DP-QPSK and DP-16QAM channels, respectively. Fig. 4.7 (a)-(d) also present the optical spectra in the input of fiber and the electrical spectra after the DSP for DP-QPSK channels with 20 dB DPR and DP-16QAM channels with 12 dB DPR.

4.2 Bidirectional U-DWDM Systems

In this section, we experimentally implement the adaptive Stokes algorithm in bidirectional ultra-dense wavelength-division-multiplexed optical metro networks. BER measurement is used to assess the quality of DP-QPSK and DP-16QAM signals in back-toback and after 80 km of SSM fiber. In addition, the resiliency of the optical metro network based on Stokes PolDemux technique is evaluated over hybrid optical fibre and free space optical link. In bidirectional

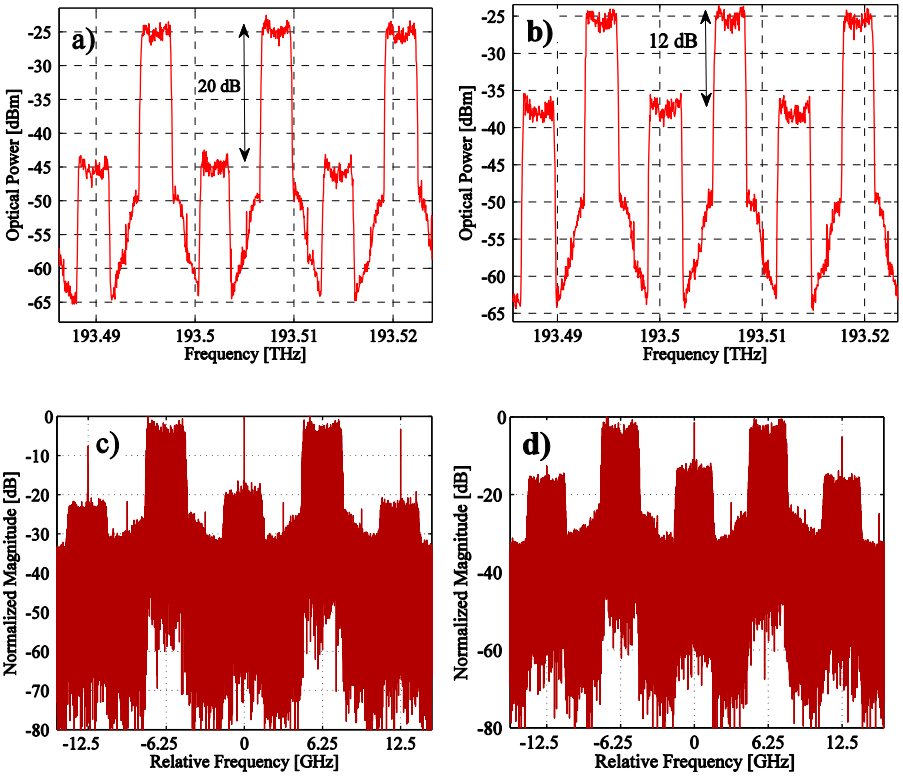

Figure 4.7: Optical spectra in the input of fiber for (a) DP-QPSK channels (b) DP-16QAM channels; the electrical spectra after the DSP for (c) 20 dB DPR of DP-QPSK channels and (d) 12 dB DPR of DP-16QAM channels.

U-DWDM systems, the downstream (DS) and upstream (US) signals are transmitted in the fibre simultaneously and in the opposite direction with small frequency spacing [5], [7]. The reason to use the US channel near to the respective DS channel is due to heterodyne detection on the OLT and ONU, and using one laser for both transmitter and receivers.

Using Nyquist pulse shaping and proper raised-cosine filtering, it is possible to reduce channel spacing down to the baud rate. However back reflections from opposite directions are one important issue that must be considered in the DP U-DWDM system based on the adaptive PolDemux technique. Moreover, in bidirectional FSO links the reflection from the lenses and even free space can increase the effect of back reflection in the receiver part of each side. Fig. 4.8 shows a bidirectional hybrid optical-wireless metro network for transmission of flexible U-DWDM systems based on DP approach with advanced modulation formats. In this section, taking advantage of Nyquist pulse shaped U-DWDM (6.25 GHz ITU-T grid) implemented by dual-polarization modulation formats, we experimentally implement the adaptive Stokes technique over a bidirectional optical metro network. The optical signals based on DP-QPSK and DP-16QAM modulation formats are transmitted over up to 80 km SSM fiber plus 54 m outdoor FSO link. Its performance is evaluated through BER calculations regarding reach, back reflection and flexibility.

At the OLT, the light from a 100 kHz linewidth ECL was injected in a MZM driven by 6.25 GHz RF signals to generate multi-tones. Note that, the optical comb used in the OLT transmitter is due to laboratorial restrictions (insufficient number of lasers with 6.25 GHz

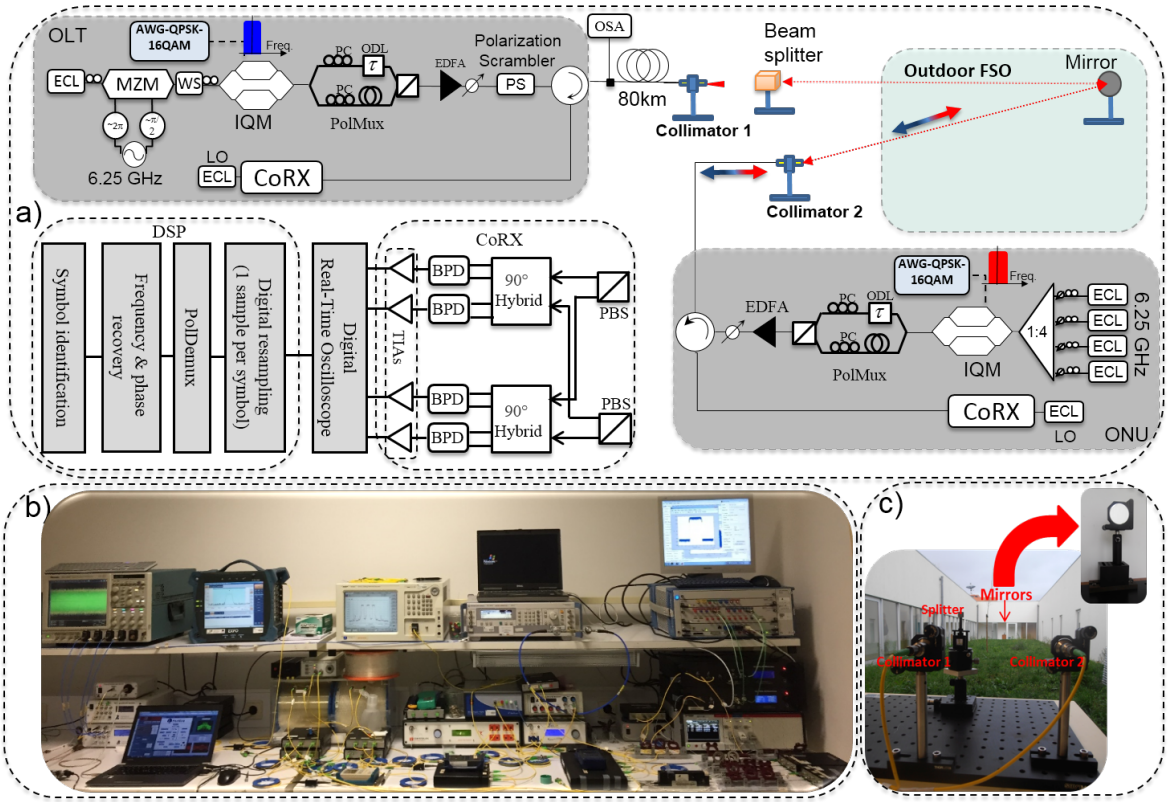

Figure 4.8: a) Bi-directional experimental setup and DSP subsystems, b) laboratory infrastructure, c) outdoor FSO setup. ECL- external cavity laser, AWG- arbitrary waveform generator, MZM- Mach-Zehnder modulator, WS- waveshaper, OSA- optical spectrum analyzer, IQM- IQ modulator, PC- polarization controller, ODL- optical delay line, PBC/S polarization beam combiner/splitter, EDFA- erbium-doped fiber amplifier, VOA- variable optical attenuator, CoRX- coherent receiver, LO- local oscillator, BPD- balanced photo-diode, TIA- transmittance amplifier.

channel spacing). The multi-tones were filtered by a WS (Finisar 4000s) to select 6 tones within 2 dB of power flatness. These wavelengths were fed into an IQ modulator, driven by a 12 GSa/s AWG, producing a 3.125 Gbaud QPSK or 16QAM signal (2^{15} PRBS) and digitally filtered by a raised-cosine filter with 0.1 roll-off factor. The signal was separated into two polarizations (69 symbols delayed for de-correlation purposes) using an ODL, and then multiplexed in polarization again by a polarization beam combiner, creating a dual-polarization 12.5 Gbps and 25 Gbps DP-QPSK and DP-16QAM, respectively. The launch power at the fibre input for 6 channels was set by an EDFA and a VOA prior to a polarization scrambler and circulator. The launch power per channel was set to -3 and -5 dBm for DP-QPSK and DP-16QAM signals, respectively. Using a polarization scrambler, the polarization state of each 6 channels was rotated randomly. Fig. 4.9 (a) presents the downstream spectrum of 6 channel 12.5 Gbps DP-QPSK or 25 Gbps DP-16QAM, which were obtained by a high resolution optical spectrum analyser at the fibre input. Also the spectrum of the 4 upstream channels is shown in Fig. 4.9(b).

The FSO link used in this setup was based on two collimators, polarization independence beam splitter and concave mirror. The beam splitter in this setup was used two divide the FSO link into two links. However, in this experiment, we just evaluated the results of straight

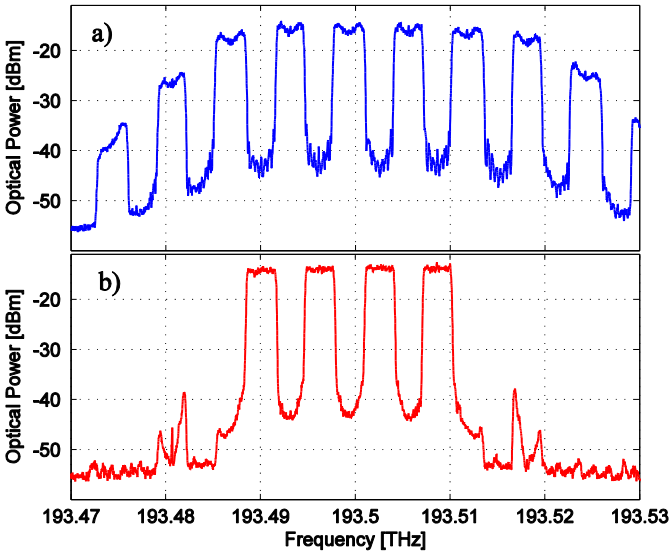

Figure 4.9: a) Downstream spectrum of of 6 channel 12.5 Gbps DP-QPSK or 25 Gbps DP-16QAM at the fibre input; b) Upstream spectrum of 4 channels 12.5 Gbps DP-QPSK or 25 Gbps DP-16QAM.

direction. The total loss of the outdoor FSO link was around 8-9 dB. At the other side, using a circulator the received signal was guided to an integrated phase- and polarization-diverse coherent receiver followed by a 50 GSa/s real-time scope. An ECL with 13 dBm optical power and 100 kHz linewidth was used as a local oscillator.

For the upstream direction (direction from user to operator) the same system was used for transmitter and receiver. The only change is that, in the transmitter part, the U-DWDM signals were implemented using 4 ECL lasers aggregated by a 4:1 coupler. The channel spacing between each channel was 6.25 GHz, with each channel being shifted by 3.125 GHz from the DS wavelengths in order to mitigate back reflection crosstalk. In addition, the IQ modulator

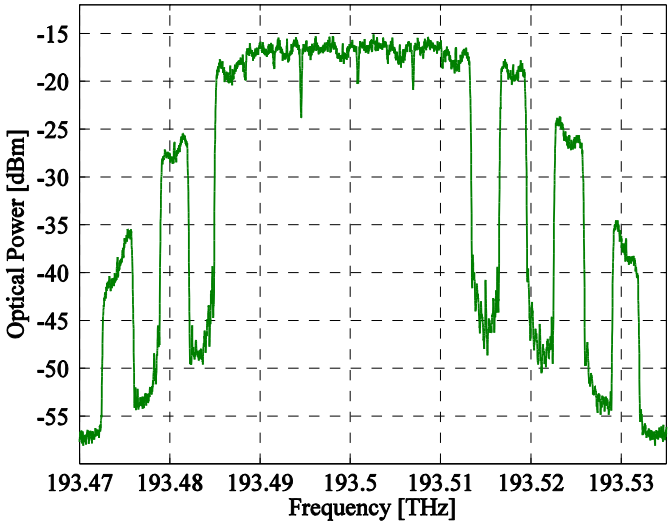

Figure 4.10: Bidirectional spectra.

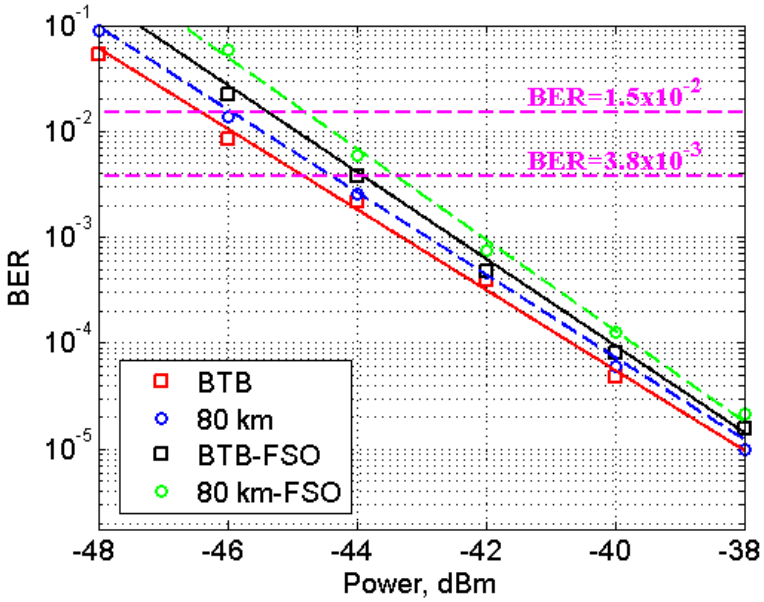

Figure 4.11: Measured BER for the central channel of 6-channels 12.5 Gbps DP-QPSK using the adaptive Stokes algorithm for BTB and 80 km of fiber length and FSO link.

in US direction was driven by a 65 GS/s AWG to generate 4×3.125 Gbaud QPSK or 16QAM signals. We used the same detection process and DSP in the receiver part of OLT for the US channels. Fig. 4.8(b) and Fig. 4.8(c) present the laboratory setup and FSO link in detail. Also the spectrum of both 6 DS and 4 US channels at the same time in the fibre and in the opposite directions are presented in Fig. 4.10,

As mentioned before, back reflections from opposite directions are a major issue, as it is highlighted in Fig. 4.10, where opposite direction channels are close together. Fig. 4.11 presents the measured BER as a function of the receiver input power per DP-QPSK channels. We evaluated the receiver sensitivity for DP signals using a DSP system based on the adaptive Stokes PolDemux technique for BTB, 80 km fibre and 80 km fibre plus 58 meters of outdoor FSO scenarios. As shown in this figure, for a hard-decision (7% overhead) FEC threshold of 3.8×10^{-3}, a sensitivity of -44.5 dBm was achieved for DP-QPSK channels and transmission over 80 km fibre, allowing an optical power budget of 41.5 dB. For 80 km plus FSO scenario the sensitivity of -43.5 dBm and consequently 40.5 dB optical power budget is observed. It is shown that there is a sensitivity penalty of around 0.4 dB when we compare U-DWDM channels in 80 km fibre with respect to the BTB case. This penalty is even increased to 1 and 1.4 dB for BTB-FSO and 80 km plus FSO, respectively.

One thing that must be pointed out is that all of the connectors used in this experimental setup were angled physical contact (APC) type for the fibre and lenses of collimators. Nevertheless, there is still a reduced reflection from opposite directions, which can be completely removed by increasing the frequency spacing between two directions. Instead, considering the soft-decision FEC threshold of 1.5×10^{-2} (20% overhead), a sensitivity of -45 dBm is achieved, enabling the 10 Gbps DP-QPSK transmission over 80 km fibre and 54 meters FSO.

A similar evolution is presented in Fig. 4.12 by measuring the receiver sensitivity of the DP-16QAM channels for BTB, BTB plus FSO, 80 km and 80 km plus FSO. In the case of 80

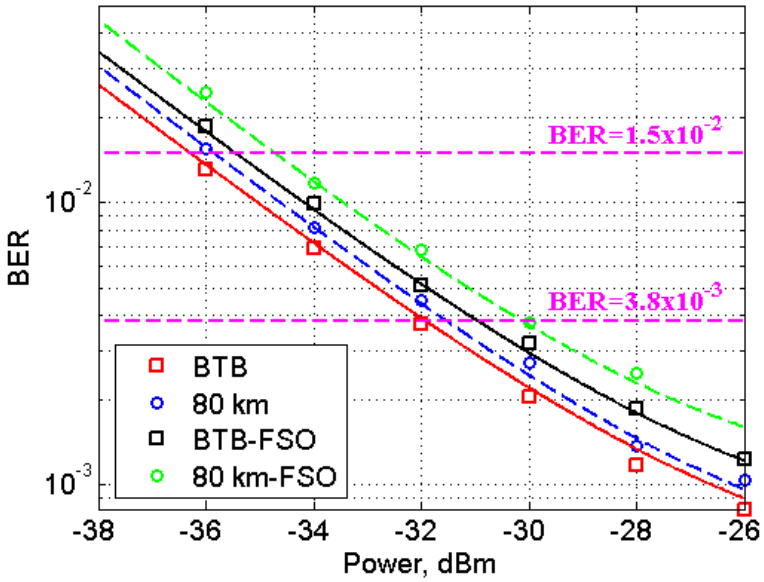

Figure 4.12: Measured BER for the central channel of 4-channels 25 Gbps DP-16QAM using the adaptive Stokes algorithm for BTB and 80 km of fiber length and FSO link.

km fibre plus FSO, we observe a sensitivity of -30 dBm and -34.5 dBm for FEC thresholds of 3.8×10^{-3} and 1.5×10^{-2}, respectively. With -5 dBm at the fibre input, a power budget of 25 dB is achieved for 25 Gbps DP-16QAM and 29.5 dB for 20 Gbps DP-16QAM over hybrid optical wireless scenario. In addition, Fig. 4.12 presents a sensitivity penalty of 2 dB at a target BER of 3.8×10^{-3}, comparing BTB with 80 km fibre plus FSO transmission.

4.3 Real-Time System

As in previous chapter stated, migration to dual-polarization coherent transceivers enables to double the spectral efficiency beside of the increased cost and complexity. The dual-polarization system requires an additional DSP subsystem for polarization demultiplexing. Despite of its widespread application, the well-known CMA presents some important challenges, such as the probability of singularity and the dependence on the transmitted modulation format [6], [8]. In the previous sections, we have proposed an adaptive Stokes PolDemux technique has several advantages over CMA such as conversion speed, flexibility and avoidance of singularity [9], [10]. However, the question related to real time implementation and complexity of algorithms in a real scenario is still open and under consideration. It has been shown for low baud rate signals as well as metro and access applications where the reach is in the short range, that dispersion is not an issue for these systems. Here we demonstrate a reconfigurable real-time DSP reception of a coherent U-DWDM-PON system based on DP-QPSK signal, supported by a commercial field-programmable gate array (FPGA), four 1.25 Gsa/s analog-to-digital converters and DSP based on the adaptive Stokes PolDemux. A test bed based on 20 U-DWDM channels with 625 Mbaud and 2.5 GHz channel spacing over 100 km of SSM fiber is used for validation of PolDemux technique in real-time operation at the coherent receiver. We note that, the 625 Mbaud DP-QPSK signal was selected due to the

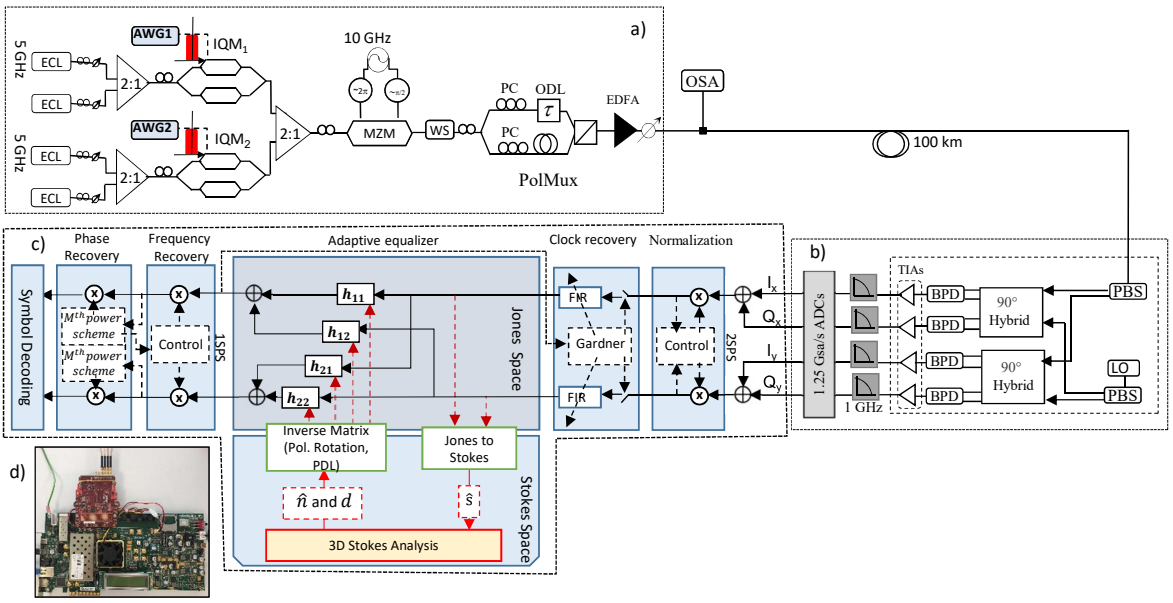

Figure 4.13: Experimental setup for 20×0.625 Gbaud DP-QPSK signals; (a) dual-polarization transmitter; (b) coherent receiver; (c) DSP subsystem based on the adaptive Stokes PolDemux; (d) FPGA and four 8-bit 1.25 Gsa/s ADCs.

limitation of the ADCs. The complexity of both PolDemux techniques based on CMA 1-tap and adaptive Stokes is investigated. The performance of this real-time system is validated for different optimization items such as sensitivity and nonlinearity. Bit error rate (BER) calculations regarding sensitivity and optical power budget is performed.

In Fig. 4.13, we show the proposed experimental setup for validating and characterizing the performance of U-DWDM system based on Nyquist pulse shaped DP-QPSK signal a real time DSP based on adaptive Stokes PolDemux techniques. At the transmitter, four ECLs (<100-kHz linewidth) with channel spacing of 2.5 GHz (wavelength λ_1 is centered at ~ 1549 nm) are injected into two IQ modulators driven by two 65 Gsa/s AWG. The AWGs generate 625 Mbaud signals from a 2^{12}-1 PRBS with a RC shaping with 0.1 roll-off factor. The modulation format for all four channels is the differential QPSK and providing 1.25 Gbps and each neighbor channel is decorrelated. After modulation, the four channels are injected into an optical comb generator1 in order to replicate the four channels in 20 channels with a channel spacing of 2.5 GHz. The U-DWDM signals were separated into two polarizations (12 symbols delayed for decorrelation purposes) using an ODL, and then multiplexed in polarization again by a polarization beam combiner, creating a dual-polarization 2.5 Gbps DP-QPSK. The launch power per channel at the input of 100 km fiber was set by an EDFA and a VOA prior to transmission link.

At the receiver side, an ECL (wavelength λ_1 and 100 kHz linewidth) with 13 dBm optical power was used as local oscillator. U-DWDM signals were detected using an integrated phase- and polarization- diversity coherent receiver followed by 1 GHz low-pass filters and four 8-bit 1.25 Gsa/s ADCs. Note that, only one output of differential outputs of TIAs was used (Fig. 4.13 (b)). The digitalized signal is sent to a Virtex-7 FPGA, where all post-detection 8-bit DSP in real-time is implemented (Fig. 4.13 (c) and Fig. 4.13 (d).

The DSP chain was comprised normalization, clock recovery, adaptive PolDemux, frequency

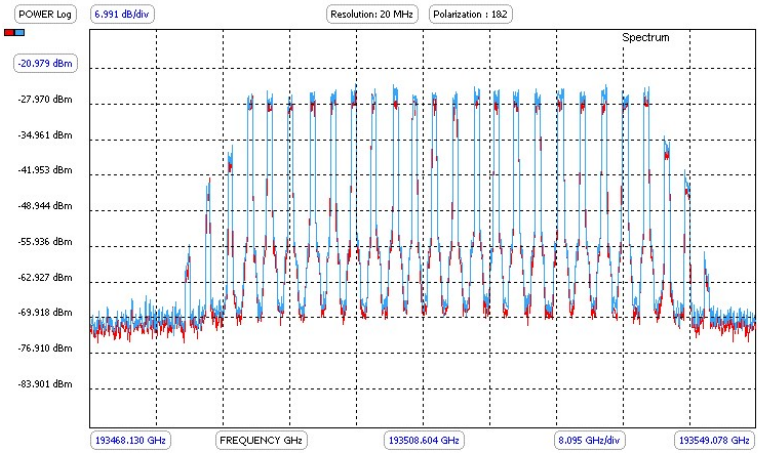

Figure 4.14: Overall optical spectrum of 20 ch in the input of fiber.

and carrier phase recovery subsystems, as depicted in Fig. 4.13 (c).

Each ADC was sampling the signal with two samples per symbol (SPS). At the DSP, firstly an amplitude normalization subsystem based on feedback control is implemented to improve the dynamic range of the overall DSP. Then, the cubic interpolation (4-taps FIR filters) supported by feedback timing-error estimation based on the Gardner power formulation and two SPS as a clock recovery was implemented [4]. As we have DP signal and we plan to implement two PolDemux techniques i.e. CMA and Adaptive Stokes, the timing-error must be estimated from the samples after PolDemux, i.e. the inputs in the feedback branch are the samples after adaptive equalization. Furthermore, since the clock is typically similar for both polarizations, the error can be estimated from only a polarization. The adaptive equalizer is designed with a MIMO configuration based on four FIR filters, supported by the CMA [11]. These filters with a 2-taps resolution are used to restore the SOP of the signal for PolDemux. After this stage, the Mth-power scheme technique proposed in [12] is used for the carrier frequency and phase recovery of one SPS signal.

Note that, the frequency is tracked by the differential phase-based method with feedback control of only one polarization. The phase recovery is based on the Viterbi and Viterbi algorithm by feedforward control and finally, the differential symbol decoding is used to overcome the cycle slip (CS) that can be induced by the blind phase recovery algorithm. The BER is calculated in real-time by bit error counting, averaged between the two polarizations [11].

Table 4.1: Complexity comparison between CMA 1-tap and the adaptive Stokes PolDemux.

PolDemux	Multiplier	Adder	LUT <= 2^{14}	Complexity(DP-QPSK)		
				0.625 GBd	1.25 GBd	2.5 GBd
CMA	$24N + 20$	$48N + 32$	0	114	264	504
Stokes	$24N + 46$	$48N + 45$	9	180.625	300.625	540.625

The clock of the DSP is set at 156.25 MHz, leading to a degree of parallelization of 8 in order to process a sampling rate of 1.25 Gsa/s, i.e. two SPS. In PolDemux part, both CMA 1-tap and the adaptive Stokes space were implemented for PolDemux algorithm and the performance of both of the techniques has been considered. By representing data in the Stokes space, the algorithm finds a best fitting plane, whose normal is then employed into the computation of the inverse polarization rotation matrix of the channel [8], [9].

The optical spectrum of 20 channels, from this setup is shown in Fig. 4.14. Also table 4.1. reports the hardware complexity of both CMA (1-tap) and Stokes algorithms for DP-QPSK signals. The evaluation only considers the real multipliers, real adders and lookup tables (LUTs) as the most critical units of the designs. The value N corresponds to the number of parallel symbols given by T_{DSP}/T_{SYM}, where T_{DSP} corresponds to the clock period of the DSP and T_{SYM} the symbol period of the signal. Thus, considering a DSP clock frequency of 156.25 MHz, N = 8 is required to process a 1.25 Gbaud DP-QPSK signal, for instance. The column Complexity, shows the total complexity of the algorithms based on an 8-bit real multiplier, considering 0.625, 1.25 and 2.5 Gbaud signals. The results should be analyzed as follows: for 2.5 Gbps DP-QPSK (0.625 Gbaud signal), for instance, the 1-tap CMA algorithm has a DSP complexity similar to 144 real 8-bit multipliers. Also, we note that that the clock frequency of the ADC is 156.25 MHz.

In addition, the results of the columns are obtained considering the following key ingredients: The bit-width of most DSP operations is 8 bits; The largest consumer of the DSP are the real multipliers, on the other hand, an adder is typically bit-width times less complex than a multiplier. Since multipliers based on LUTs are typically the most cost-effective solution for multiplier-intensive applications [13], the complexity of the reported LUTs (all in size of <= 2^{14} bits) may be less than an 8-bit multiplier. Thus, it is simply considered that the complexity of a LUT is equal to a real multiplier.

The estimation flow of both algorithms can be designed with a degree of parallelization

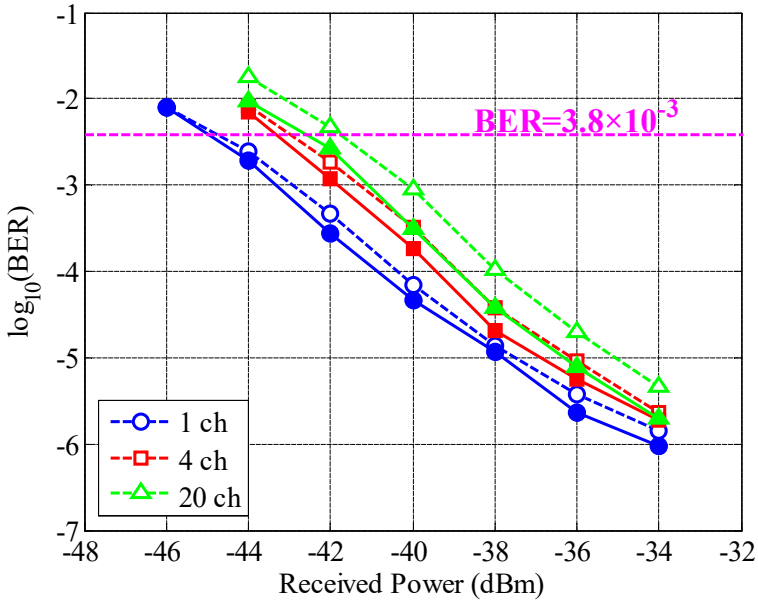

Figure 4.15: BER results for the adaptive Stokes (solid lines) and CMA 1-tap (dashed lines) with the received power per channel transmitted in 100 km fiber.

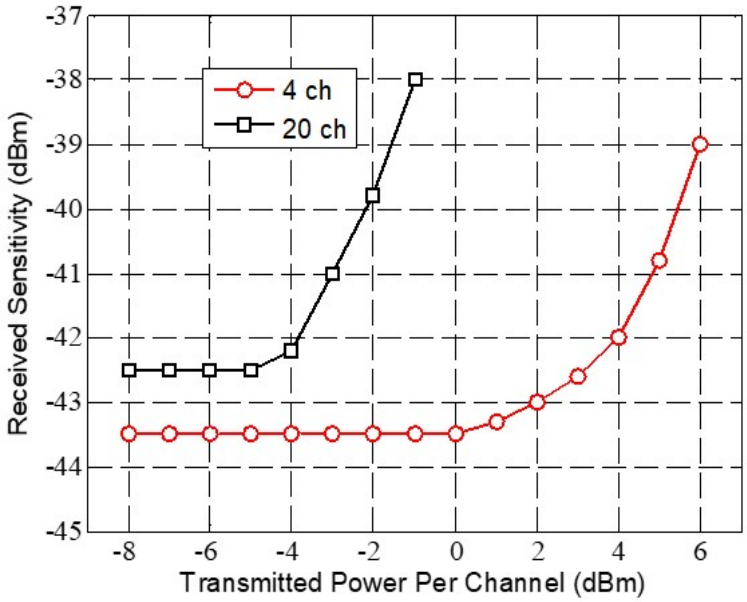

Figure 4.16: ODN power budget for U-DWDM channels: required received power vs. transmitted power per channel to keep the BER at 3.8×10^{-3}.

of one, i.e. only one of the $2N$ received parallel samples (when the signal is sampled with 2 samples per symbol) is used in the estimation process. Since the polarization rotation is generally slow, the feedforward branch of the algorithm requires a degree of parallelization of $2N$ to achieve the sampling high-speed throughput. Thus, as observed in the last column, the complexity between both algorithms (when parallelized hardware implementations are used) is similar when the symbol rate increases (N value grows), since the Stokes differs from the CMA only in the estimation flow of the Matrix coefficients. The complexity of the subsystem is given almost by the feedforward processing of the algorithm, which is equal for both algorithms.

In order to verify and assess the performance of both CMA 1-tap and proposed Stokes PolDemux, Fig. 4.15 shows the measured BER as a function of the receiver input power per multi-channel after transmission on 100 km SSM fiber. The launched optical power per channel in the input of fiber was set to -5 dBm. Results show an acceptable -42 dBm sensitivity considering a forward error correction compatible of BER=3.8×10^{-3}. For received optical powers at this threshold, both algorithms present almost a similar performance for 20 U-DWDM channels.

In addition, Fig. 4.16 analyses the ODN power budget in 100 km SSM fiber of the center channel of 4 and 20 U-DWDM channels. By changing the transmitted power at the input of fiber, the required received optical power for maintaining at the target BER of 3.8×10^{-3} is determined. As shown in Fig. 4.16, maximum power budget of 38 dB for 20 channels is obtained with -42 dBm sensitivity and the input power of -4 dBm. For 4 channels, maximum ODN power budget is 46 dB which obtained with 4 dBm transmitted power.

Results in Fig. 4.17 represents the dynamic power range of the center channel for 4 channels and 20 channels when 100 km fiber was used as a transmission link. The dynamic power range characterizes the maximum power unbalance between adjacent channels, which is an important consideration for the US traffic due to the different link budget between the OLT and each end-user in a real scenario. To report these results for 4 channels transceivers, the power of

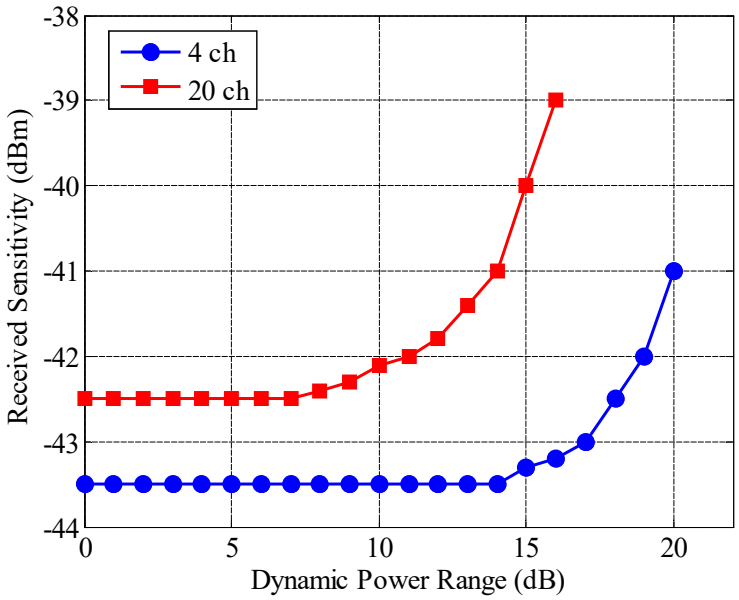

Figure 4.17: Received sensitivity for the central channel of U-DWDM channels vs. DPR in the input of 100km fiber.

two laser was fixed and the other two laser which was interleaved in the other channels was decreased using an optical attenuator. The VOA was before IQM modulator as shown in Fig. 4.13. The obtained results show with 17 dB dynamic power range that can be supported by the center channel of 4 channels scenario, only 0.5 dB penalty in the sensitivity of receivers is created. However, 20 dB dynamic power range gives a penalty of 2.5 dB in the sensitivity for channels systems. This dynamic range can help us to optimize the link budget and number of the users in a U-DWDM system based on proposed Stokes PolDemux. To study the same results for 20 channels, we turned on the comb generator and decrease the power of the laser before comb. Firstly, we make all channels flat as show in Fig. 4.14 and then start to decrease the power of lasers at the input of IQM1. Fig. 4.18(a) and Fig. 4.18(b) present the the optical spectra for 4 and 20 channels when the dynamic power range is around 16 dB. The results in Fig. 4.17 represents the penalty of 0.5 and 2.5 dB is created when the dynamic power range is set to 10 dB and 15 dB, respectively.

In the next step, we have repeated the examination, with adding 54 m FSO to the transmission link, and compare the performance of the adaptive Stokes algorithm and CMA 1-tap as the received optical power per multi channel for 100 km fiber plus 54 m FSO. The FSO link that used in this setup is same as the one, we have used in section 1. Fig. 4.19 depicts BER results for the adaptive Stokes and CMA with the received power per channel for DP-QPSK channels transmitted in 100 km fiber plus FSO link. Considering the FEC threshold of 3.8×10^{-3}, results in this figure show an acceptable -42 dBm sensitivity for 20 channels for both algorithms, and no penalty compared with the setup without the FSO link. In addition, the acceptable sensitivity of -44 dBm was achieved in the case of one channel for both algorithm.

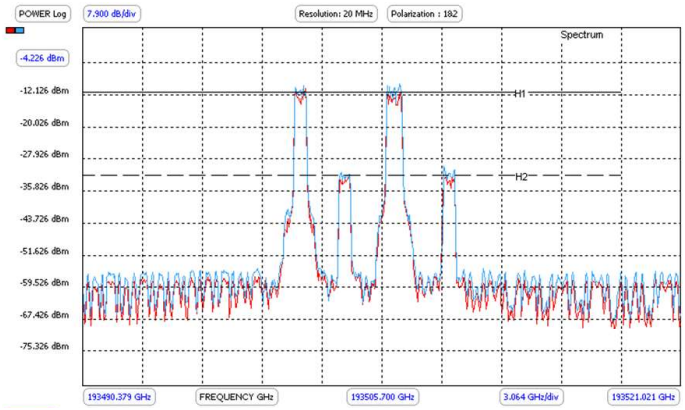

a)

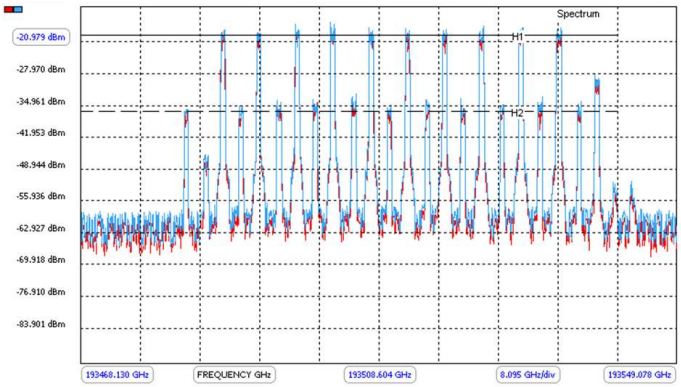

b)

Figure 4.18: Optical spectrum of 4 channels (a) and 20 channels (b), with 16 dB DPR.

4.4 Final Remarks

In this chapter, the adaptive Stokes algorithm was experimentally validated in a coherent U-DWDM system. First, a flexible coherent U-DWDM system with support to optical-wireless links and adaptive DP-QPSK/DP-16QAM modulation was demonstrated. A dynamic bandwidth and power range optical metro and access network, considering back-to-back and transmission scenarios over 80 km fibre, FSO links and field-trial was experimentally assessed. Hybrid DP-QPSK and DP-16QAM modulation was enabled by format-transparent Stokes space PolDemux, simultaneously providing high sensitivity and flexibility with reasonable dynamic power range at 6.25 GHz channel spacing. Performance in field trial was also evaluated in terms of sensitivity confirmed by the penalty-free comparison with the laboratory results. Then, the applicability of using an adaptive Stokes PolDemux technique in bidirectional flexible optical metro networks was experimentally investigated. Employing DP-QPSK modulation, it has been shown that using Stokes-based PolDemux in the DSP part of coherent U-DWDM, an optical power budget of 40.5 dB is achieved for the fibre plus FSO scenario. This power budget is decreased to 25 dB for DP- 16QAM signals of U-DWDM channels. It is concluded that, the back reflection from opposite directions generates a sensitivity penalty of around 2 dB.

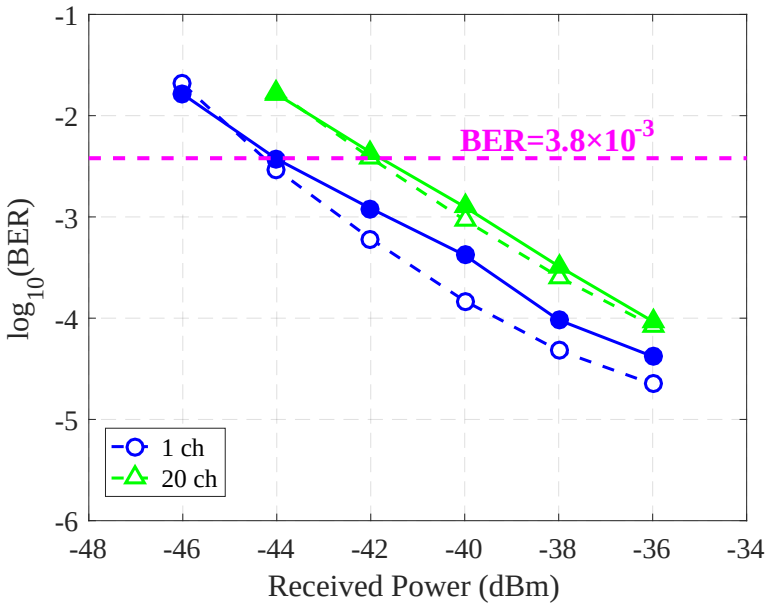

Figure 4.19: BER results for the adaptive Stokes (solid lines) and CMA 1-tap (dashed lines) with the received power per channel for DP-QPSK channels transmitted in 100 km fiber plus FSO link.

Also, a real time U-DWDM DP-QPSK system based on both CMA 1-tap and the adaptive Stokes space PolDemux technique was implemented . The comparisons between both adaptive equalizers were performed in terms of complexity and receiver sensitivity. In addition, the resiliency of the adaptive Stokes PolDemux technique was evaluated in terms of nonlinearity and an optical power budget of >38 dB was achieved dependent to number of channels.

Besides the fast convergence speed and transparency of the adaptive Stocks technique, it was also shown that this technique can be implemented for PolDemux stage of any flexible data rate in optical metro systems as well as hybrid optical wireless scenarios. Allying its fast convergence speed and format-transparency, the adaptive Stokes algorithm is a promising technique to be used in adjustable systems, which means that it can be easily employed in a flexible scenario with different modulation for each channel.

Bibliography

[1] H. Rohde, E. Gottwald, A. Teixeira, J. D. Reis, A. Shahpari, K. Pulverer, and J. S. Wey, "Coherent ultra dense WDM technology for next generation optical metro and access networks," *Journal of Lightwave Technology*, vol. 32, no. 10, pp. 2041–2052, May 2014.

[2] J. D. Reis and A. L. Teixeira, "Architectural optimization of coherent ultra-dense WDM based optical access networks," in *Proc. optical Fiber Communication Conf. and Exposition (OFC)*. IEEE, 2011, paper OTuB7.

[3] A. Shahpari, R. Ferreira, V. Ribeiro, A. Sousa, S. Ziaie, A. Tavares, Z. Vujicic, F. P. Guiomar, J. D. Reis, A. N. Pinto, and A. Teixeira, "Coherent ultra-dense wavelength division multiplexing passive optical networks," *Optical Fiber Technology, Elsevier*, vol. 26, pp. 100–107, December 2015.

[4] A. Shahpari, R. M. Ferreira, F. P. Guiomar, S. Amado, S. Ziaie, C. Rodrigues, J. D. Reis, A. N. Pinto, and A. L. Teixeira, "Real-time bidirectional coherent Nyquist UDWDM-PON coexisting with multiple deployed systems in field-trial," *Journal of Lightwave Technology*, vol. 34, no. 7, pp. 1643–1650, 2015.

[5] D. Lavery, R. Maher, D. S.Millar, B. C. Thomsen, P. Bayvel, and S. J. Savory, "Digital coherent receivers for long-reach optical access networks," *Journal of Lightwave Technology*, vol. 31, no. 4, pp. 609–620, 2013.

[6] S. J. Savory, "Digital coherent optical receivers: algorithms and subsystems," *Selected Topics in Quantum Electronics, IEEE Journal of*, vol. 16, no. 5, pp. 1164–1179, 2010.

[7] J. D. Reis, A. Shahpari, R. M. Ferreira, S. Ziaie, D. M. Neves, M. Lima, and A. L. Teixeira, "Terabit+ (192x10 Gb/s) nyquist shaped UDWDM coherent PON with upstream and downstream over a 12.8 nm band," *Journal of Lightwave Technology*, vol. 32, no. 4, pp. 729–735, Feb. 2014.

[8] N. J. Muga and A. N. Pinto, "Adaptive 3-D Stokes space-based polarization demultiplexing algorithm," *Journal of Lightwave Technology*, vol. 32, no. 19, pp. 3290–3298, 2014.

[9] S. Ziaie, N. J. Muga, F. P. Guiomar, G. M. Fernandes, R. M. Ferreira, A. Shahpari, A. L. Teixeira, and A. N. Pinto, "Experimental assessment of the adaptive Stokes space-based polarization demultiplexing for optical metro and access networks," *Journal of Lightwave Technology*, vol. 33, no. 23, pp. 4968–4974, December 2015.

[10] S. Ziaie, N. J. Muga, R. Ferreira, F. Guiomar, A. Shahpari, A. L. Teixeira, and A. N. Pinto, "Adaptive Stokes space based polarization demultiplexing for flexible UDWDM metro-access networks," in *Proc. Optical Fiber Communication Conf. and Exposition (OFC)*, 2017, paper Th1K–6.

[11] R. M. Ferreira, A. Shahpari, J. D. Reis, and A. L. Teixeira, "Coherent UDWDM-PON with dual-polarization transceivers in real-time," *IEEE Photonics Technology Letters*, vol. 29, no. 11, pp. 909–912, 2017.

[12] R. M. Ferreira, A. Shahpari, S. Amado, M. Drummond, J. D. Reis, A. N. Pinto, and A. L. Teixeira, "Optimized carrier frequency and phase recovery based on blind Mth power

schemes," *IEEE Photonics Technology Letters (PTL)*, vol. 28, no. 21, pp. 2439–2442, 2016.

[13] A. Hazanchuk, "Soft multipliers for dsp applications," in *Global Signal Processing Expo Conf. (GSPx)*, April 2003.

Chapter 5

Stokes Algorithm for Long-Haul Multi-Subcarrier Systems

Due to the impact of chromatic dispersion, demonstrations of the Stokes-based PolDemux algorithm have been restricted to short-reach and/or low symbol-rate systems. Therefore, it is of great importance to find a transmission technology that may enable the extension of Stokes PolDemux to long-haul transmission systems. In this sense, digital multi-subcarrier (MSC) systems provide an opportunity to extend the range of validity of Stokes PolDemux, while keeping its advantages of robust demultiplexing and format transparency.

In this chapter, a solution based on the use of digital multi-subcarrier, which has been demonstrated to efficiently improve the performance of long-haul optical systems, without increasing complexity and cost, will be considered. In addition, we experimentally demonstrate a joint-subcarrier PolDemux strategy for multi-subcarriers systems, which takes into account the PMD effect and clearly shows significant gains in computational complexity. In fact, we carry out an in-depth analysis of the impact of residual CD on the performance of Stokes-based PolDemux, providing clear directives for the required precision of CD compensation at the implementation level. In this regard, in section 5.1, we demonstrate the feasibility and implementation of digital MSC, section 5.2 addresses the extension of the adaptive Stokes algorithm to long-haul optical links. Section 5.3 details the experimental setup and DSP algorithms. The experimental results are presented in section 5.4 and the main conclusions of this chapter are presented in Section 5.5.

5.1 Digital Multi Subcarrier Systems

Recently subcarrier multiplexing and its application in the optical communication systems have been widely considered in the researches. Digital MSC multiplexing has been proposed as an alternative optical transmission technique for the widely deployed single-carrier (SC) systems [1]. MSC presents an additional dimension of multiplexing, which can significantly improve bandwidth efficiency, capacity and flexibility of the optical transmission system [2], [3].

In fact, through symbol rate optimization (SRO), the nonlinearity tolerance of the system can be increased [4], [5]. Also benefiting from the fact that wideband MSC signals are actually composed of several narrowband subcarriers, this technique can enhance its robustness against CD [6], [7]. The QAM is the most commonly advanced modulation format, which employed by MSC systems, since multiple bits are sent in a single signaling interval, utilizing a mapping

method that includes both amplitude and phase. However, with optimization of the modulation format allocation in the hybrid subcarrier system, MSC presents similar performance compared to the time-domain hybrid modulation format (TDHMF), and can provide time-independent procedure in the transceiver side [4]. Although, nonlinearity impairments may appear, due to the unbalanced power between subcarriers, which can be compensated through polarization interleaving.

In the MSC system, digital subcarriers are created by generating signals in the transmitter DSP and loading the samples to high-speed DAC. Then this electrical signal containing multiple subcarriers linearly up-converted to an optical carrier by a single laser and an electro-optic IQ modulator. The idea of employing high-speed DACs, is to move the processing of subcarrier multiplexing and demultiplexing from analog to the digital domain and simplifying the transmitter design. Furthermore, the spacing between subcarriers and also the pulse shaping of each subcarrier can be precisely controlled.

Note that the digital MSC system in this study requires only 1 transmitter for multi-subcarrier, and in case of transmitter configuration has the same structure as a SC system. This means that a SC signal can be considered as a special case of MSC signal, when the number of subcarriers N_{SC} = 0. Fig. 5.1 shows the transmitter-side of a MSC system for subcarrier multiplexing.

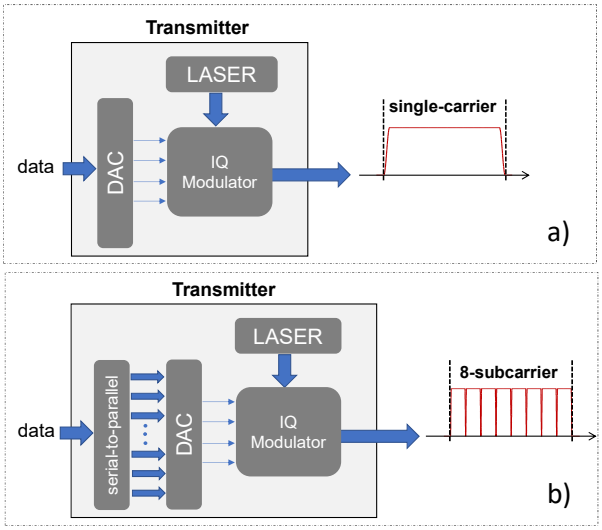

Figure 5.1: Splitting high low symbol rate single carrier to low symbol rate subcarriers in the transmission side.

5.2 Extending Stokes PolDemux to MSC Signals

The performance of the memoryless Stokes PolDemux can be significantly degraded by memory effects [8], which are mostly due to residual CD. For this reason, the application of this algorithm has been so far limited to short-reach systems [9]. In the context of long-haul optical systems, it has been recently demonstrated that digital multi-subcarrier modulation enables to efficiently improve the nonlinear transmission performance, providing up to 20% increased propagation reach with no additional DSP overhead [10], [11]. Furthermore, at the typical optimum symbol-rates per subcarrier of 2–6 Gbaud, the system also benefits from higher

tolerance towards CD comparing with traditional single-carrier systems (≥32 Gbaud) [6]. Under these circumstances, it is of great interest to test the application of the Stokes PolDemux approach with MSC modulation, providing a format-agnostic PolDemux solution for long-haul transmission systems. Benefiting from the fact that wideband MSC signals are actually composed of several narrowband subcarriers, which enhances its robustness against CD [6], in this chapter we experimentally demonstrate the implementation of Stokes-based PolDemux for long-haul optical transmission (> 2000 km) [12]. In addition, by observing that the polarization rotation is strongly correlated between subcarriers, we demonstrate that the complexity of PolDemux for MSC signals can be substantially reduced. This is achieved by performing polarization rotation monitoring over a subset of N_{ref} reference subcarriers, and then applying the extracted PolDemux rotation matrices to the remaining N_{SC} subcarriers, in groups of N_{SC}/N_{ref} nearest neighbor subcarriers. Moreover, we experimentally assess the requirements in terms of CD compensation precision for penalty-free Stokes PolDemux, while demonstrating its compatibility with the well-known SRO benefit in MSC systems.

The adaptive Stokes algorithm proposed in [8] can be divided into two stages, as shown in Fig. 5.2. The first stage corresponds to the cascade of sub-stages that go from the computation of the Stokes parameters of the received data to the estimation of the inverse SOP rotation matrix, which we designate as polarization tracking (PolTrack). After representing the received data in the Stokes space, the algorithm finds a best fitting plane, whose normal is then employed in the computation of the transformation matrix capable of reversing the mixing of the two orthogonal polarization components [8].

As completely explained in chapter 3, Stoks algorithm uses the Stokes vector of each sample, $\hat{s}(k+1)$, to continuously compute the normal $\hat{n}(k+1)$. Sample by sample, and agnostically to the modulation format, the orientation of the normal $\hat{n}(k)$ is therefore updated following the rule,

$$\hat{n}(k+1) = (\hat{n}(k) + \vec{\Gamma}(k+1))B, \tag{5.1}$$

where B represents a normalization factor, and k is the sample number. $\vec{\Gamma}(k+1)$ represents a vector lying in the Stokes plane with direction perpendicular to $\hat{s}(k+1)$,

$$\vec{\Gamma}(k+1) = \mu A[\hat{s}(k+1) \times \hat{n}(k)] \times \hat{s}(k+1), \tag{5.2}$$

where μ is the step-size parameter and $A = \left|\hat{s}(k) \cdot \hat{n}(k)\right|$. The $\hat{s}(k+1)$ is the Stokes vector representing the SOP of the optical field at sample $k+1$. The inverse SOP rotation matrix

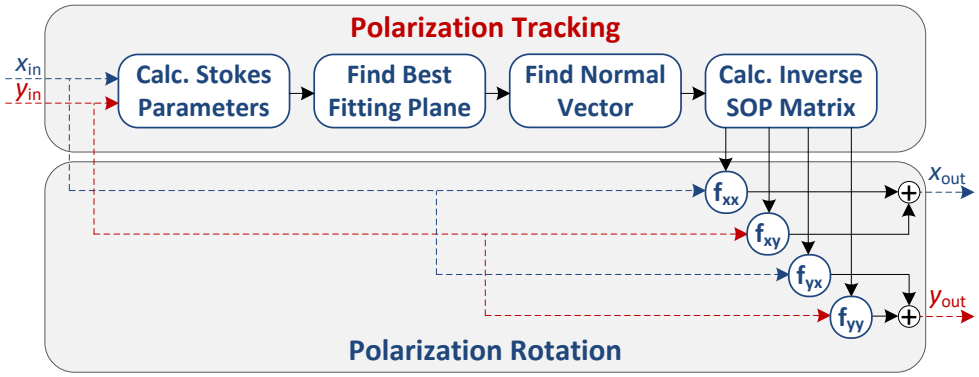

Figure 5.2: Schematic representation of the adaptive Stokes PolDemux algorithm.

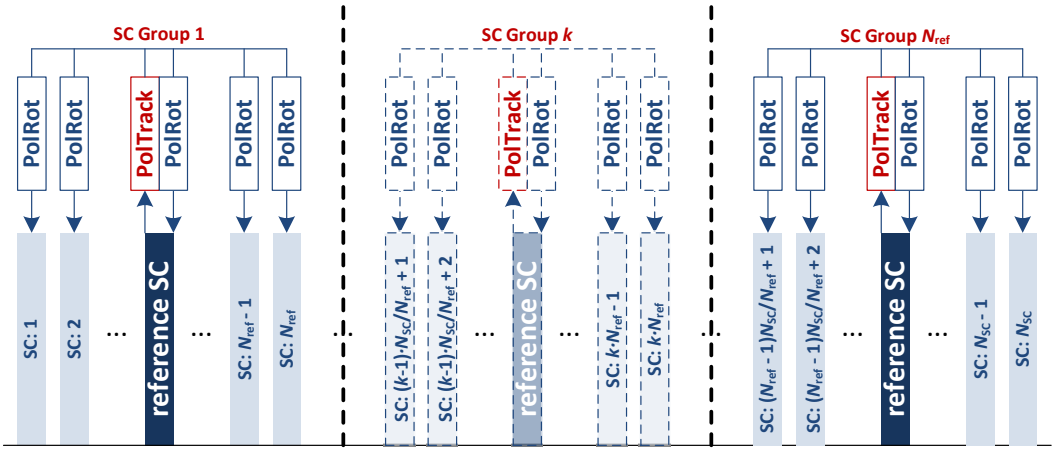

Figure 5.3: Applying the Stokes PolDemux over an MSC signal, using a subset of N_{ref} reference subcarriers for polarization tracking.

$F(\hat{n}(k))$ can be calculated as,

$$\mathbf{F} = \begin{bmatrix} \cos(p)\exp(j\,q/2) & \sin(p)\exp(-j\,q/2) \\ -\sin(p)\exp(j\,q/2) & \cos(p)\exp(-j\,q/2) \end{bmatrix} \tag{5.3}$$

where $p = 1/2\,\text{atan}(a, (b^2 + c^2)^{1/2})$ and $q = \text{atan}(b, c)$, with a, b and c representing the normal vector components, $\hat{n}(k) = (a, b, c)^T$ in the Stokes space [8]. The second stage of the algorithm consists of the polarization rotation (PolRot) part, which basically corresponds to the multiplication of the incoming signal by the previously estimated SOP rotation matrix of expression (5.3) [8]. For each polarization-multiplexed component, x_{in} and y_{in}, the PolRot output signals, x_{out} and y_{out}, are calculated as $x_{out}/y_{out} = f_{xx/yx}x_{in} + f_{xy/yy}y_{in}$, where f_{xx}, f_{xy}, f_{yx} and f_{yy} are the complex-valued scalar components of the inverse SOP rotation matrix $\mathbf{F}$.

As can be easily perceived, most of the complexity of the Stokes PolDemux algorithm lies in the PolTrack stage, which includes several trigonometric operations and multiplications. Moreover, the process of adaptively finding the best fitting plan and normal vectors also introduces some processing latency, as it requires a minimum convergence time. In contrast, the PolRot stage is actually very simple, as it requires only 8 real multiplications and 6 additions per polarization. Therefore, it can be safely stated that the complexity of the PolTrack stage is much larger than the complexity of the PolRot stage.

Thus, the overall complexity of Stokes PolDemux can be significantly reduced by narrowing the bandwidth over which PolTrack is performed. Taking advantage of the subcarrier multiplexing concept, this can be seamlessly done by selecting just a few designated reference subcarriers for the application of the PolTrack stage. The proposed reduced complexity Stokes PolDemux is illustrated in Fig. 5.3. The MSC signal is first divided into N_{ref} groups of $N_{\text{SC}}/N_{\text{ref}}$ subcarriers, where PolTrack stage is applied only over a reference (central) subcarrier, and the PolRot stage is then applied equally to all subcarriers within the same group. The total number of reference subcarriers can be adjusted based on the performance requirements. Assuming that the complexity of PolTrack is largely dominant, it therefore becomes apparent that this strategy enables to approximately reduce the overall PolDemux complexity by a factor of $N_{\text{SC}}/N_{\text{ref}}$.

We must mention that estimating the complexity of the whole DSP chain is an interesting

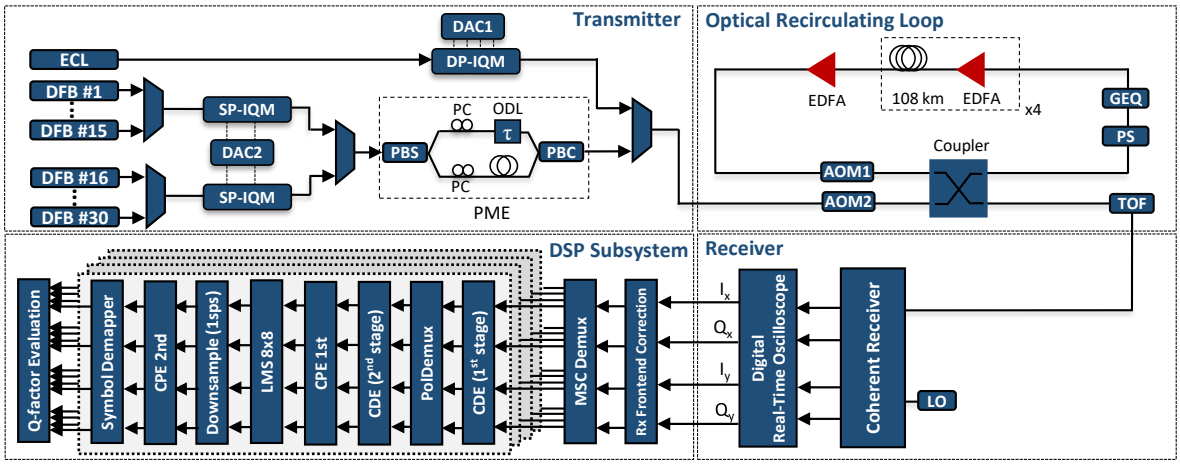

Figure 5.4: Experimental setup for long-haul MSC transmission and DSP subsystems.

but quite challenging topic, which falls outside of the scope of this work. However, we would like to highlight that our claims of DSP complexity in this study are not in relative terms to other adaptive equalization techniques, but only regarding the Stokes implementation itself due to the joint subcarrier processing scheme.

5.3 Experimental Setup and DSP Subsystems

The experimental setup depicted in Fig. 5.4 has been used to validate the performance of Stokes PolDemux implemented in a long-haul optical link, transmitting 31 WDM channels with spacing of 28 GHz. Each optical channel is composed of root raised-cosine (0.05 roll-off) PM-16QAM MSC signals with an aggregate symbol-rate of R_S = 24 Gbaud and variable number of subcarriers, $N_{SC} \in [1, 2, 4, 6, 8, 12]$, with an inter-subcarrier spacing of $1.05 \times R_S/N_{SC}$.

Each 16QAM subcarrier carries bit-level information originated by uncorrelated PRBS, with length varying between 2^{15} (highest symbol-rate) and 2^{11} (lowest symbol-rate) symbols. For each optical channel, the digital MSC signal, including pre-emphasis, is converted to an analog electrical signal by a 64 Gsa/s digital-to-analog converter.

The channel under test (CUT) is generated using an ECL with <100 kHz linewidth, modulated by a dual-polarization IQ modulator. The remaining 30 interfering channels are generated using distributed-feedback (DFB) lasers, modulated (separately for even and odd channels) by a single-polarization IQM followed by polarization multiplexing emulation (PME), resorting to the use of a PBS, polarization controllers (PC), an ODL and a PBC. The recirculating loop is composed of 4 spans of pure silica core fiber (PSCF) with 108 km length, 20.12 ps/(nm·km) dispersion parameter and 0.16 dB/km attenuation coefficient. The total link loss, including insertion losses, is 18.75 dB. EDFA-only amplification (5.2 dB noise figure) is used with a spectrally-resolved gain equalizer (GEQ) that compensates for the EDFA gain-tilt and ripples. Finally, a loop synchronized polarization scrambler (PS) is applied to statistically average the polarization effects. At the receiver, the CUT is filtered by a tunable optical filter (TOF) and mixed with a local oscillator (ECL with <100 kHz linewidth).

Finally, the coherently detected signal is sampled by a 50 Gsa/s real-time oscilloscope. Offline DSP is then applied to the stored waveforms, starting with the compensation of the

optical front-end imperfections, including Gram-Schimdt orthonormalization, DC component removal and compensation of IQ skew introduced by the receiver. The carrier frequency offset is then estimated digitally and the MSC signal is frequency-demultiplexed into N_{SC} subcarriers. In order to assess the impact of the residual accumulated CD on the performance of Stokes PolDemux, we split the CDE into two stages. In the first CDE stage, $x\%$ ($x \in [0, 100]$) of the total accumulated CD is compensated, leaving the remaining residual CD at the input of the PolDemux stage, which implements the algorithm described in section II. Then, the second stage of CDE will exactly compensate for the remaining $(100 - x)\%$ of the accumulated CD. This strategy allows to analyze the impact of the residual CD on the performance of our memoryless Stokes PolDemux algorithm, emulating a real condition in which the CD estimation is performed with a given error.

Therefore, the only DSP stage that processes a signal with residual CD is the PolDemux stage, while it is guaranteed that the overall system performance is not directly affected by uncompensated CD. Note that the Stokes PolDemux in this study is applied with 2 samples per symbol, using the same implementation scheme originally proposed in [8]. Thereby maintaining the 2× oversampling rate for the subsequent 8×8 linear equalizer filter. However, due to the inherently geometrical nature of the Stokes algorithm, it has the possibility to work with only one samples per symbol. Although this signal is then downsampled to 1 sample per symbol in the Downsample block. After the PolDemux, a first coarse carrier phase estimation is applied over one of the central subcarriers, using the 16QAM-modified (QPSK partitioning) Viterbi and Viterbi algorithm with 101 taps. The estimated phase noise is then removed from all subcarriers, allowing for the compensation of the transmitter IQ skew with a 51-tap LMS-driven 8×8 real-valued equalizer [13], initialized in data-aided mode for tap convergence and then switched to decision-directed mode. It is important to mention that all cross-polarization filters in the 8×8 LMS matrix are removed, reducing the total number of individual filters from 64 down to 32. This guarantees that, except for the Stokes PolDemux algorithm, no other DSP subsystems are attempting to perform polarization demulplexing. Also note that the dedicated Stokes PolDemux stage enables the first carrier phase estimation (CPE) stage, which avoids the need for an embedded phase tracker within the 8×8 LMS equalizer.

Performing PolDemux in a preliminary stage allows to perform a first coarse carrier phase estimation before the 8×8 MIMO filter, which simplifies the DD-LMS implementation by avoiding the need for an embedded phase tracker within the filter adaptation loop. Meanwhile, since polarization demultiplexing is fully performed in the initial PolDemux stage, the 8×8 MIMO filter can be simplified by pruning all its cross polarization filter branches, effectively reducing the total number of filter coefficients by half.

Regarding the complexity of the MIMO filters, all its filter components will be in practice implemented in parallel. This means that the processing latency should in principle be kept the same regardless of the number of MIMO filters. Nevertheless, the use of parallelization implies the replication of hardware resources for each filter, and therefore a reduction by 50% on the number of constituent filters should roughly correspond to a similar reduction in terms of required number of hardware gates, thus contributing as well to the optimization of power consumption and chip area.

After down sampling to 1 sample per symbol, a second Viterbi and Viterbi CPE stage is applied to each subcarrier with an optimized block length, aimed at the removal of residual nonlinear phase noise, similarly to what has been done in [11]. It should be mentioned that the second CPE is actually optional, and is used in this work just for the purpose of providing a

fine tune compensation of the nonlinear phase noise (NLPN), thus maximizing the symbol-rate optimization effect. Finally, symbol demapping is performed and the Q-factor per subcarrier is evaluated from the counted BER.

5.4 Experimental Results

Applying the DSP chain described in the previous section, the Stokes PolDemux performance is experimentally evaluated for all considered MSC configurations at the optimum launch power of 0 dBm per optical channel [11] and at a fixed transmission distance of 2160 km (5 recirculations). The system performance as a function of the residual CD (bottom x-axis) and the error percentage on CD estimation (top x-axis), after the 1st CDE stage, is shown in Fig. 5.5, for a number of subcarriers ranging from 1 to 12.

Also, Fig. 5.6 shows the total residual CD that can be tolerated as a function of the number of subcarriers, assuming a maximum Q-factor penalty (Q_{pen}) of 0.1 dB relatively to the case when CD is fully compensated in the 1st stage. These results clearly show the enhanced tolerance against residual accumulated CD that is enabled by an increasing number of subcarriers.

Indeed, for the typical single-carrier signal (1×24 Gbaud) the system is very sensitive to residual CD before the PolDemux stage (< 1 ns/nm is tolerated for $Q_{\text{pen}} \leq 0.1$ dB). Besides, very steep degradation of performance is observed when the CD compensation error is >1%, which roughly corresponds to 700 ps/nm of residual CD.

With single subcarriers modulation a 0.1 dB penalty on Q-factor is already found at about 1.7% CD compensation error, which corresponds to approximately 700 ps/nm. A zoomed version of Fig. 5.5, is depicted in Fig. 5.7 for the single-carrier case.

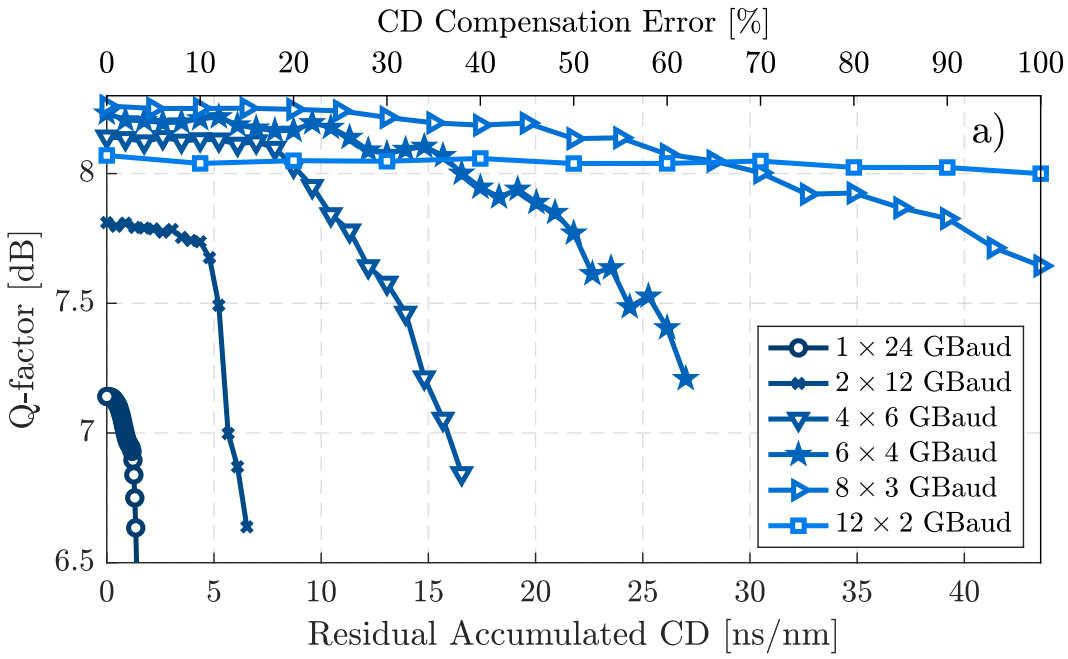

Figure 5.5: Q-factor vs. residual accumulated dispersion and error percentage on CD estimation after the 1st CDE stage.

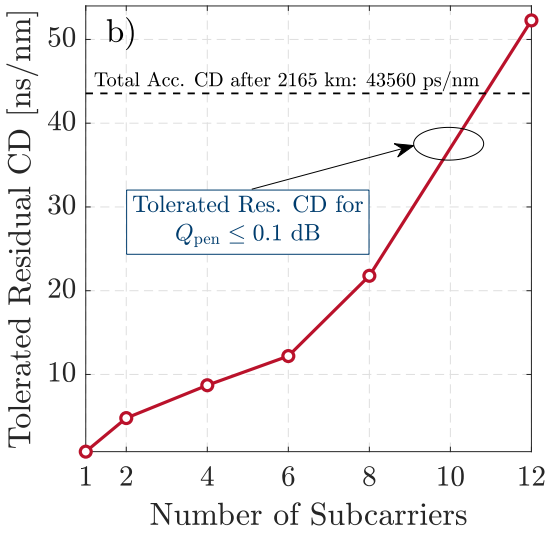

Figure 5.6: Tolerated residual CD (considering $Q_{\text{pen}} \leq 0.1$ dB) vs. number of subcarriers.

In contrast with the above single-carrier results, with only 2 subcarriers, the 0.1 dB penalty on Q-factor is already found for a significantly higher CD compensation error of >10%, corresponding to >4 ns/nm of residual CD.

By using 2×12 Gbaud, this tolerance is substantially increased to ~10%. In contrast, when the signal is composed of 12 subcarriers (12×2 Gbaud) the system performance remains stable for all range of tested residual CD values, thus enabling Stokes PolDemux to be applied without any prior CD compensation at all (CD is entirely compensated in the second CDE stage, after PolDemux). Taking into account that advanced CD estimation algorithms can typically provide an accuracy of ±300 ps/nm [14], we may conclude that the considered 24 GBaud single-carrier system could still be supported with minimal implementation penalty. Nevertheless, with the current trend towards ultra-high symbol-rates, the margin for CD

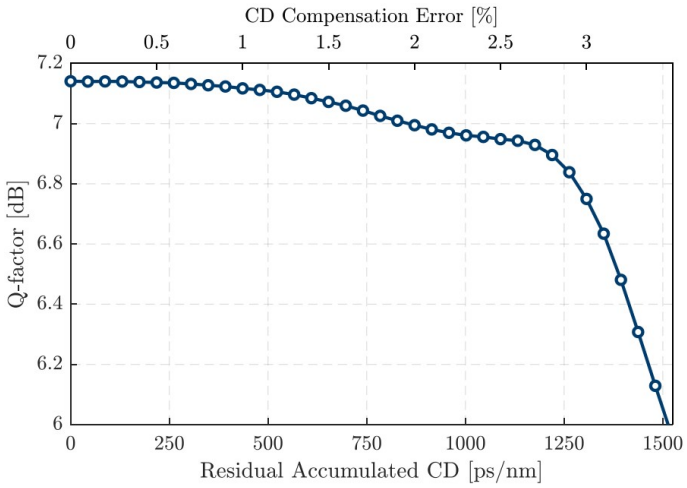

Figure 5.7: Q-factor vs. residual accumulated dispersion and error percentage on CD estimation for one subcarrier.

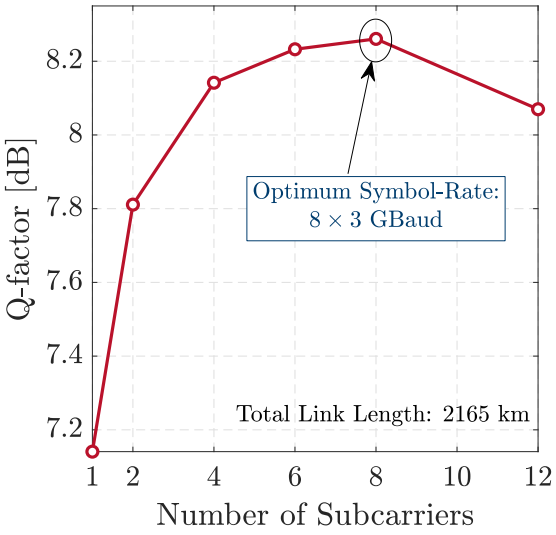

Figure 5.8: Symbol-rate optimization.

estimation errors is rapidly closing. Considering the quadratic dependence of the residual CD on the transmitted symbol-rate [6], the tolerated CD values here reported are expected to suffer a ~16× reduction by increasing the baseline symbol-rate to 100 GBaud, thereby challenging the precision of state-of-the-art CD estimation algorithms. In that case, the use of MSC transmission might become a key enabler for memoryless Stokes-based PolDemux.

It is also worth noting that the well-known SRO advantage is still kept using the proposed DSP. This is evidenced in Fig. 5.8, which shows the best Q-factor obtained for each MSC configuration, corresponding to the case of perfect CD compensation in Fig. 5.5. The optimum symbol-rate is found at 3 Gbaud per subcarrier, providing ~1 dB of gain in terms of Q-factor relatively to the single-carrier case, in accordance with the results from our previous experimental campaign [11].

However, due to the quadratic dependence on the symbol-rate, which can be clearly confirmed in Fig. 5.5 and also in the results of reference [6], the tolerated residual CD will rapidly become very small for the next-generation commercial long-haul optical systems, which are currently targeting 64-100 GBaud per channel. Considering that a symbol-rate increase by a factor of N will roughly correspond to a reduction of tolerated residual CD by a factor of N^2, then the current value of 700 ps/nm tolerated CD at 24 Gbaud is expected to become as low as 100 ps/nm at 64 Gbaud and 40 ps/nm at 100 GBaud. Considering the accuracy of state-of-the-art CD estimation algorithms, it will be much more challenging to provide the required CD estimation accuracy that guarantees penalty-free operation with a memoryless PolDemux algorithm for next-generation transceivers. In those cases, the use of subcarrier-multiplexing might become a crucial enabling factor for Stokes-based PolDemux.

Besides the enhanced robustness towards residual CD, the use of MSC signals together with Stokes PolDemux can also be advantageous from the complexity point of view. In Fig. 5.9 we experimentally validate the reduced complexity Stokes PolDemux strategy depicted in Fig. 5.3 and described in section II, in which the PolTrack stage is only applied over a group of reference subcarriers. The obtained results show that a minimum of 2 to 4 reference subcarriers are needed to achieve the maximum performance (within < 0.2 dB penalty) of the PolDemux algorithm.

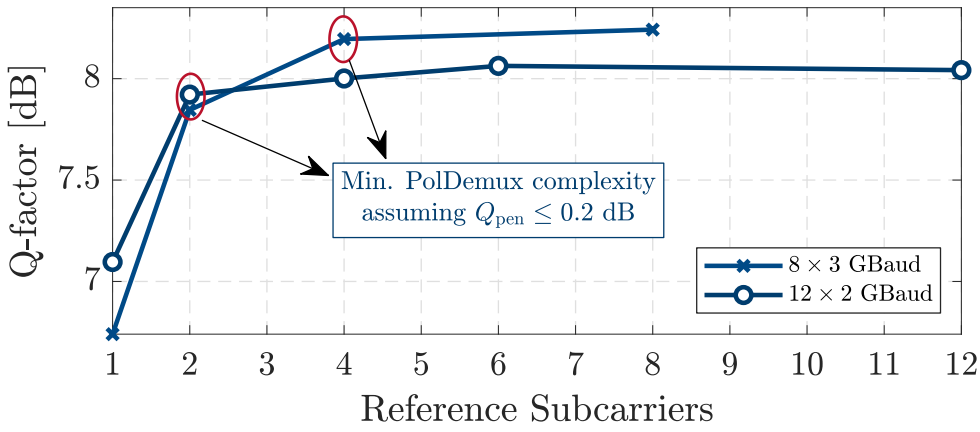

Figure 5.9: Impact of the number of reference subcarriers for PolTrack on the overall performance of the Stokes PolDemux algorithm.

For the cases of 8×3 Gbaud and 12×2 Gbaud, this roughly corresponds to a computational effort reduction by a factor of 2 and 6 respectively, when compared to an independent Stokes-based PolDemux of all subcarriers. These results show that the frequency-dependent variation of the PolDemux coefficients caused by PMD can be efficiently taken into account without the need to replicate the PolTrack stage over all subcarriers.

In practice, the (first-order) PMD effect will translate into a frequency-dependent polarization axis, which in the case of subcarrier-multiplexed signals can be more easily observed by analyzing the inverse SOP matrix coefficients estimated for each subcarrier. In fact, our proposed joint subcarrier PolDemux algorithm described in Fig. 5.3, already addresses the impact of PMD in these systems, we apply the PolDemux algorithm to a subset of reference subcarriers (evenly spaced) then same parameters are used for neighbor subcarriers. Following this approach, the results presented in Fig. 5.9 show that a minimum number of 2-4 reference subcarriers are required for high performance PolDemux. This is indeed due to the impact of PMD, which results in a frequency-dependent variation of the PolDemux coefficients: our results show that within a reasonably narrow frequency range (5-10 GHz) the PMD-induced variation of the PolDemux coefficients is almost negligible, allowing for the PolDemux estimation on a single reference subcarrier and application of the estimated coefficients to the remaining neighbor subcarriers.

5.5 Final Remarks

Benefiting from the fact that wideband MSC signals are actually composed of several narrowband subcarriers, which enhances its robustness against CD [6], we experimentally demonstrate the implementation of Stokes-based PolDemux for long-haul optical transmission (> 2000 km). We have shown, the adaptive Stokes PolDemux algorithm, which has been previously utilized for short reach (<100 km) applications only, can also be efficiently applied to long-haul transmission systems. The enabling factor is the use of MSC modulation, which has been demonstrated to significantly enhance the PolDemux tolerance against residual accumulated CD, thereby potentially allowing for a practical implementation of the modulation transparent Stokes PolDemux algorithm in long-haul scenarios.

We have detailed assessm ent of the impact of mismatched CD compensation on the performance of Stokes-based PolDemux, demonstrating that >10% tolerance in CD estimation error can be tolerated for symbol-rates per subcarrier of <6 GBaud. This provides a clear indication of the practical feasibility of the memoryless Stokes PolDemux for long-haul transmission enabled by subcarrier multiplexing.

In addition, by observing that the polarization rotation is strongly correlated between subcarriers, we demonstrated that the complexity of PolDemux for MSC signals can be substantially reduced. This was achieved by performing polarization rotation monitoring over a subset of N_{ref} reference subcarriers, and then applying the extracted PolDemux rotation matrices to the remaining N_{SC} subcarriers, in groups of N_{SC}/N_{ref} nearest neighbour subcarriers. Moreover, we have experimentally assessed the requirements in terms of CD compensation precision for penalty-free Stokes PolDemux, while demonstrating its compatibility with the well-known SRO benefit in MSC systems.

Bibliography

[1] R. Hui, B. Zhu, R. Huang, C. T. Allen, K. R. Demarest, and D. Richards, "Subcarrier multiplexing for high-speed optical transmission," *Journal of lightwave technology*, vol. 20, no. 3, p. 417, 2002.

[2] Y. Zhang, M. O Sullivan, and R. Hui, "Digital subcarrier multiplexing for flexible spectral allocation in optical transport network," *Optics Express*, vol. 19, no. 22, pp. 21 880–21 889, 2011.

[3] F. P. Guiomar, L. Bertignono, D. Pilori, A. Nespola, G. Bosco, A. Carena, and F. Forghieri, "Comparing different options for flexible networking: Probabilistic shaping vs. hybrid subcarrier modulation," in *Proc. European Conf. on Optical Communication (ECOC)*, 2017, pp. 1–3.

[4] F. P. Guiomar and A. Carena, "Achieving fine bit-rate granularity with hybrid subcarrier modulation," in *Signal Processing in Photonic Communications*. Optical Society of America, 2016, paper SpW3F–2.

[5] M. Qiu, Q. Zhuge, M. Chagnon, Y. Gao, X. Xu, M. Morsy-Osman, and D. V. Plant, "Digital subcarrier multiplexing for fiber nonlinearity mitigation in coherent optical communication systems," *Optics Express*, vol. 22, no. 15, pp. 18 770–18 777, 2014.

[6] M. Malekiha, I. Tselniker, and D. V. Plant, "Chromatic dispersion mitigation in long-haul fiber-optic communication networks by sub-band partitioning," *Optics Express*, vol. 23, no. 25, pp. 32 654–32 663, 2015.

[7] F. P. Guiomar, S. B. Amado, J. D. Reis, S. M. Rossi, A. Chiuchiarelli, J. R. F. Oliveira, A. L. Teixeira, and A. N. Pinto, "Ultra-long-haul 400g superchannel transmission with multi-carrier nonlinear equalization," in *Proc. European Conf. on Optical Communication (ECOC)*, 2015, pp. 1–3.

[8] N. J. Muga and A. N. Pinto, "Adaptive 3-D Stokes space-based polarization demultiplexing algorithm," *Journal of Lightwave Technology*, vol. 32, no. 19, pp. 3290–3298, Oct. 2014.

[9] S. Ziaie, N. J. Muga, F. P. Guiomar, G. M. Fernandes, R. M. Ferreira, A. Shahpari, A. L. Teixeira, and A. N. Pinto, "Experimental assessment of the adaptive Stokes space-based polarization demultiplexing for optical metro and access networks," *Journal of Lightwave Technology*, vol. 33, no. 23, pp. 4968–4974, December 2015.

[10] M. Qiu, Q. Zhuge, M. Chagnon, Y. Gao, X. Xu, M. M. Osman, and D. V. Plant, "Digital subcarrier multiplexing for fiber nonlinearity mitigation in coherent optical communication systems," *Optics Express*, vol. 22, no. 15, pp. 18 770–18 777, Jul 2014.

[11] F. P. Guiomar, A. Carena, G. Bosco, L. Bertignono, A. Nespola, and P. Poggiolini, "Nonlinear mitigation on subcarrier-multiplexed PM-16QAM optical systems," *Optics Express*, vol. 25, no. 4, pp. 4298–4311, Feb 2017.

[12] S. Ziaie, F. P. Guiomar, N. J. Muga, A. Nespola, G. Bosco, A. Carena, and A. N. Pinto, "Adaptive Stokes-based polarization demultiplexing for long-haul multi-subcarrier systems," *IEEE Photonics Technology Letters*, vol. 31, no. 10, pp. 759–762, 2019.

[13] G. Bosco, S. M. Bilal, A. Nespola, P. Poggiolini, and F. Forghieri, "Impact of the transmitter IQ-skew in multi-subcarrier coherent optical systems," in *Proc. Optical Fiber Communication Conf. and Exposition (OFC)*. IEEE, 2016, paper W4A.5.

[14] R. A. Soriano, F. N. Hauske, N. G. Gonzalez, Z. Zhang, Y. Ye, and I. T. Monroy, "Chromatic dispersion estimation in digital coherent receivers," *Journal of Lightwave Technology*, vol. 29, no. 11, pp. 1627–1637, 2011.

Chapter 6

Conclusions and Future Research

The exponential growth of bandwidth-consuming internet applications and services leads to the development and adoption of new optical transmission paradigms for telecommunication networks. However, due to the very heterogeneous nature of services, the plurality of end-users, the cost constraints and unpredictable Internet data traffic, there are a lot of challenges for developing and implementing optical transmission systems. In this regard, next-generation optical networks require high-performance and flexible optical transceivers to support a very-high capacity optical network as well as optimization of the network concept. Coherent U-DWDM technologies together with multi-level modulation formats and a powerful DSP, lead to high aggregated capacity per fiber as well as long transmission distances.

The central topic of this thesis is related to research and characterization of cost-effective novel coherent systems based on polarization demultiplexing techniques for the development of new generation practical, flexible and high capacity transceivers for future optical technologies. In this final chapter, in section 6.1, we overview the developed work and summarize the most relevant conclusions. Also some guidelines and suggestions for future research topics are presented in section 6.2.

6.1 Conclusion

The first contribution of this thesis was presented in Chapter 2, in which we presented implementation details of an optical recirculating loop and discussed experimental issues related to this technique. In a general context, we review digital coherent transmitters and receivers, which can used for high-capacity long-haul optical networking and data center interconnect. In addition, we presented experimental results of 100 Gbps DP-QPSK propagated over 8000 km of SSM fiber. We use the digital backward propagation method employing the split-step Fourier algorithm, in order to compensate nonlinearities in the transmission system and compare its performance with the results of the system without applying a nonlinear equalizer.

One of the major conclusions of this study was to validate adaptive Stokes polarization demultiplexing techniques for the development of new generation practical, flexible and high capacity transceivers for future optical technologies. We have experimentally validated the performance and convergence speed of the adaptive Stokes technique with constant frequency SOP rotation for DP-QPSK and DP-16QAM Nyquist signals at 3.125 Gbaud and compared it with conventional CMA. Although both algorithms could achieve identical performance by properly adjusting their step-size, the convergence of the adaptive Stokes algorithm has been

found to be approximately three times quicker than that of CMA.

In addition, performance of a flexible coherent U-DWDM with support to optical-wireless links and DP-QPSK and DP-16QAM modulation formats enable by the adaptive Stokes algorithm was evaluated. A dynamic bandwidth and power range optical metro and access network, considering back-to-back and transmission scenarios over 80 km fiber, FSO links, and field-trial have been experimentally demonstrated. Hybrid DP-QPSK and DP-16QAM modulation are enabled by format-transparent Stokes space PolDemux, simultaneously providing high sensitivity and flexibility with reasonable dynamic power range at 6.25 GHz channel spacing. Performance in the field trial was also evaluated in terms of sensitivity confirmed by the penalty-free comparison with the laboratory results. Allying fast convergence speed and format-transparency of the adaptive Stokes space PolDemux, we have shown, this technique is a promising technique to be used in reconfigurable DSP for flexible optical metro-access networks, as well as optical wireless scenarios.

Furthermore, taking advantage of Nyquist pulse shaped U-DWDM, we experimentally implement the adaptive Stokes algorithm over a bidirectional optical metro network. The optical signals based on DP-QPSK and DP-16QAM modulation formats were transmitted over up to 80 km SSM fiber plus 54 m outdoor FSO link. Besides the fast convergence speed and transparency of the adaptive Stokes algorithm, it was also shown that this technique can be implemented for the PolDemux stage of any flexible data rate in optical metro systems as well as hybrid optical wireless scenarios.

We showed that the Stokes PoldDem technique can be implemented in FPGA. We experimentally demonstrated a real-time U-DWDM DP-QPSK system based on both CMA 1-tap and the adaptive Stokes space PolDemux technique considering transmission over 100 km fibre. The comparisons between both adaptive equalizers were performed in terms of complexity and receiver sensitivity. In addition, the resiliency of the adaptive Stokes PolDemux technique was evaluated in terms of nonlinearity and an optical power budget of >38 dB was achieved dependent on the number of channels.

For the data center interconnect and long-haul transmission systems, we also have been working on the efficient implementation of the adaptive Stokes PolDemux algorithm for high bit rate signals. As in high baud rate signal using subcarrier scenario, the tolerance to errors in CD estimation and compensation is very low, making the application of the technique extremely challenging. We have shown that the adaptive Stokes PolDemux algorithm, which has been previously utilized for short reach (<100 km) applications only, can also be efficiently applied to long-haul transmission systems. The enabling factor is the use of MSC modulation, which has been demonstrated to significantly enhance the PolDemux tolerance against residual accumulated CD, thereby potentially allowing for practical implementation of the modulation transparent Stokes PolDemux algorithm in long-haul scenarios. By restricting the polarization tracking circuitry to a subset of N_{ref} subcarriers, we also demonstrated that the overall PolDemux complexity can be significantly reduced (approximately by a factor of $N_{\mathrm{SC}}/N_{\mathrm{ref}}$) with negligible performance degradation.

6.2 Future Work

We believe that the outcomes and results, which have presented in this thesis contribute to an advance of the field, although some subjects can be explored more thoroughly. Therefore, from the efforts of this work, some potential future research directions remain as open and

challenging topics, as listed in the following

- The geometrical nature of the adaptive Stokes method imposes memory-less processing. It will be useful to develop the Stokes PolDemux algorithm that not restricted to this issue. Therefore, it can account for memory effects and consequently increase capacity of the flexible optical communication systems.
- In recent years, lower-cost schemes based on direct-detection transmission technologies that have been proposed, e.g. Stokes vector receiver [1] and Kramers-Kronig algorithm [2]. Despite using DD, they allow recovering the complete information of the optical field, offering notable advantages such as smaller footprint, lower power consumption, and considerable lower cost. In this context, the PolDemux techniques experimentally validated in this work could be extended to these new approaches.
- Employing advanced modulation formats, allow the increase rate per channel as well as the system spectral efficiency. As future work, it is very interesting to validate the adaptive Stokes algorithm with higher-order modulation formats, such as 128QAM, and even 256QAM.
- The adaptive Stokes algorithm is modulation format transparent, which means it can easily be employed in a flexible scenario. It is very interesting to extend the MSC system, in order to have a different modulation format for each subcarrier.
- Above mentioned coherent architectures in burst mode operation and investigating burst mode issues in the laboratory.
- Implementing novel and reliable hybrid optical wireless networks (fiber optic plus FSO parallel with fiber optic plus RF) for higher network resiliency.

Bibliography

[1] A. Li, D. Che, V. Chen, and W. Shieh, "Spectrally efficient optical transmission based on Stokes vector direct detection," *Optics Express*, vol. 22, no. 13, pp. 15 662–15 667, 2014.

[2] A. Mecozzi, C. Antonelli, and M. Shtaif, "Kramers–Kronig coherent receiver," *Optica*, vol. 3, no. 11, pp. 1220–1227, 2016.